2019

Molecular Mechanisms Underlying Stress-Induced GLIA Remodeling in the Nematode C. Elegans

In Hae Lee

MOLECULAR MECHANISMS UNDERLYING STRESS-INDUCED GLIA REMODELING IN THE NEMATODE *C. ELEGANS*

A Thesis Presented to the Faculty of

The Rockefeller University

in Partial Fulfillment of the Requirements for

the degree of Doctor of Philosophy

by

In Hae Lee

June 2019

MOLECULAR MECHANISMS UNDERLYING STRESS-INDUCED GLIA REMODELING IN THE NEMATODE *C. ELEGANS*

In Hae Lee, Ph.D.

The Rockefeller University 2019

Animals can adapt to long-term environmental changes by modifying their behavior, which can be accompanied by structural alterations of the nervous system. Such alterations are common in sensory organs, composed of sensory neurons and glia, which initially detect environmental stress. The molecular mechanisms driving cell shape remodeling following environmental stress and the effects of such remodeling on animal survival are not well understood. *C. elegans* is an excellent model in which to study neuronal and glial cell remodeling. Under normal growth conditions, the sensory receptive endings of the bilateral AWC sensory neurons, which respond to volatile odorants, are individually ensheathed by processes of adjacent amphid sheath (AMsh) glial cells. Upon exposure to high temperature, starvation, or crowding, animals enter an alternative developmental state, called dauer, in which bilateral AMsh glia membranes surrounding the AWC neuron fuse, connecting the two glial cells, and allowing the AWC neuronal receptive endings to expand. Previous studies from our lab identified several AMsh glia proteins required for remodeling. These include (1) the cell fusion protein AFF-1, (2) a VEGFR-related protein VER-1, (3) the Otd/Otx transcription factor TTX-1, and (4) the zinc-finger transcription factor ZTF-16. *ver-1* expression in AMsh glia is induced by dauer entry or by cultivation

at high temperature, and requires direct binding of TTX-1 to *ver-1* regulatory sequences. To identify additional genes involved in stress-induced sensory organ remodeling, we performed a forward genetic screen, seeking mutants in which *ver-1* expression at high temperature is not induced. One mutant recovered from this screen harbors a causal lesion in *F47D2.11* gene, which encodes a 7-transmembrane G-protein coupled receptor (GPCR). Mutations in *F47D2.11* not only block *ver-1* induction, but also prevent dauer-induced AMsh glia remodeling and result in a delay in exit from the dauer state following exposure to a favorable environment. *F47D2.11* mutants can be rescued by expression of the wild-type cDNA in AMsh glia but not in AWC neurons. These results implicate *F47D2.11* in the sensation of dauer conditions in AMsh glia, required for dauer-induced glial remodeling and timely dauer exit.

To my parents.

어머니, 아버지~

수고 많으셨습니다.

감사합니다.

ACKNOWLEDGEMENTS

First, I thank **Shai Shaham**, my thesis advisor, for his mentorship and guidance. His deep and contagious enthusiasm for understanding how the world works is truly inspiring. Thank you for always pushing me and believing in me. I am very lucky to have been a student of yours.

I am honored and privileged to have **Cori Bargmann** and **Vanessa Ruta** as my thesis committee members. Their keen insights and discussions were critical for the development of my project. Thank you for all of your advice during the completion of this thesis. I also want to thank **Maureen Barr** for graciously accepting to serve as my external thesis committee member.

I want to thank all the members of the Shaham lab, past and present, who have created such a collegial, enriching work environment. It has been an enjoyable place to work, even during periods of scientific frustration. I especially want to thank my first benchmate and friend **Menachem** for providing a critical scientific eye and his willingness to always lend a hand. Our never-ending discussions kept me motivated and curious for the next step. I also want to thank **Sean** and **Lena**, who inspire me with their tenacity and thoughtfulness. Their willingness to always stop and answer my questions has been invaluable. I also thank our lab manager **Maya**, who keeps the lab running smoothly with ease and patience.

I thank the Dean's office (**Sid, Emily, Cris, Kristen, Marta,** and **Stephanie**) for making it so easy to be a graduate student at Rockefeller. They enabled me to focus on the science throughout my time here and I really appreciate all your hard work.

I also thank the housing office **Marnel** and **Joe** as well as the housing/maintenance staff for keeping our apartments running smoothly. I especially thank them for keeping this west coast lady warm and safe when my heater broke down in the middle of a snowstorm (twice).

I also want to thank my undergraduate mentors, **Robert Steiner, Don Clifton** and **Daniel Marks** for instilling in me a love of science and encouraging me every step of the way.

I would not be here without my **friends** from all around the globe. Thank you for always being a call (or snap) away, despite the time differences.

I am always and forever grateful to my **mother** and **father** for their endless love and sacrifices. Thank you for being the unwavering source of happiness in my life. I'm also grateful for my little **brother**. His optimism and humor kept me afloat

and smiling even through the toughest of times. Without my family, I truly would not be here today.

Last but not least, I thank my fiancé **Eugene**, who is tirelessly supportive, patient and loving. Thank you for encouraging me every step of the way. I am so glad you found me in NYC and bringing so much joy and light to my life. Thank you for always being by my side and I cannot wait to marry you!

Table of Contents

List of Figures

List of Tables

List of acronyms

aGPCR	Adhesion G-protein-coupled receptor
AMsh	Amphid sheath
AMso	Amphid socket
Arg1	Arginase 1
ASD	Autism spectrum disorder
ATP	Adenosine 5’-triphosphate
BBB	Blood-brain barrier
bp	Base pair
celo	Coelomocyte
cfa	Cyclopropane fatty acyl phospholipid synthase
CFA	Cyclopropane fatty acid
CNS	Central nervous system
CRISPR	Clustered regularly interspaced short palindromic repeats
CTF	Carboxy-terminal fragment
Daf-c	Dauer formation constitutive
Daf-d	Dauer formation defective
ECD	Extracellular domain
EM	Electron microscope
EMS	Ethyl methanesulfonate
GAIN	G-protein-coupled receptor autoproteolysis-inducing

GDP	Guanosine diphosphate
GFAP	Glial fibrillary acidic protein
GFP	Green fluorescent protein
GPCR	G-protein-coupled receptor
GPS	G-protein-coupled receptor proteolysis site
GTP	Guanosine triphosphate
IGF	Insulin/insulin-like growth factor
kb	kilobase
MUFA	Monounsaturated fatty acid
NR	Nerve ring
NTF	N-terminal fragment
RFP	Red fluorescent protein
ROS	Reactive oxygen species
RPE	Retinal pigmented epithelial
SASP	Small acid soluble spore protein
SDS	Sodium dodecyl sulfate
SNP	Single nucleotide polymorphism
TGF-β	Transforming growth factor-β
TREM2	Triggering-receptor expressed on myeloid cells-2
VEGFR	Vascular endothelial growth factor receptor
Wnt	Wingless/int
WT	Wild type

YA	Young adult
Ym1	Chitinase-like protein 1

1 Introduction

1.1 Adaptation to environmental stress is crucial for survival.

Proper adaptation to environmental stress is crucial for survival and maximizing reproductive success. Extreme environments threaten the survival of the animal as well as propagation of the next generation. Organisms are often capable of modifying their development to better suit their environment. As the environment fluctuates, organisms must properly sense and adapt to the changes in order to maintain optimal metabolism and growth. Evolution has intelligent ways for organisms to adapt in otherwise lethal conditions by undergoing drastic developmental alterations and behavioral modification to survive and reproduce.

Stress refers to any threatening situation that induces behavioral or physiological readjustments aimed to preserve homeostasis [1]. In response to environmental stressors, some organisms have evolved developmental strategies to persist under high stress conditions. For example, some organisms enter a specialized, stress-resistant state that permits both the temporal avoidance of the environmental insult as well as the dispersal of the organism from one environment to another. In response to nutrient depletion, some species of bacteria become endospores—metabolically inactive cellular structures with a thick, multi-layered protein coat and a dehydrated core [2]. Endospores have incredible longevity; some endospores of a *Bacillus* species have been recovered

from an extinct symbiotic bee host preserved in amber over 25 million years ago [3]. During sporulation, specialized endospore proteins called α/β-type small acid soluble spore proteins (SASPs) are synthesized and bind to the DNA, generating a protective, conformational change. These developmental changes in the bacterium provide resistance to environmental stressors, including high temperature, noxious chemicals and DNA-damaging ultraviolet radiation [2].

Some organisms enter a developmental period of metabolic arrest known as estivation. Estivation is a state of aerobic hypometabolism used by organisms to endure seasonally arid conditions, often in desert environments. Estivating species are often active for only a few weeks each year to feed, breed, and then retreat to estivate in sheltered sites, often underground. In general, estivation includes (1) a strong reduction in metabolic rate, (2) a primary reliance on lipid oxidation to fuel metabolism, and (3) methods of water retention, both physical (e.g. cocoons) and metabolic (e.g. urea accumulation) [4-7]. Invertebrates like land snails have evolved annual cycles of estivation during unfavorable environmental periods with low water availability and high temperature. Land snails dramatically reduce their metabolism [4] and generate a protective calcium carbonate membrane called an epiphragm to seals off their shell from the environment [5]. This allows estivating land snails to become resistant to desiccation and high temperatures, allowing them to survive prolonged periods of stress.

Vertebrates, including mammals, also undergo periods of estivation when faced with harsh conditions. For example, most species of lungfish enter estivation state during the dry seasons. To prevent desiccation, estivating African lungfish *Protopterus annectens* will dig a burrow in the mud and secrete a protective mucous cocoon from its epithelial mucous glands [6]. Similarly, some species of amphibians also enter reversible estivation by generating a protect cocoon to conserve their energy and prevent desiccation [6]. Estivating mammals also switch from carbohydrate to lipid metabolism to conserve energy [7]. These estivating animals can survive for many months, waiting for more favorable environmental conditions.

Some species escape periods of environmental stress by generating stress-resistant offspring. Many fresh and saltwater sponges reproduce asexually to generate gemmules in response to unfavorable water temperature. Gemmules are collagenous glass capsules filled with metabolically-repressed cells and they are resistant to environmental stressors such as freezing and desiccation [8]. In response to freezing winters and summer droughts, the sponge species *Eunapius fragilis* gemmules will produce sorbitol that allows the buildup of high osmotic pressure, which in turn represses germination. Once faced with a favorable environment, gemmules synthesize sorbitol dehydrogenase, which relieves the osmotic pressure and allows these gemmules to continue their development into a new sponge [8,9].

Some organisms enter a specialized physiological state of dormancy called diapause, characterized by profound metabolic depression and extreme stress tolerance. For example, the annual killifish *Austrofundulus limnaeus* adapt to the dry season by producing stress-tolerant embryos that can survive for months encased in drying mud [10-13]. The killifish rely on diapause as an integral part of their breeding cycles. Newly laid embryos quickly enter diapause state, which suspends all developmental processes including reduced metabolism, decreased heart rate, reduced oxygen consumption [14]. It also provides higher tolerance to various stresses, including long seasonal drought [14-17]. Exposure to increased temperature and light promotes exiting out of diapause [18,19]. In killifish, a diapause is regulated through temperature-dependent vitamin D signaling where vitamin D_3 promotes active development in fish embryos while inhibition of vitamin D_3 synthesis leads to developmental arrest [20]. Other species of killifish have diverse survival mechanisms. Some adult killifish can survive out of water for an extended period while others can survive in extreme cold and anoxia [21]. While some organisms remain relatively immobile in a developmentally suspended, inactive state, other organisms remain physiologically active. For example, monarch butterfly in its reproductive diapause form can migrate over 3,000 miles from southern Canada and Midwestern United States to overwintering sites in central Mexico in search for favorable environment [22,23].

Environmental stressors can cause short or long-term progression of changes that alter physiological function and reproductive development in a given organism. The adaptive tuning of development and behavior requires specialized cells to monitor environmental changes.

1.2 Glia are important for appropriate response to stress

Through evolution, different cell types have developed adaptive functions to appropriately respond to different stressors. In the nervous system, glial cells play a central role in compensatory responses designed to protect against stressors and consequent damaging effects on the organism.

Glia are the most abundant cell type in the vertebrate brain and are intimately associated with neurons. Glia display diverse morphological complexity and specialization [24-26]. For example, glia secrete neurotrophic factors [27], provide guidance for neuronal migration and patterning [28,29], modulate dendritic morphologies [30,31], form the myelin sheath around axons required for fast nerve impulses, and regulate neuronal communication at synapses [32,33].

Glia, like neurons, can sense changes in their extracellular environment. Glia can directly sense stimuli such as Na^+ levels [34], neurotransmitters [35], and protons [36]. Furthermore, glia can regulate behavior in response to sensory stimuli. Previous studies have shown glia in the ventral brainstem surface can sense CO_2-induced acidosis, triggering the release of adenosine 5'-triphosphate (ATP) to activate neurons that control inspiratory breathing movements [37,38].

Glial cells possess the machinery to gauge the environment surrounding their receptive endings.

Glia also function in response to stress. Inflammatory responses are a major part of all central nervous system (CNS) insults, such as acute trauma, infection, malnutrition and chronic neurodegenerative diseases [39,40]. Inflammation in the brain recruits and activates glial cells as part of the immune response. A growing number of studies recognize diverse exposures to environmental stressors pose as risk factors for neurodevelopmental disease like ASD (autism spectrum disorder) [39,41]. In response to CNS insults, the brain signals a coordinated inflammatory response that includes glia, neurons, and other CNS cells. Chief inflammatory responders among CNS glial cells are microglia, the resident myeloid cells of the brain, as well as astrocytes. Both microglia and astrocytes have pro- and anti-inflammatory functions dependent on the mode of injury [42-47]. Recent studies indicate microglia can trigger astrocyte reactivity and these coordinated glia interactions are required regulation and resolution of the CNS inflammatory response [45].

1.2.1 Microglia

One of the glial subtypes activated by the stressors is microglia. First identified by Rio-Hortega in 1932, microglial cells are part of the innate immune system and are the resident tissue macrophages of the CNS [48-50]. Microglia originate from the embryonic yolk sac and are incorporated into the CNS during the earlier stages of development [51]. Microglia are rapid responders to any

disruption of homeostasis or immune challenges, and are major producers of cytokines, chemokines, and other neuromodulators within the brain [49,52].

In response to CNS damage or infection, microglia can rapidly change their phenotype to express different receptors according to the stressor stimuli [53]. Microglia in the normal adult brain have a highly ramified “resting” morphology, with low levels of “activation markers” (e.g., complement protein CD11b, major histocompatibility molecules MHC II) on the cell surface. However, resting microglia are far from dormant or inactive. Throughout the neural tissue, resting microglia build a dense network of dynamic and reactive cells to survey, scan, and maintain brain homeostasis [54,55]. They play an important role as phagocytes and are essential for the development of the CNS, as they eliminate apoptotic neurons, produce growth factors and contribute to function and organization of the nerve tissue [56,57]. Later in life, microglia play a major role in adult neurogenesis [58] and in CNS remodeling of synapse structure and function [59-61]. The microglia processes are continually extending and contracting into nearby synapses in order to monitor their microenvironments and are likely responsible for synapse removal via phagocytosis [62]. Overall, the resting microglia survey and maintain a neuroprotective environment under normal physiological conditions [63,64].

Various danger signals to the CNS can induce inflammatory events and activate microglia [65-67]. Activated microglia can migrate toward the signals, proliferate, and engulf the injured cells [68]. There are two general phenotypes of

the active state of microglia—M1 and M2. The M1 phenotype is known as the classically activated state and M2 is referred to as an alternative active state that has other subpopulations [53,69-74]. In response to neuronal injury, these two phenotypes have opposite characteristics.

Upon the M1 activation state, microglia can release various proinflammatory cytokines, chemokines and free radicals to inhibit neuronal repair and regeneration [75-82]. Conversely, the M2 state can improve brain repair and regeneration by attenuating neuroinflammation, inducing phagocytosis, and promoting the repair gene expressions that leads to wound healing and restores tissue homeostasis [78,80,81,83-94]. Recent studies have shown that microglia do not act on their own, but they coordinate their action with neurotoxic reactive astrocytes (described below) [45,95]. In addition, microglia help sustain the blood-brain barrier (BBB) [96,97]. Balancing both pro- and anti-inflammatory responses is necessary for maintenance of a healthy CNS. Chronically activated microglia can lead to substantial damages to CNS function and structure.

1.2.2 Astrocytes

Astrocytes are also highly involved in protection of the CNS. Astrocytes are the most abundant cells in the CNS that provide many homeostatic maintenance functions, including providing trophic support for neurons, promoting the formation and function of synapses, pruning synapses by

phagocytosis as well as the assisting in the formation and maintenance of the BBB [98-101].

Stressors to the brain can cause an unbalance of extracellular nutrients and ions [102], damage the BBB [103,104], and release excessive amounts of excitatory neurotransmitters, such as glutamate [105,106]. These responses can damage mitochondria and produce reactive oxygen species (ROS) that in turn increase DNA damage and inflammation, eventually leading to cell death [107-109]. Astrocytes protect the brain through multiple mechanisms. Astrocytes regulate homeostasis in the brain by managing excess neurotransmitters, ions, and other metabolic products [110-112]. Astrocytes can also assist injured neurons by exchanging damaged mitochondria for healthy mitochondria [113]. Furthermore, astrocytes can protect neurons by producing an antioxidant response [114,115].

In response to brain stressors, astrocytes undergo a dramatic transformation called reactive astrocytosis [42,43]. Reactive astrocytes are characterized by high levels of glial fibrillary acidic protein (GFAP). GFAP is the main intermediate filament protein in mature astrocytes, and it is highly relevant to the pathogenesis of various CNS pathologies [116]. Reactive astrocytes form a glial scar after acute CNS trauma [43,98,117]. Previous studies indicate reactive astrocytes can both hinder and support CNS recovery [43,98,117-119]. However, it remains unclear under what contexts reactive astrocytes may be helpful or harmful. There are two forms of reactive astrocytes, A1 and A2 [42]. A1s

upregulate many genes that are destructive to synapses while A2s upregulate neurotrophic factors, suggesting A1s are harmful while A2s are protective [42]. Activated microglia induce A1 reactive astrocytes to drive scar formation, which allows astrocytes to regulate and contain the immune responses in a manner that controls neuroinflammation [45]. Crosstalk between microglia and astrocytes is crucial for the maintenance and protection of the CNS.

1.3 GPCR-mediated signaling in response to stress

Microglia and astrocytes express many G-protein-coupled receptors (GPCRs) to regulate their activation and signaling for proper response to the disturbance in neuronal damage. GPCR expressions in microglia provide important mechanisms in regulating parts of the activation process (e.g., proliferation, migration and differentiation into active phenotypes) [120]. Similarly, mGlu3 and mGlu5 GPCR expression in astrocytes have been shown to be crucial in sensing and responding to changes in glutamate [121].

GPCRs were first identified in 1986 [122] and are the largest and most versatile family of signaling receptors in humans [123,124]. GPCRs have seven transmembrane domains and their classic signaling pathway is to couple to G proteins to activate second messengers [125-127]. Heterotrimeric G proteins consist of Gα, β and γ subunits [128,129]. Upon activation by ligands, GPCR act as guanine-nucleotide exchange factor (GEF) for the Gα subunit, facilitating the exchange of guanosine diphosphate (GDP) for guanosine triphosphate (GTP), which results in dissociation of Gβ/Gγ dimers from the complex. Activated Gα

proteins and dissociated Gβ/Gγ subunits regulate many downstream signaling pathways. Gα i/o act through second messengers cAMP, Gα q acts through second messengers IP3 and DAG, while Gα 12/13 act through Rho GEFs. Gβ/Gγ signaling acts primarily on ion channels [130,131]. GPCRs respond to diverse external signals and play critical roles in various physiological processes, such as vision, olfaction, and neurotransmission. Many GPCRs have been found to be selectively localized to cilia on numerous mammalian and non-mammalian cell types.

GPCRs can be classified into five families: glutamate, rhodopsin, frizzled, secretin, and adhesion [132]. Glutamate is a major excitatory neurotransmitter in the nervous system. Glutamate GPCRs play important roles in synaptic transmission, synapse formation, axon guidance, and the development of neuronal circuits [133,134]. The rhodopsin GPCRs are the most abundant GPCR family and are involved in photoreception and neurotransmission [135]. Frizzled GPCRs are activated by wingless/int (Wnt) proteins and control numerous cellular processes including neural crest development, patterning, and adult neurogenesis [136]. Secretin receptors are hormone receptors and have neuroprotective functions in the CNS [137]. Finally, adhesion GPCRs (aGPCR) represent the second largest GPCR family. aGPCRs play key developmental roles in many tissues and in nervous system development and disease [138,139].

aGPCRs have two unique features: first, a long amino-terminal extracellular domain (ECD) for many family members that contains motifs important for cell–cell adhesion; and second, the presence of a GPCR autoproteolysis-inducing (GAIN) domain within the ECD, which encompasses the highly conserved GPCR proteolysis site (GPS) [140,141]. Many aGPCRs undergo autoproteolysis at the GPS, which results in a protein that is separated into an N-terminal fragment (NTF) and a carboxy-terminal fragment (CTF) [142]. aGPCRs can function as adhesion molecules due to the NTF and can function as classical GPCRs through the CTF [138]. Several aGPCRs undergo homophilic trans-trans interactions, where they interact with other versions of themselves on neighboring cells [143]. Often these homophilic associations are signaled through NTF to promote adhesion. For example, the Celsr2 and Celsr3 aGPCRs increase intracellular calcium levels through homophilic N terminus-N terminus interactions and are thought to signal neurite outgrowth in cultured neurons [144]. Likewise, GPR56 aGPCR undergo N terminus-N terminus interactions to induce its downstream G protein signaling to activate Rho [143]. In *Drosophila,* aGPCR Flamingo can also undergo homophilic trans-trans interactions but it is unclear whether these interactions promote receptor signaling [144]. Some studies speculate that aGPCRs undergo N terminus-N terminus interaction to create a binding site for larger ligands while others suspect these receptors require large adhesive ligands to bind and stabilize N terminus-N terminus interactions to promote receptor signaling [138,143,145].

GPR124 is another example of adhesion GPCR, which plays a pivotal role in brain angiogenesis and in ensuring a tight BBB [146-148]. Ectopic expression of GPR124 in cell culture promoted cell adhesion and filopodia formation [149]. Filopodia are highly dynamic, needle-like, actin-rich protrusions from the cell surface [150]. They are presumed to act as sensory organelles, extending and retracting very quickly to explore the external environment [150]. Work on GPR124 suggests that aGPCR may be important for cell-to-cell adhesion to maintain the BBB as well as induce some type of sensory function in the expressing cell to sense its external environment.

1.4 Sensory organs detect environmental stressors

In animals, specialized sensory organs detect environmental stimuli to regulate proper developmental and behavioral responses to the changing environment. Environmental sensory organs in animals are composed of neurons and their associated glia or glia-like cells. Neurons collect and convert environmental cues to electrical signals while glia are known to have several functions which include modulating neuronal activity [27-33]. Recently studies reveal important glial roles in regulating sensory organ morphology and function in response to environmental stressors. For example, the supporting cells in the mammalian ear are thought to contribute to hearing sensitivity. Deiters' cells express the glial marker, glial fibrillary acidic protein (GFAP), and form the physical structure that supports the sensory outer hair cells of the cochlea [151]. Following high-intensity sound exposure, Deiters' cells are displaced towards the

outer hair cells and this displacement is correlated with a loss of sensitivity in the cochlea [152]. Since continued acoustic stress can damage the outer hair cells, this suggests decreased sensitivity to sound by displacement of the Deiters' cells is a protective response against acoustic stressors [152].

In the vertebrate eye, Müller glia make contacts with photoreceptor cells in the retina. High levels of light can induce damage to the photoreceptor cells. In response to such injury, a subset of Müller glia dedifferentiate to produce embryonic retinal progenitor cells and ultimately form new photoreceptors, neurons or glia [153,154]. Similarly, retinal pigmented epithelial (RPE) cells ensheath the outer segment of the photoreceptors. Retina degeneration can be caused by exposure to high levels of light. Exposure triggers photo-oxidative reactions in the photoreceptors that, at high levels, can lead to a build up of reactive products, thus damaging the retina. RPE cells protect photoreceptors by reducing photo-oxidative stress using antioxidants and detoxifying agents within the photoreceptor cell [155]. Altogether, these observations suggest glial cells in the sensory organs play an important role in regulating stress-induced responses.

1.5 *Caenorhabditis elegans* sensory organs

Like vertebrates and other animals, the nematode *C. elegans* sense the environment through sensory organs composed of specialized sensory neurons and glia. Worms have six types of sensory organs, all sharing a basic structure of one or more sensory neurons extending the ciliated endings of its dendrite into or

through a lumen generated by two glial cells [156]. The primary sensory organ of the worm is the bilaterally symmetric amphid sensilla, located at the anterior tip of the animal. Each amphid consists of twelve sensory neurons and two ensheathing glial cells, the amphid sheath (AMsh) and amphid socket (AMso) cells (Fig. 1-1). Amphid neuron cell bodies are located near the posterior bulb of the pharynx. The axons of these amphid neurons extend into the nerve ring while their dendrites extend to the anterior tip of the animal (Fig. 1-1 b). The AMsh cell body is located near the amphid neuronal cell bodies while the AMso cell body is near the anterior bulb of the pharynx (Fig. 1-1 b). AMsh and AMso glia also extend their processes anteriorly, making contact with the dendrite projections of amphid neurons (Fig. 1-1 b). All amphid neuronal sensory endings are ensheathed by the sheath glia at the anterior tip (Fig. 1-1 c) [157,158]. Four of these amphid neurons have their dendritic endings fully embedded within the AMsh glia and surrounded by an undefined matrix material secreted by the sheath cell. The remaining neurons extend their sensory cilia through the amphid channel, formed by the AMsh and AMso glia. The amphid channel is open to the outside environment and also filled with AMsh-secreted matrix [156]. Each dendrite enters the sheath cell through an individual lumen before converging in a common lumen.

The amphid dendrites terminate in specialized cilia, the shape of which are diverse and important for sensory responses [159]. Different cell-surface receptors, ion channels, and signal transduction machinery are localized at

Figure 1-1. The amphid is the primary chemosensory organ in *C. elegans*. (A) Schematic of an adult *C. elegans* hermaphrodite. The amphids are located in the head. (B) Each amphid consists of 12 neurons (in red; only one is drawn here for simplicity) and two glial cells, the amphid sheath (AMsh, green) and the amphid socket (AMso, blue). (C) Processes from the neurons and glia come together at the tip of the nose to form the amphid sensory organ. The glial cells align to form a tube, the amphid channel, through which some amphid neuron dendrites extend sensory cilia that adopt distinct morphologies: single cilia (neurons ASE, ASG, ASH, ASI, ASJ, and ASK), double cilia (neurons ADF and ADL), wing cilia (neurons AWA, AWB, and AWC) and the finger cilia of AFD. Adherens junctions between the dendrites and the sheath glia, as well as between the sheath and socket glia establish a niche for the sensory cilia. This niche is filled with matrix material secreted by the sheath glia; thus, the site where the nervous system of the animal meets the environment is under the direct control of glia. Adapted from Perkins et al., 1986 [159].

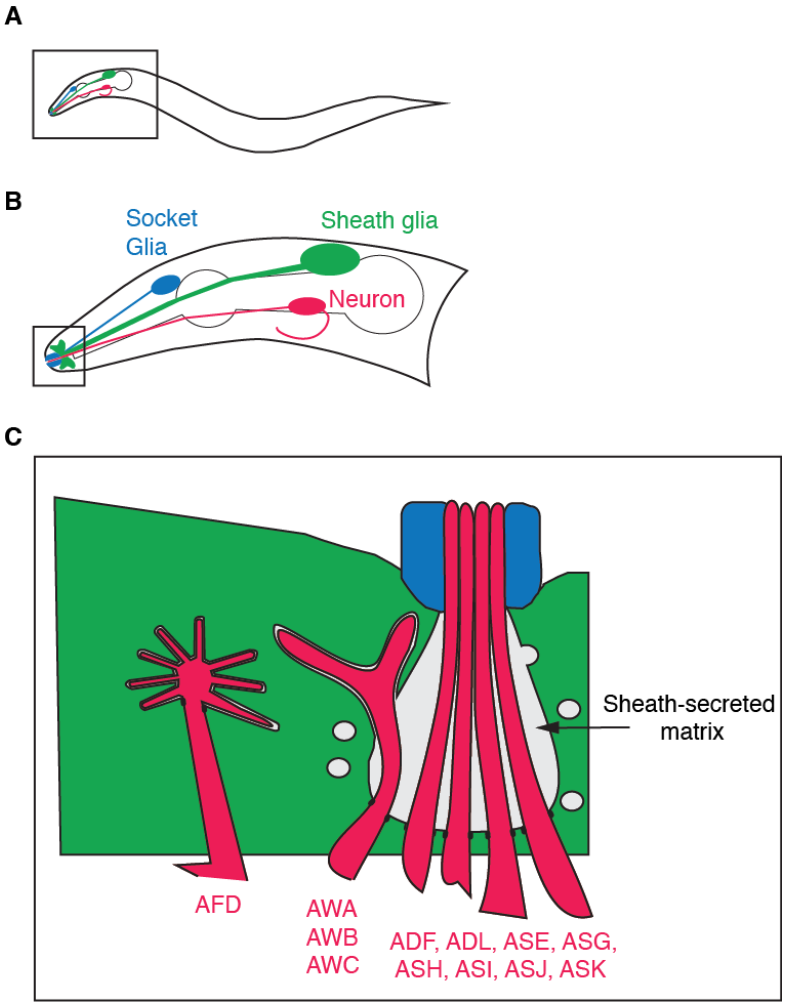
A
B
Socket
Glia
Sheath glia
Neuron
C
Sheath-secreted
matrix
AFD
AWA
AWB
AWC
ADF, ADL, ASE, ASG,
ASH, ASI, ASJ, ASK

these ciliated sensory endings [160]. Amphids are required for many behavioral responses such as movement in response to tastants and odorants [161,162], temperature seeking behavior [163], nose touch responses [164], and dauer development in response to environmental stress (see below) [156,159,161,165]. For example, ASI and ASJ neurons have single, microtubule-based cilia that project through an open amphid channel formed by the glia and are directly exposed to the outside environment [156]. ASI neurons can sense temperature and secrete endocrine signals in response to environmental stressors that induce dauer while ASJ neurons control both entry and exit from dauer stage [156,165-167]. By contrast, the dendrites of AWC neurons terminate in butterfly wing-like structures [157]. These elaborate endings are embedded in the AMsh glia in a hand-in-glove configuration and can respond to odorants to alter odor-associated behavior [156,159,161,165]. In response to removal of odorants from the environment, AWC neurons signal the release of glutamate at the AWC synapses, which affects downstream neuronal circuits that regulate animal turning behavior [168]. AWC can also respond to temperature to regulate temperature-associated behavior [169,170].

In the head of the worm, separate from the amphid, are six symmetrically arranged inner labial sensilla. Each of these sensilla contains two dendrites, IL1 and IL2 neurons, as well as IL sheath (ILsh) and IL socket (ILso) glia. During development, ILsh cells are suggested to guide axons entering the nerve ring neuropil, the “brain” of the worm, from the anterior via the six labial nerves

[171,172]. IL1 neurons are mechanosensory and regulate head withdrawal in response to dorsal or ventral nose touch [173,174] while IL2 neurons are thought to be chemosensory [159].

At the tail of the worm are bilateral sensory organs called the phasmids. These organs consist of only two neurons, one phasmid sheath (PHsh) and two phasmid socket (PHso) glial cells. Phasmids are required for measuring nose-to-tail environmental gradients [175].

1.6 *C. elegans* enter a stress-resistant state called dauer

In addition to the organisms described earlier, the nematode *C. elegans* provides another striking example of an animal that enters an alternative developmental state in response to environmental stressors. In favorable conditions, *C. elegans* undergo normal reproductive growth, progressing through four larval stages (L1 through L4) to become egg-laying adults (Fig. 1-2). In contrast, unfavorable conditions trigger late L1s to enter the L2d (pre-dauer state) and then proceed into a protective, developmentally-arrested larval stage termed dauer, from the German for “enduring” larva (Fig. 1-2) [176].

Dauer animals are morphologically distinct from larvae that develop in favorable conditions. For example, the dauer body circumference shrinks radially and the cuticle is altered, having a thicker outer cortex and an additional striated underlayer compared to non-dauer animals [176]. The thick protective cuticle occludes the buccal cavity, which prevents toxins from entering the body and helps retain solutes and fluids within the body [176]. The pharyngeal pumping

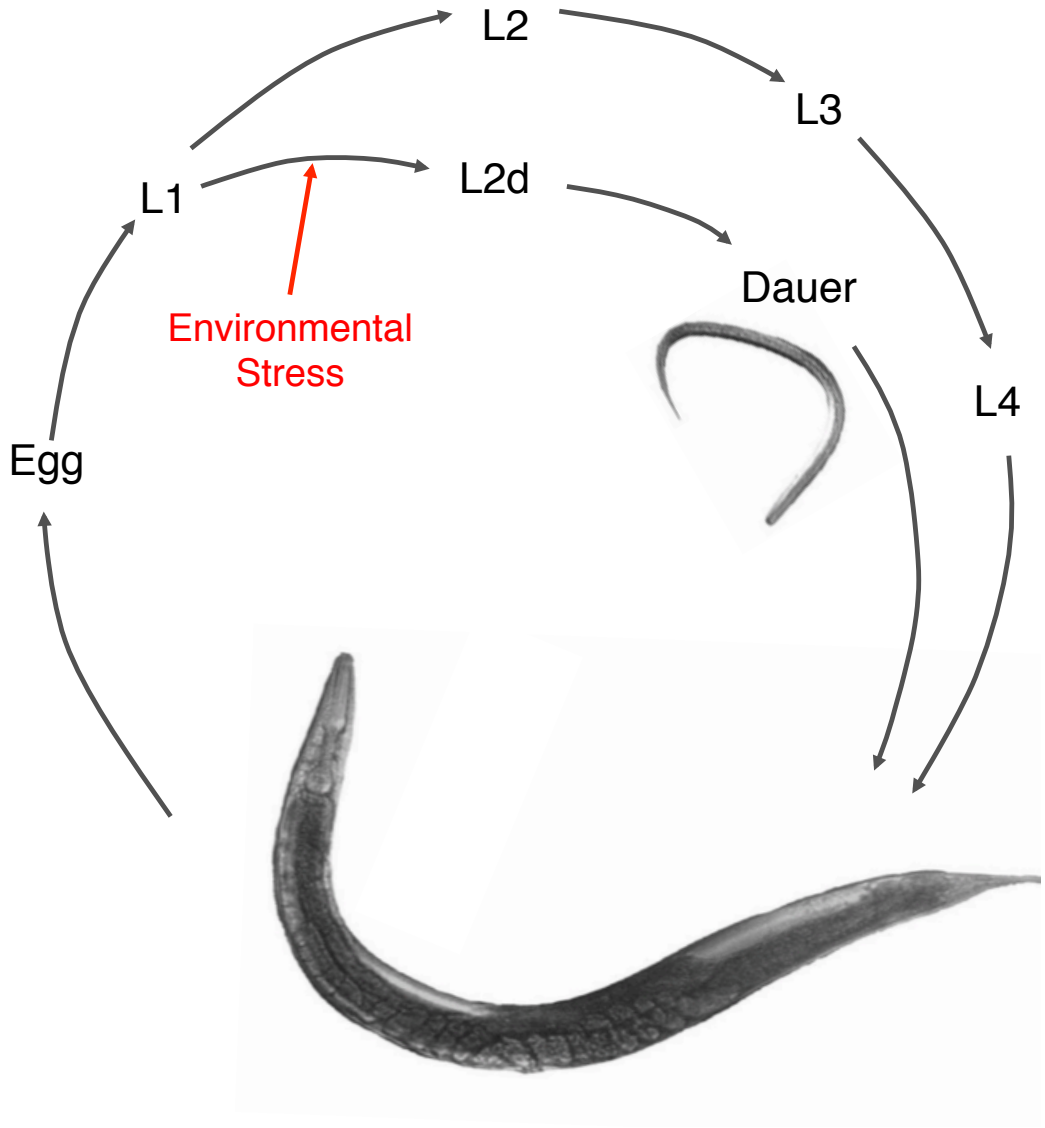

Figure 1-2. The life cycle of *Caenorhabditis elegans*. During reproductive development, *C. elegans* progresses through four larval stages, L1 to L4, before becoming an egg-laying adult. In unfavorable environments, *C. elegans* select an alternative developmental pathway developing into L2d and then dauer larvae. When environmental conditions become favorable, *C. elegans* will exit the dauer state and become fertile adults. (adapted from WormAtlas).

used to rhythmically suck in and trap bacteria ceases, perhaps since the buccal plug blocks access to the environment [176]. Therefore, dauer metabolism is altered for long-term survival [177]. Compare to non-dauer animals that continuously explore their environment in search of food or for feeding, dauer animals are mostly motionless for long periods and their overall movement is suppressed [176,178]. Dauers also display a specialized behavior called nictation, where the animal lifts its body off the surface, waving its head in the air [176]. Dauer animals can also nictate as a group, entwining their bodies into a waving rope. Nictation helps dauer animals attach to moving hosts to find new environments [179]. These morphological changes increase resistance to environmental challenges and enable dauer animals to persist in harsh environments for an extended period of time [176]. When environmental conditions improve, *C. elegans* resumes pharyngeal pumping for normal feeding and continues development to a fertile adult, sometimes called post-dauer (Fig. 1-2). Thus, the dauer state provides a temporal escape from harsh environments and allows for dispersal of the worm from one environment to another.

Dauer entry in *C. elegans* is promoted by high population density, low food abundance and high temperature[176,180]. Population density is measured by the levels of dauer pheromone in the environment, a complex mixture of chemicals secreted constitutively by the animal [180]. Dauer pheromone is the most potent dauer entry signal and this induction is temperature-dependent [180,181]. In the presence of pheromone, shifting to higher temperature

enhanced dauer formation while shifting to lower temperatures promoted dauer recovery [182]. The dauer pheromone consists of structurally related derivatives of the sugar ascarylose, termed ascarosides [183-185]. These are sensed through multiple receptors, one pair of which is the guanosine-5'-triphosphate (GTP)-binding protein (G-protein)-coupled receptors (GPCRs) SRBC-64 and SRBC-66, that are expressed specifically in a pair of environmental ASK sensory neurons and function together to mediate responses to dauer pheromone [166]. While it is clear that certain G proteins play a role in dauer formation, not all of the relevant G proteins have been identified. Studies have shown Gα subunits GPA-2 and GPA-3 are expressed in several amphid neurons and are involved in the decision to form dauer larvae primarily in response to dauer pheromones [185]. G proteins also have functions independent of their traditional signaling roles. For example, Gα proteins *odr-3* loss-of-function mutants and *gpa-3* gain-of-function transgenes disrupt the morphogenesis of their associated sensory cilia [184,185]. There are two general classes of dauer formation mutants: dauer formation constitutive (Daf-c) mutants, which inappropriately form dauer larvae under favorable conditions and dauer formation defective (Daf-d) mutants, which fail to form dauer larvae under dauer-inducing conditions.

Dauer pheromone and environmental stressors that induce dauer state are sensed by specialized amphid sensory neurons in the head of the animal [165]. In order to induce the organism-wide morphological and metabolic changes in dauers, these neurons must communicate their acquired environmental

information about the environment to other tissues. Insulin/insulin-like growth factor (IGF) and transforming growth factor-β (TGF-β) signaling pathways are the two major neuroendocrine pathways that facilitate physiological changes in dauer [186,187]. When hormone levels are high in both pathways, animals proceed with reproductive development. If either hormone is low, the dauer state is promoted.

ASI amphid sensory neurons express the TGF-β-related hormone, DAF-7. Mutations in the *daf-7* (*dauer formation-7*) gene induce mutant animals to enter dauer constitutively in otherwise favorable environments [187]. *daf-7* transcription is inhibited by dauer cues such as pheromone and high temperature [167,187]. DAF-7 binds to widely expressed DAF-1 and DAF-4 receptors [188,189]. Likewise, one of the insulin/IGF-like peptides, DAF-28, is expressed in the ASI and ASJ amphid sensory neurons. *daf-28* transcription in these sensory neurons is regulated by environmental cues that normally trigger dauer arrest [183]. DAF-28 and other potential insulin-like peptides signal through broadly expressed insulin receptor tyrosine kinase DAF-2, which in turn inhibits the downstream Forkhead transcription factor DAF-16 to inhibit dauer entry [186,190,191]. Altogether, sensory neurons communicate information about the environment systemically through both TGF-β/DAF-7 and insulin/DAF-28 neuroendocrine pathways to affect dauer development.

Both TGF-β/DAF-7 and insulin/DAF-28 neuroendocrine pathways converge onto the nuclear hormone receptor DAF-12. *daf-12* is widely expressed in most

cells of the animal [192] and loss of function mutations in *daf-12* cause a Daf-d phenotype [193,194]. Both TGF-β/DAF-7 and insulin/DAF-28 pathways signal downstream cells to synthesize DAF-12 ligand, dafachronic acid steroid hormones, which act systemically on all DAF-12 expressing cells [195]. Under favorable conditions, DAF-12 is bound to its ligand to induce normal development. However, in unfavorable environments, dafachronic acid synthesis is reduced due to decreased TGF-β/DAF-7 and insulin/DAF-28 signaling, and the unbound DAF-12 receptor promotes gene transcription for dauer development [196].

Once dauer larvae encounter favorable conditions that are more conducive to growth, animals are able to exit the dauer state and develop into fertile adults. Recovery from dauer state can be promoted by food signals derived from bacteria [197]. Compared to dauer entry cues, little is known about the exact chemical nature of the food signal that promotes dauer recovery.

The typical bacterial strain used as a food source for *C. elegans* in the laboratories is *E. coli* OP50. During the exponential growth phase of *E. coli*, the majority of bacterial fatty acids are either saturated or monounsaturated [198]. However, when bacteria enter stationary phase, they induce the enzyme cyclopropane fatty acyl phospholipid synthase (*cfa*), which catalyzes the formation of cyclopropane fatty acids (CFA) from monounsaturated fatty acids (MUFA) [198]. Worms under standard culture conditions ingest a significant amount of CFA [199].

Recent study showed in the presence of *cfa* mutant *E. coli* K12 strain, which fails to synthesize CFA during stationary phase, the recovery from dauer state increased [200,201]. This enhancement in dauer recovery was related to the corresponding increase in MUFA, not CFA, in these bacteria [201]. In addition, exposure to exogenous saturated and monounsaturated fatty acids without bacteria increased dauer recovery [201]. This implies that the dauer animals are sensing the fatty acids and not other metabolites produced by the bacteria [201].

In genetically ablated ASJ animals, dauer recovery in response to fatty acids was absent. This suggests that dauer recovery in response to fatty acids is likely to be mediated by ASJ sensory neuron [201]. Furthermore, this dauer recovery regulated in part by guanylate cyclase *daf-11* and the insulin peptide *ins-6* [201]. *daf-11* is expressed in a subset of sensory neurons, including ASJ, and acts to integrate environmental chemosensory inputs into the TGF-β/DAF-7 and insulin/DAF-28 signaling pathways [183,202]. Activation of DAF-11 stimulates cGMP production and promotes INS-6 secretion from the ASJ sensory neuron through the insulin receptor DAF-2 to enhance dauer recovery [201,203]. *daf-11* functions downstream of chemosensory GPCRs [203] and MUFA-induced dauer recovery requires *daf-11* [201]. These results suggest that an unknown chemosensory GPCR detects fatty acids from the bacteria to signal its downstream G-proteins to influence DAF-11 activity. This model presents the possibility that dauer larvae can sense the nutritional content of their food source to adjust their recovery accordingly [201].

1.7 Environmental stressors promote nervous system remodeling in dauer larvae

Dauer state induces morphological alterations in many organs including the amphid sensilla and inner labial sensilla. Electron microscope (EM) reconstructions of the amphid sensory endings at the nose tip reveal four out of twelve bilateral neuron pairs and both AMsh glia are remodeled in dauer larvae [204]. In dauer animals, the two single-ciliated ASG and ASI neurons are shortened and displaced posteriorly in the amphid channel. In comparison, AFD and AWC neurons show changes in their morphology. In dauer animals, the AFD dendrites increase in the number of microvillar extensions compared to non-dauer animals. AWC neurons and AMsh glial cells exhibit the most dramatic changes in dauer animals. Under normal conditions, the sensory receptive endings of the bilateral AWC sensory neurons are individually ensheathed by processes of adjacent AMsh glial cells (Fig. 1-3 b). Upon dauer entry, the bilateral AMsh glia membranes surrounding the AWC neurons fuse around 50% of the time, connecting the two glial cells and allowing AWC neuron receptive endings to expand and overlap (Fig. 1-3 c) [204]. EM analysis of 2-day post-dauer animals demonstrates these animals maintained glial fusion (Carl Procko, unpublished). Dauer remodeling induces a permanent change in AMsh glia architecture but the functional consequences of this change remains to be explored.

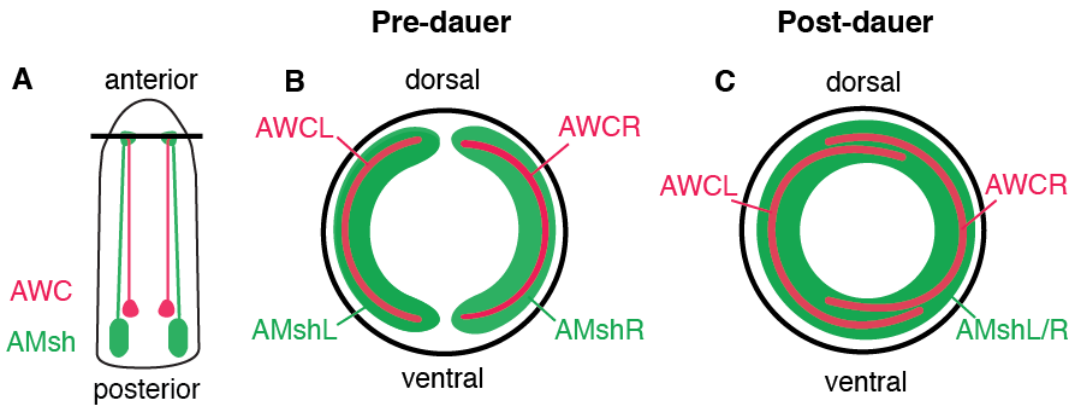

Figure 1-3. AWC neuron receptive endings and AMsh glia remodel in dauer larvae. (A) Diagram of the head of the worm, showing the two bilateral AMsh glia (green) and AWC sensory neurons (red); see also Figure 1-1. The horizontal line at the nose tip indicates the position of the transverse sections shown in (B&C). **(B&C)** Cross-section diagrams through the tip of the nose indicating the positioning of the AWC neuron receptive endings and the ensheathing AMsh glia in non-dauer (B) and dauer (C) animals. (Left (L) and right (R)). AMsh glia fusion may occur on either the ventral or dorsal side or both. Adapted from Albert and Riddle, 1983; Ward et al., 1998 [204,205]. Not to scale.

From previous studies in our lab, we identified several AMsh glia proteins required for amphid glial remodeling. These include the cell fusion protein AFF-1, a vascular endothelial growth factor receptor (VEGFR)-related protein, VER-1, the Otd/Otx transcription factor TTX-1, and the zinc-finger transcription factor ZTF-16 [206,207]. *ver-1* expression in AMsh glia is induced by dauer entry or by cultivation at high temperature and requires direct binding of TTX-1 to *ver-1* regulatory sequences [206]. Fluorescent assay and EM serial analysis confirmed

either *ttx-1(p767)* or *ztf-16(ns171)* mutations in dauer-constitutive *daf-7(e1372)* temperature-sensitive mutation background failed to induce AMsh glial fusion upon dauer entry [206,207]. However, AWC dendritic expansion was inhibited in only *ztf-16(ns171)* mutant, showing that the AMsh glial fusion and AWC dendritic expansion can be uncoupled [206,207]. We confirmed that AMsh glial fusion can still occur when AWC neurons are ablated, further showing the AMsh glia can remodel independently of AWC receptive ending growth [206].

In addition to amphid remodeling, the inner labial sensilla also undergo drastic remodeling in all dauer animals. EM image analyses demonstrate IL2 cilia are approximately two-thirds shorter during dauer than nondauer and no longer extend through the opening of the inner-labial pore [204]. In addition, the four dorsal and ventral IL2 neurons undergo dendrite arborization during dauer formation [208]. In comparison, the two lateral IL2 neurons branch only once at the distal end of the dendrite during dauer. IL2 arborization is regulated by the proprotein convertase KPC-1 and the POU homeodomain transcription factor UNC-86 [208]. The IL2s are required for nictation behavior in dauer animals [179]. While IL2-specific rescue of *kpc-1* mutants rescues nictation defects, further studies are needed to understand how IL2 arbors regulate nictation [208]. Unlike the amphid remodeling, the IL2 remodeling is almost fully reversed upon dauer recover.

1.8 What are the physiological consequences of amphid remodeling?

Why do the amphid structures remodel in dauer animals? The purpose of stress-induced amphid remodeling in *C. elegans* has not been ascertained. It may be that dauer remodeling is a passive outcome of the radial shrinkage of the body, bringing the glia and sensory neurons close in proximity [204]. Alternatively, morphological remodeling of both AMsh glia and AWC neurons may have functional consequences such as altered sensitivity to food or other signals indicating favorable environmental conditions and the opportunity to exit dauer for reproduction.

In line with this hypothesis, dauer animal exhibit an altered repertoire of odorant receptors in a given sensory neuron [209]. Moreover, previous studies suggest AMsh glia have a sensory function to detect changes in its extracellular environment that affect the behavior of the worm [36]. In addition, mutants with defective AMsh glial fusion (*ttx-1*(*p767*); *daf-7*(*e1372*)) exit dauer prematurely compared to *daf-7*(*e1372*) single mutants [206,210]. This suggests the structure of the amphid sensory organ may be important for modulating the perception of dauer exit signals.

Intriguingly permanent changes in the AMsh glial morphology in post-dauer animals may suggest that post-dauer animals retain memory of some past experiences (Carl Procko; unpublished). A previous study reported differences in the expression profiles of post-dauer animals and animals that did not pass

through dauer [211]. In addition, post-dauer animals have been shown to have longer life spans and larger pools of offspring [211]. It remains unclear if the permanent changes in amphid structure have functional relevance post-dauer.

In my thesis, I aimed to understand how organisms adapt to unfavorable condition. Dauer-induced amphid remodeling in *C. elegans* offers a unique opportunity to study nervous system plasticity for several compelling reasons. First, amphid remodeling in dauer is both inducible and reproducible. In addition, *C. elegans* have facile genetics and molecular biology, making them a prime candidate for study. Here, I set out to identify molecular mechanisms governing stress-induced glial remodeling in *C. elegans* and to investigate the developmental consequences of this plasticity. I will describe a novel gene important for regulating stress-induced glial remodeling. In addition, I will explore a potential functional consequence of this remodeling that mediates proper adaption to the changing environment.

2 F47D2.11 GPCR regulates *ver-1* induction and dauer-induced amphid remodeling

2.1 Introduction

In response to environmental stressors, the nematode *C. elegans* become developmentally arrested dauer larvae. Stress-induced dauer entry promotes drastic morphological changes including remodeling of the bilateral amphid sensory organs in the head of the animal (Fig. 1-1). However, the underlying mechanisms controlling dauer remodeling are mostly unknown because there are no high-throughput assays available to study this process directly. Changes in the remodeling structures are smaller than the resolution limit of current fluorescence microscopes and screening for mutants defective in glial fusion by electron microscopy (EM) is time consuming.

Previous work in our lab and others has established that dauer-dependent remodeling requires the transmembrane receptor tyrosine kinase, *ver-1*, whose expression in the AMsh and PHsh glia is induced by entry into the dauer state as well as by exposure to environmental stressors such as high temperature (Fig. 2-1) [206]. Therefore, *ver-1* expression in AMsh glia following exposure to high temperature can be used as a proxy to study dauer-induced remodeling. This fluorescent reporter yields an easier and more high-throughput screening to indirectly identify dauer-remodeling defective mutants. To study how glial remodeling is regulated, Carl Procko (previous graduate student in the lab) performed a forward genetic screen using transgenic animals (*nsIs22*) in which a

Figure 2-1. Temperature- and dauer-induced expression of P*ver-1*::GFP in wild-type sheath glia. (A-C) Representative fluorescence images and DIC and fluorescence merged images of P*ver-1*::GFP (*nsIs22*) expression in one of the two AMsh glial cells of wild-type adults cultivated at 25°C (A) and 15°C (C) and a wild-type dauer induced by starvation at 25°C (B). Exposure time 800ms. Scale bar, 50 µm. Anterior is up. Reprinted from Procko et al., 2011, 2012 [206,207]. **(D)** Histogram of P*ver-1*::GFP (*nsIs22*) expression in AMsh (black) and PHsh glia (grey) in wild-type animals at 25°C and 15°C . Animals were screened at young adult and dauer state. Number of animals scored inside bar. n.s. $p>0.05$, ****, $p<0.0001$, Fisher's exact test.

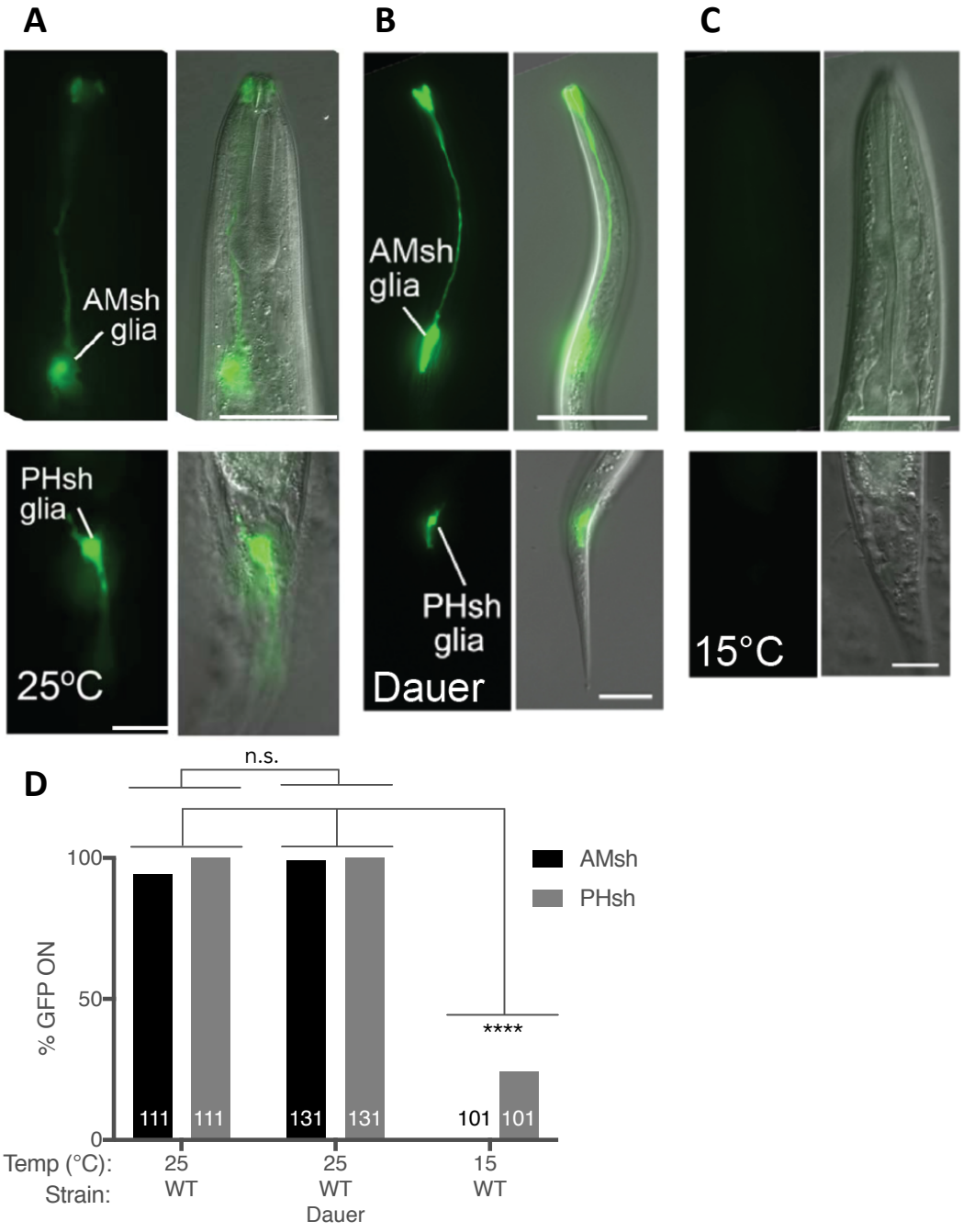
A
B
C
AMsh glia
AMsh glia
PHsh glia
25ºC
PHsh glia
Dauer
15°C
D
n.s.
****
AMsh
PHsh
% GFP ON
100
50
0
111
111
131
131
101
101
Temp (°C):
Strain:
25
WT
25
WT
Dauer
15
WT

ver-1 promoter element drives green fluorescent protein (GFP) transgene expression (P*ver-1*::GFP) to identify mutant animals defective in GFP induction at high temperature. Wild-type animals carrying a P*ver-1*::GFP transgene were mutagenized with ethyl methanesulfonate (EMS) and screened for adult F2 animals grown at high temperature (25°C) (see Chapter 6). More than 35,000 F2 animals were screened, and a total of 21 independent mutant alleles were isolated with reduced GFP expression in the AMsh glia at 25°C [206,207]. From this screen and other assays, we identified several AMsh glia proteins required for dauer-remodeling. These include cell fusion protein AFF-1, a VEGFR-related protein, VER-1, the Otd/Otx transcription factor TTX-1, and the zinc-finger transcription factor ZTF-16. *ver-1* expression in the glia requires direct binding of TTX-1 to *ver-1* regulatory sequences. These glial proteins are required for AMsh glial and associated AWC sensory neuronal remodeling in dauer animals [206,207]. To date, all mutants that have been characterized from this screen also show defective dauer remodeling [206,207].

2.2 *ns250* mutation impairs P*ver-1*::GFP expression at high temperature and upon dauer entry

In my thesis work, I set out to further characterize the molecular mechanisms governing dauer-induced remodeling and to investigate the physiological purpose of this plasticity by focusing on the remaining uncharacterized mutants from Carl's initial screen. I found an interesting mutant *ns250* which fails to turn on P*ver-1*::GFP transgene expression at high

temperature and in dauer state. To eliminate background mutations, I backcrossed the *ns250* mutant to N2 wild-type animals three times. *ns250* mutation continued to impair GFP induction in the AMsh glia after backcrossing. To identify the causal gene, I mapped the *ns250* mutation using single nucleotide polymorphism (SNP) mapping techniques against the polymorphic Hawaiian strain background [212]. I was able to map the *ns250* mutation to a 5 M.U. interval on chromosome V and isolated 6 candidate genes in this region by comparing whole genome sequencing (WGS) data of *ns250* mutant to the wild type N2 reference genome. To make sure *ns250* was not a redundant mutation in one of the previously characterized genes from the P*ver-1*::GFP off genetic screen (such as *ttx-1*, *ztf-16*, *aff-1*, etc.), I verified that *ns250* animals do not harbor any mutations in these genes.

To identify the causal mutation, I targeted individual knockdown of these candidate genes using RNAi in *nsIs22* background (see Chapter 6) [213]. Standard RNAi libraries (Ahringer and Vidal labs) had RNAi-targeting probes for 5 out of 6 candidates. While control RNAi plasmids (GFP and lethal) worked efficiently, demonstrating that RNAi works well in my experiments, the 5 candidate probes failed to repress P*ver-1*::GFP expression. While this result could be explained by insufficient knockdown of the target genes, it suggested that the remaining candidate gene, *F47D2.11*, may be the cause of the phenotype.

Next, I proceeded to analyze the remaining candidate gene. *F47D2.11* gene is a predicted serpentine receptor class z (Srz) G-protein coupled receptor (GPCR). Little is known about this family of receptors. There are no known mammalian homologs based on sequence alignment, but several Srz GPCR orthologs exist in other nematode species. WGS data reveal *ns250* allele as a point mutation (G→ A) at the start of the C' tail of F47D2.11 GPCR, which alters the negatively charged glutamic acid to a positively charged lysine on the 278th amino acid (E278K) (Fig. 2-2 a, b).

The *ns250* mutation has variable effects on the P*ver-1:*:GFP expression, depending on the animal's environment. In Figure 2-3, I characterized and compared the P*ver-1*::GFP expression pattern in the AMsh and PHsh glia between *nsIs22* wild type and *ns250* animals under various growth conditions. For both strains, the developmental stage does not affect the P*ver-1*::GFP expression pattern at all tested temperatures. Therefore, I selected and scored young adult (YA) stage animals to facilitate easier screening. YA animals were cultured at the respective temperature for at least two generations without starvation while dauer larvae were induced by starvation at respective temperature before screening (see Chapter 6).

In *nsIs22* control animals, ~100% of the animals grown at 25°C show strong induction of P*ver-1*::GFP expression in both AMsh and PHsh glia. At 20°C, AMsh glial expression is not induced but GFP is fully expressed in the PHsh glia. At 15°C, AMsh glial expression continues to be off while GFP expression in the

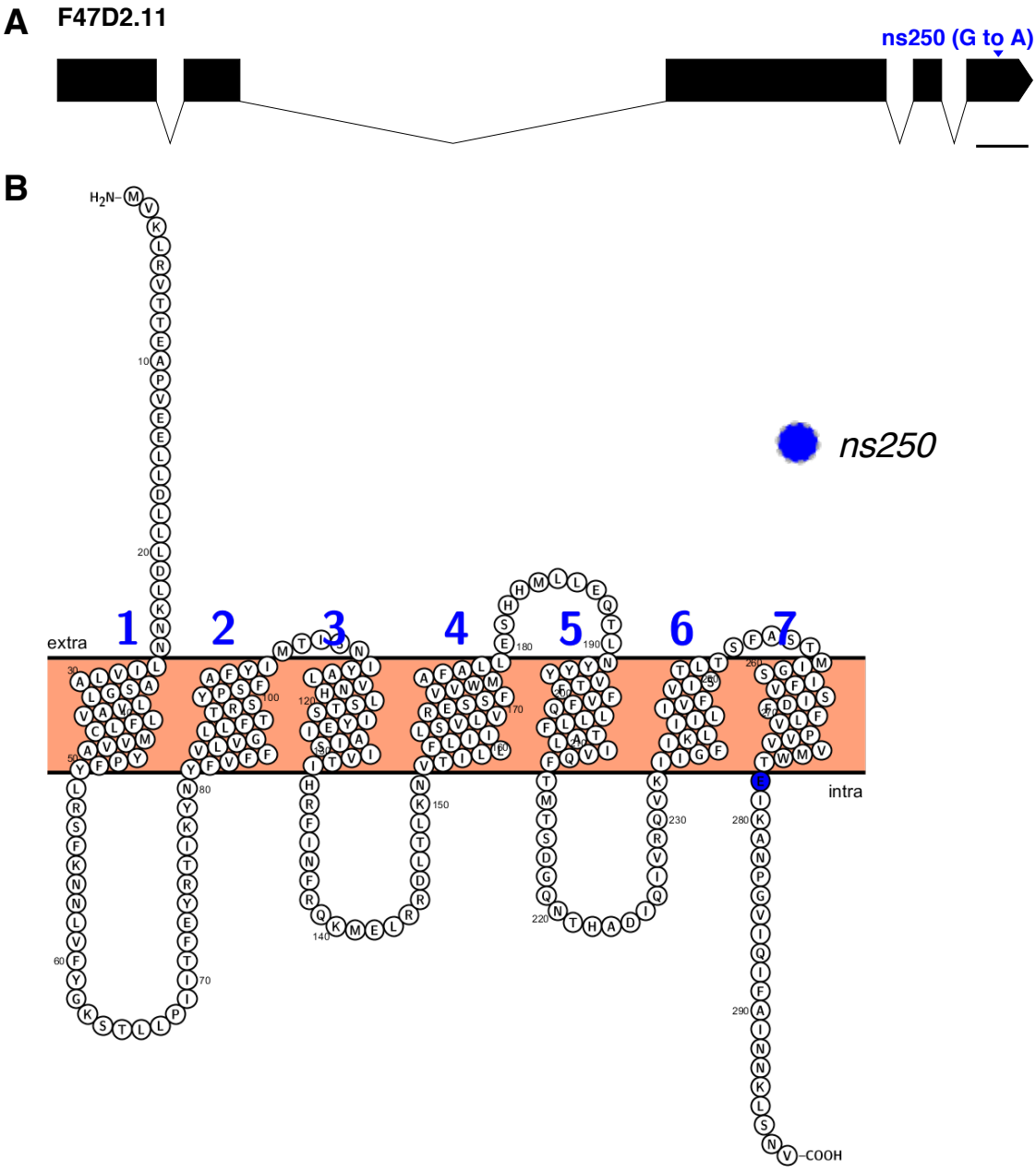

Figure 2-2. *F47D2.11* gene organization and protein sequence and structure. (A) Schematic of the *F47D2.11* gene: exons are represented by boxes. Scale length 100bp. **(B)** Two dimensional schematic of predicted F47D2.11 GPCR structure set in a lipid bilayer. The seven transmembrane spanning domains are labeled by numbers. *ns250* point mutation labeled in yellow (E278K). Protein structure schematic predicted using Protter.

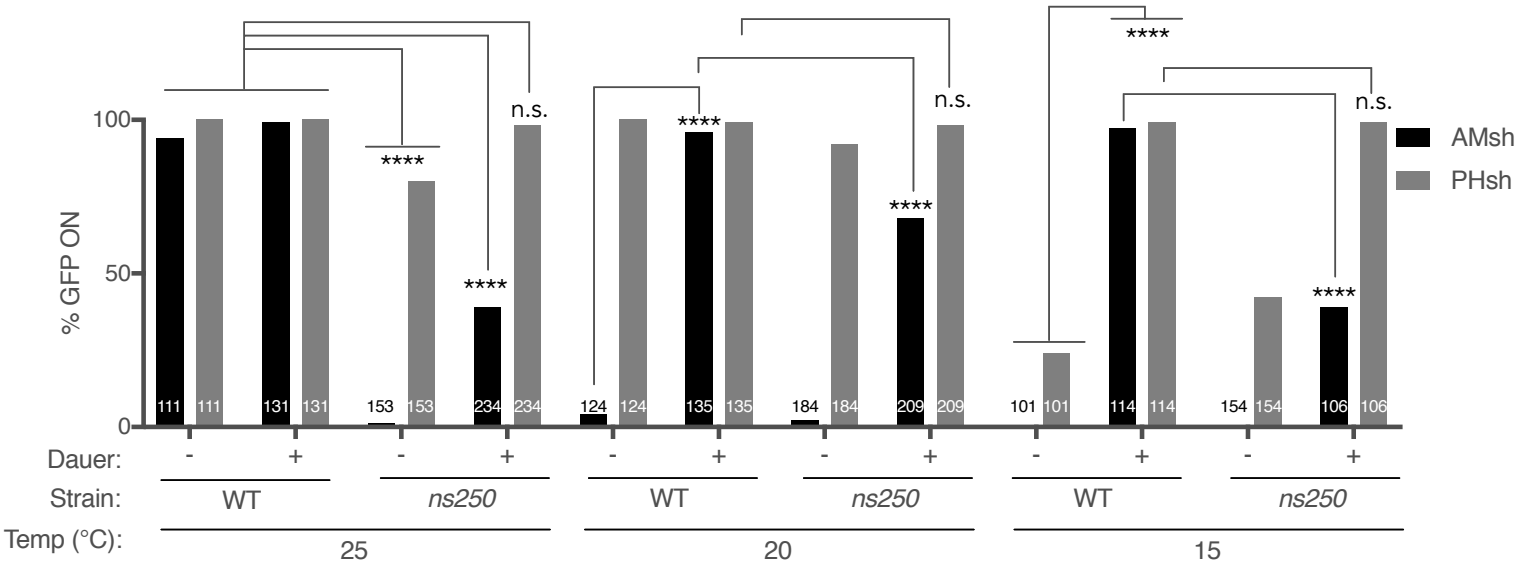

Figure 2-3. Temperature- and dauer-induced expression of P*ver-1*::GFP in wild-type and *ns250* mutant animals. Histogram depicting the percentage of P*ver-1*::GFP (*nsIs22*) expression in AMsh (black) and PHsh glia (grey) of the indicated genotype and temperature. Animals were screed as young adults or starvation-induced dauers. n.s. $p>0.05$, ****, $p<0.0001$, Fisher's exact test. Number of animals scored inside bars.

PHsh glia is reduced to 20%. In comparison, *ns250* point mutation completely fails to induce GFP expression in the AMsh glia at 25°C. At 20°C and 15°C, GFP expression remained off in *ns250* mutants. As for the PHsh glia, GFP induction is slightly impaired to 80% on at 25°C. At 15°C this impairment in the PHsh is more pronounced (40% on). Interestingly, PHsh GFP remains high in *ns250* mutant animals grown at 20°C. In all wild type dauer larvae, dauer entry by starvation induces AMsh and PHsh glial expression regardless of the cultivation temperature. In *ns250* dauer mutants, GFP fails to be expressed only in the AMsh glia at all tested temperatures. However, this impairment is weaker compared to *ns250* YA raised at 25°C. Because GFP induction failure is more pronounced in AMsh glia compared to PHsh in *ns250* mutant, I focus on AMsh glia from this point onwards. In summary, the *ns250* mutant animals fail to induce P*ver-1*::GFP expression in AMsh glia both at high temperatures and upon dauer entry.

To test if *ns250* is a loss-of-function allele, I looked for other mutants in *F47D2.11* gene. There were none available so I made *F47D2.11* mutants using CRISPR (Chapter 6). I generated several targeted *F47D2.11* gene deletions in the *nsIs22* reporter animals using CRISPR to generate predicted loss-of-function mutations (Fig. 2-4 a). First, I made three different lines of partial deletion mutants by excising out the 4th transmembrane domain of the GPCR (*ns843*, *ns844*, and *ns845* alleles). Interestingly, these partial deletion mutants showed

Figure 2-4. *F47D2.11* mutant alleles differentially regulate P*ver-1*::GFP expression. (A) Schematic of the *F47D2.11* gene: exons are represented by boxes. *ns250* mutant allele isolated from our screen is shown with the corresponding nucleic acid change. CRISPR-induced mutant alleles are also marked with corresponding nucleic change and deletions. 4TM is deletion of the entire 4th transmembrane sequence of the GPCR. Scale length 100bp. **(B-C)** Histogram of P*ver-1*::GFP expression in the strains of the indicated genotype at high temperature (B) or dauer larvae (C). *F47D2.11* deletion alleles did not alter *ver-1* expression at high temperature or in dauer state. **(D-E)** As is in (B). *F47D2.11*(E278K) alleles failed to induce *ver-1* expression at high temperature (D) and dauer larvae (E) n.s. $p>0.05$, ****, $p<0.0001$, Fisher's exact test. Number of animals scored inside bars.

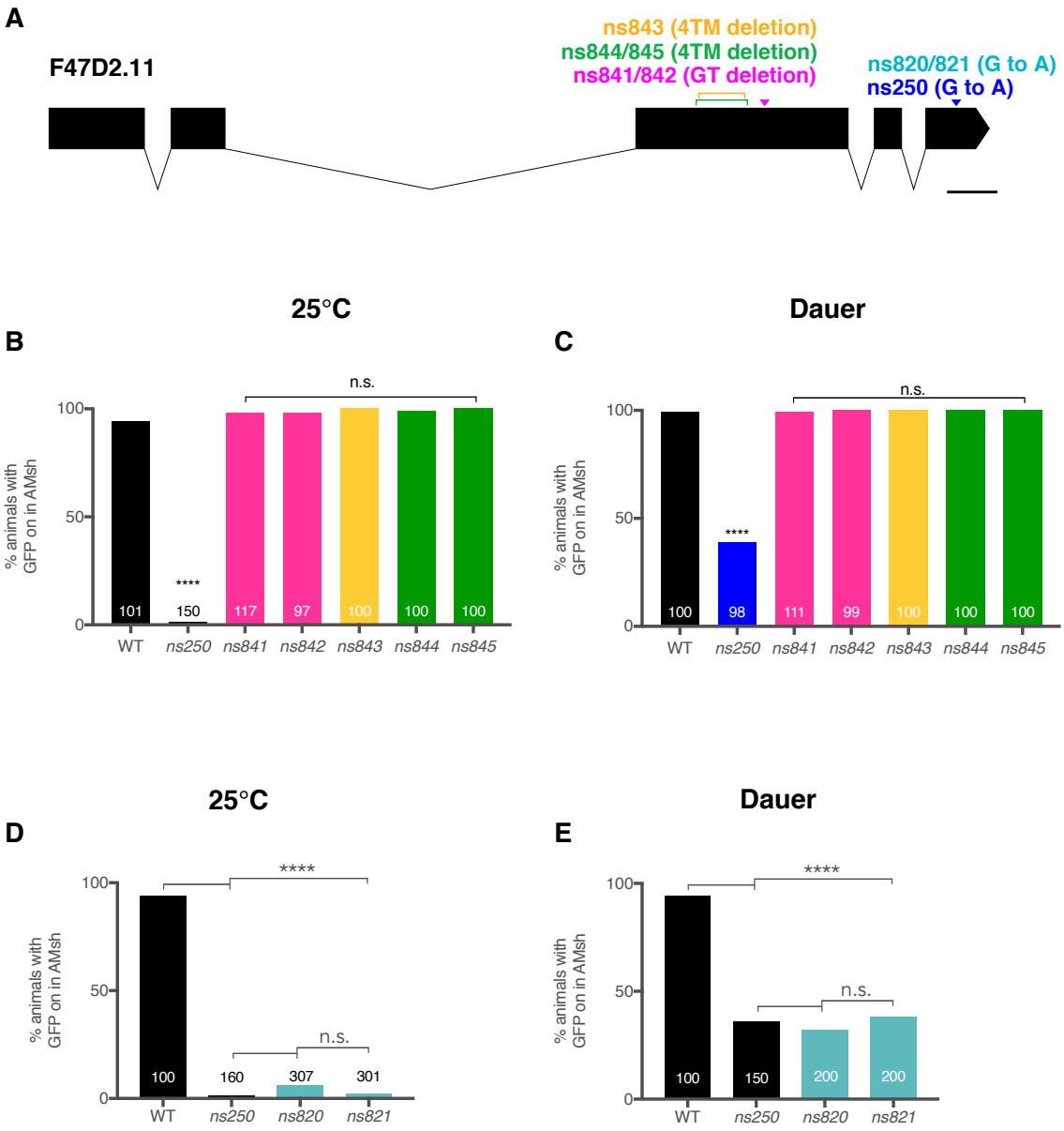
A
F47D2.11
ns843 (4TM deletion)
ns844/845 (4TM deletion)
ns841/842 (GT deletion)
ns820/821 (G to A)
ns250 (G to A)
25°C
Dauer
B
C
% animals with GFP on in AMsh
n.s.
****
101
150
117
97
100
100
100
100
98
111
99
100
100
100
WT
ns250
ns841
ns842
ns843
ns844
ns845
D
E
25°C
Dauer
160
307
301
200
200
ns820
ns821

wild type P*ver-1::GFP* expression pattern in the AMsh glia at 25°C and dauer state (Fig. 2-4 b, c). Similarly, introducing an early stop codon mutation in the *nsIs22* reporter animals using CRISPR (*ns841* and *ns842*) did not affect the GFP expression in the AMsh glia at high temperature and upon dauer entry (Fig. 2-4 b,c). The difference between *F47D2.11* deletion alleles and *ns250* mutant suggests that *ns250* could be a gain-of-function allele. It is all exactly as expected for gain-of-function allele that either activates *F47D2.11* or actively inhibit another gene. Another explanation is that perhaps *F47D2.11* is not the causal gene and might have been incorrectly mapped, raising the possibility that there may be a linked causal mutation close by *F47D2.11* gene that regulates the expression of P*ver-1::GFP* expression instead. However, if *F47D2.11* is the correct candidate, this would suggest *ns250* may be a gain-of-function allele.

To confirm that *ns250* is the causal mutation, I introduced the *ns250* mutation (E278K) into the genome of *nsIs22* reporter animals using CRISPR (*ns820* and *ns821*). Interestingly, both CRISPR-induced E278K alleles fail to induce P*ver-1*::GFP expression at high temperature and dauer entry (Fig. 2-4 d, e). This result confirms that the E278K mutation gives rise to the mutant phenotype.

Next, I tested for transgene rescue. Restoring wild type *F47D2.11* expression rescued the *ns250* defect. Injecting fosmids WRM0612aF01 and WRM0638cF08, which include the *F47D2.11* gene region, could independently rescue GFP expression in AMsh glia at high temperature (Fig. 2-5). In addition, a

Figure 2-5. Restoration of P*ver-1*::GFP (*nsIs22*) expression in AMsh glia in *ns250* mutant. Histogram depicting the percentage of P*ver-1*::GFP (*nsIs22*) expression in AMsh glia in the strains of the indicated genotype. All strains are *ns250* mutant background, except for wild-type animals on the left. Fosmid rescue constructs are either WRM0612aF01 or WRM0638cF08, which includes *F47D2.11* transgene. Genomic rescue plasmids have *F47D2.11* genomic sequence. AMsh glia promoter (*F16F9.3)* and amphid sensory neuronal promoter (*dyf-7)* were used to drive F47D2.11 cDNA. All rescue constructs were injected with co-injection marker (coelomocyte::RFP). Animals screened at young adult. n.s., $p>0.05$, ****, $p<0.0001$, ####, $p<0.0001$, Fisher's exact test. Number of animals scored inside bars.

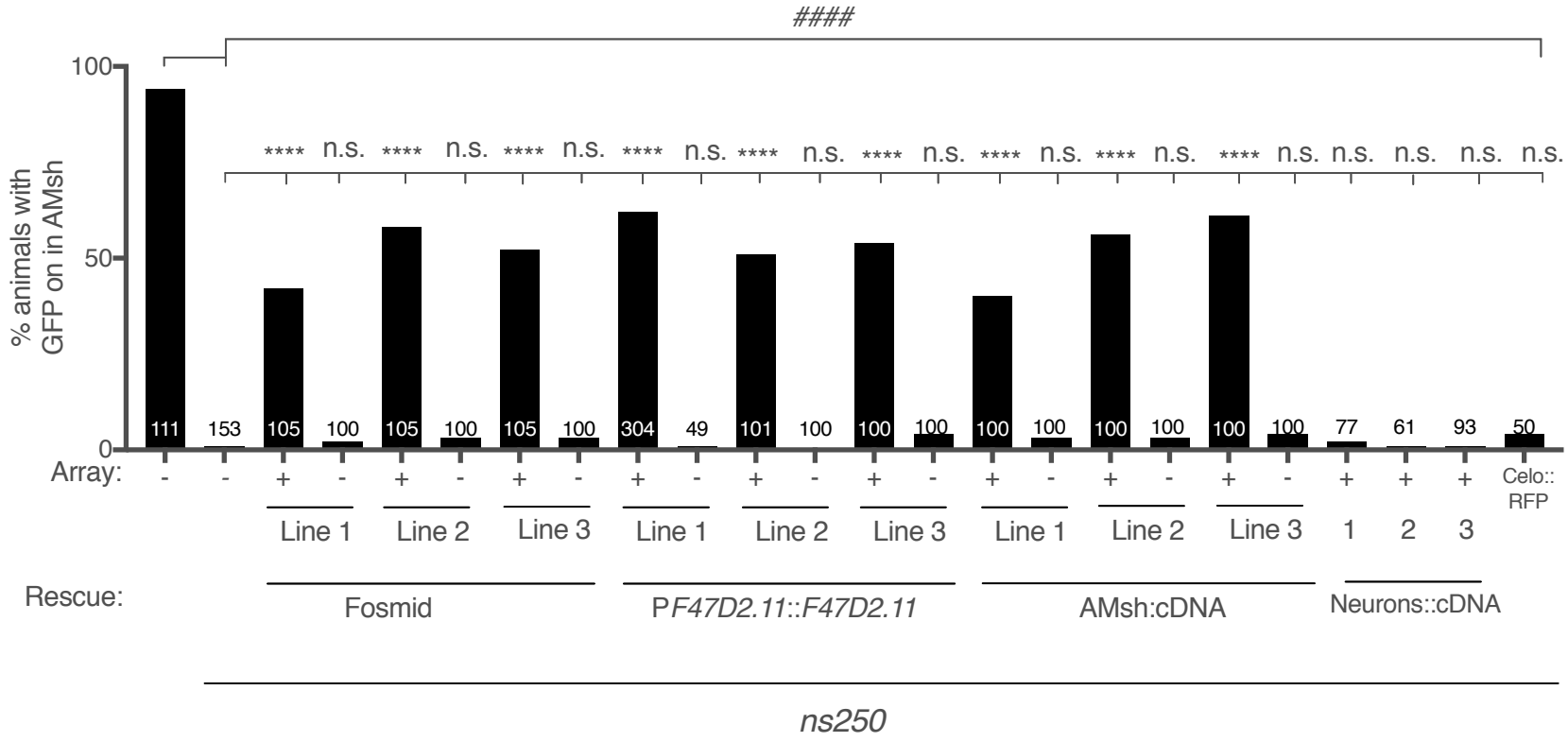
####
100
50
0
% animals with GFP on in AMsh
**** n.s. **** n.s. **** n.s. **** n.s. **** n.s. **** n.s. **** n.s. **** n.s. **** n.s. n.s. n.s. n.s. n.s.
111 153 105 100 105 100 105 100 304 49 101 100 100 100 100 100 100 100 100 100 77 61 93 50
Array: - - + - + - + - + - + - + - + - + - + - + - + + + Celo:: RFP
Line 1 Line 2 Line 3 Line 1 Line 2 Line 3 Line 1 Line 2 Line 3 1 2 3
Rescue:
Fosmid
P*F47D2.11*::*F47D2.11*
AMsh:cDNA
Neurons::cDNA
ns250

smaller genomic fragment with *F47D2.11* alone was also sufficient to rescue the *ns250* phenotype (Fig. 2-5). Three independent lines were observed to rescue the phenotype for each rescue constructs. Rescue data confirmed *F47D2.11* as the causal gene, eliminating the possibility of a linked causal gene. These results strongly support the identification of *F47D2.11* as the affected gene. However, it is still unclear whether *ns250* is a gain- or loss-of-function allele.

In the various rescue strains in Figure 2-5, GFP was never fully restored to 100% wild type level. This suggested maybe *ns250* allele has a semi-dominant nature that inhibits the normal function of wild type F47D2.11 GPCR. To further characterize the genetic trait of *ns250* mutation, I conducted a dominance test (see Chapter 6). First, I backcrossed *ns250* mutant to its parental *nsIs22* strain, which also express a co-injection marker (Pcelo::RFP= coelomocyte promoter element driving red fluorescent protein transgene) to track the F1 cross-progenies. I picked red YA heterozygote progeny under the dissecting scope and scored for GFP fluorescence in the AMsh glia at 25°C. At 20°C and 15°C, P*ver-1*::GFP expression is turned off in the control *nsIs22* animals (Fig. 2-3), therefore not suitable conditions for this dominance test. The hermaphrodite heterozygote cross progeny had significant impairment in GFP induction compared to the control at 25°C, suggesting *ns250* is a semi-dominant mutation (Fig. 2-6). During the scoring, I noticed that the male heterozygote cross-progeny also had similar GFP expression level as the hermaphrodite equivalent. Interestingly, *ns250* mutants showed differences in *ver-1* expression pattern between the sexes at

high temperature. While GFP induction completely fails in hermaphrodites mutants, there is a weaker impairment (34% on) in the male mutant counterparts (Fig. 2-6). At all other temperatures, there were no significant differences in GFP expression between *ns250* mutant hermaphrodites and males (not shown). The heterozygote male cross-progeny also showed significant impairment in GFP expression compared to the control males cultivated at 25°C (Fig. 2-6).

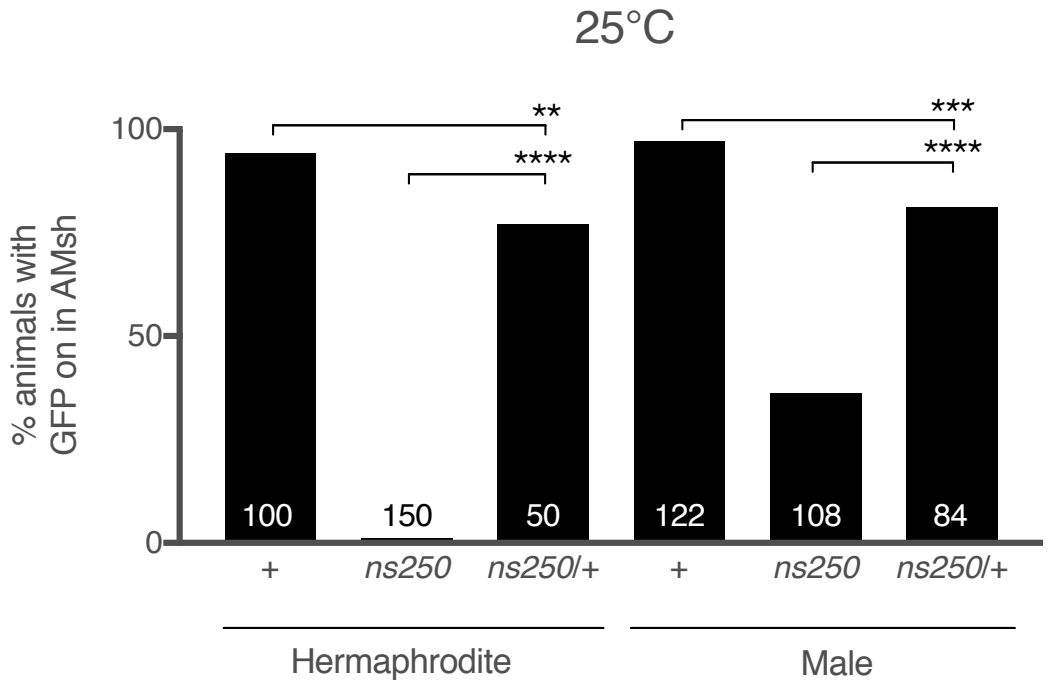

Figure 2-6 The *ns250* mutation has semi-dominant effect on P*ver-1*::GFP expression. Histogram of P*ver-1*::GFP expression in the F1 cross progeny of *ns250* dominance test cross at 25°C. Both hermaphrodite and male heterozygotes (ns250/+) show significant suppression of GFP expression. Animals screened as young adults. **, p<0.01, ***, p<0.001, ****, p<0.0001, Fisher's exact test. Number of animals scored inside bars.

Therefore, *ns250* mutation has a semi-dominant effect on P*ver-1*::GFP expression in both sexes. It was challenging to induce F1 cross-progeny into dauer state by starvation before the birth the F2 progeny. Due to mixed population, I was unable to test for dominance in dauer larvae.

In conclusion, I identified a novel gene *F47D2.11* as a new regulator of the *ver-1* transcriptional network. *F47D2.11(ns250)* fails to induce P*ver-1::GFP* expression in the AMsh glia in response to environmental stressors such as high temperature and upon dauer entry. *ns250* allele is likely a semi-dominant mutation at 25°C, but it remains unclear how *ns250* allele regulates *ver-1* induction.

2.3 *F47D2.11* gene regulates dauer-induced amphid remodeling

Previous work in our lab showed *ver-1* expression was important for regulating AMsh glial remodeling in the dauer state [206]. Since *F47D2.11(ns250)* regulates *ver-1* expression in response to high temperature and upon dauer entry, I wondered if the *ns250* mutation could also affect stress-induced AMsh glial remodeling. To monitor AMsh glial cell fusion, I performed cytoplasmic mixing assay to monitor AMsh glial cell fusion using fluorescence (Fig. 2-7) (see Chapter 6) [206,207]. In this assay, first-stage (L1) *daf-7(e1372*) larvae expressing an AMsh glia::GFP reporter from an unstable extrachromosomal array (*nsEx1391*, *F16F9.3* promoter::GFP) were selected for mosaic expression of GFP in only one of the two glial cells. These animals were then cultivated for more than 48 h at 25°C, which induces dauer entry due to the *daf-7(e1372)* temperature-sensitive

mutation. The presence of GFP in both glial cells in dauers was taken as evidence of cytoplasmic mixing between the cells, indicative of cell fusion (Fig. 2-7). Previous reports from our lab also demonstrated that *daf-7(e1372)* mutation did not change the glial remodeling rate compared to the wild type dauer animals induced by starvation and other natural stressors [206,207].

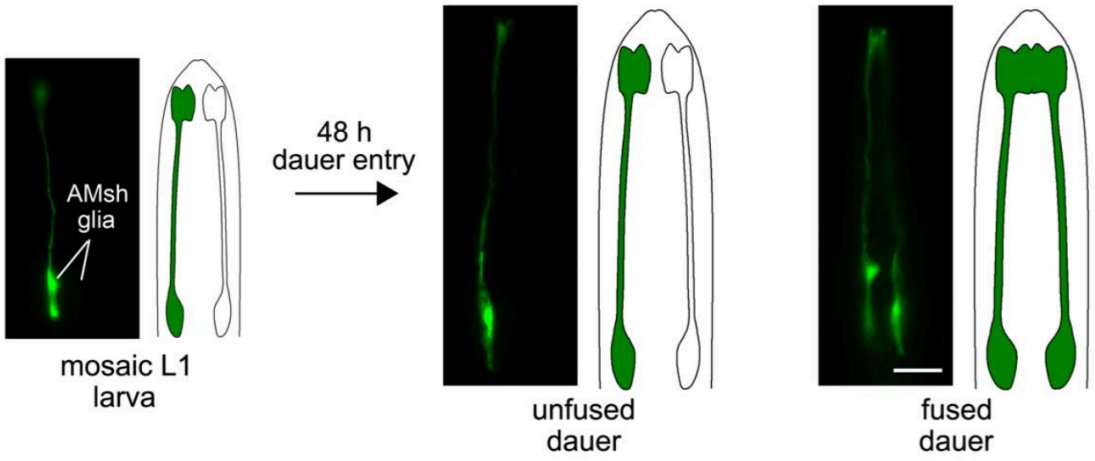

Figure 2-7 Scoring AMsh glia fusion by cytoplasmic mixing assay. Animals chimerically express an AMsh::GFP reporter from an unstable extrachromosomal array (*nsEx1391*). First-stage mosaic larvae expressing GFP in one of the two AMsh glia were picked and cultivated for 48 h at 25°C, which induces dauer entry due to the dauer-constitutive *daf-7(e1372)* temperature-sensitive mutation. If the left and right AMsh do not fuse at the nose tip, the animals continue to express GFP in only one of the two AMsh glia. If AMsh glia undergo fusion, cytoplasmic mixing occurs and animals express GFP in both cells. Examples of *daf-7*(*e1372*) dauers with and without fusion are shown. Scale bar, 20 µm. Anterior is up. Adapted from Procko, et al. 2011 [206].

Using this fluorescence assay, AMsh glia fusion was never observed in wild-type, non-dauer adult animals, whereas 46% of animals induced to enter dauer by the *daf-7(e1372)* mutation had fused AMsh glia (Fig. 2-8 a-c). The 46% wild type glial fusion rate is consistent with the expected rate of 51% previously reported [206,207]. Moreover, electron microscopy (EM) was used to directly evaluate AMsh glial fusion for some of these animals. EM serial reconstructions demonstrated that glia are unfused in dauer animals expressing GFP in only one AMsh glial cell (n=3), whereas dauers expressing GFP in both AMsh glia have fused glia (n=2), confirming that the presence of GFP in both glial cells is a good readout for cell fusion.

Next, I analyzed the effects of *F47D2.11* gene on glial remodeling. As shown in Figure 2-8a, AMsh glia fusion failed in the following mutant dauer animals (each in a *daf-7(e1327)* background to induce dauer entry): 1) *F47D2.11(ns250)*, 2) CRISPR-induced E278K mutant *ns820*, and 3) CRISPR-induced E278K mutant *ns821*. EM serial reconstructions of these mutants further confirmed that AMsh glial cells remain unfused (Fig. 2-8 d-e; n=8). Thus, *F47D2.11* is likely to be a component of the glial remodeling machinery.

I have described above that unlike *ns250* mutation, *F47D2.11* loss-of-function mutations did not exhibit defects in P*ver-1*::GFP expression at high temperature or in the dauer state. Therefore, I expected these loss-of-function mutants to show normal dauer-dependent glial remodeling as wild type animals.

Figure 2-8. *F47D2.11* required for amphid sensory organ remodeling in dauers. (A) Percentage of animals with fused AMsh glia as scored by cytoplasmic mixing. All strains carry a *daf-7*(*e1372*) mutation. Listed alleles are mutations in *F47D2.11* gene: *ns250*, *ns820*, *ns821* are point mutation E278K; *ns841* is an early stop deletion alleles;*ns844* is a 4th transmembrane deletion allele (see Figure 2-4 a). ****, $p<0.0001$, Fisher's exact test. Number of animals scored inside bars. **(B-H)** Representative electron micrographs (EM) and schematic outlines of amphid sensory organs in dauer animal with corresponding genotypes. Dauer larvae were induced by *daf-7(e1372)* mutation cultivated at high temperature. All EM images show no AMsh glial fusion. Scale bar, 1µm. (G) and (H) are reprint from Procko et al., 2011 and 2012 [206,207].

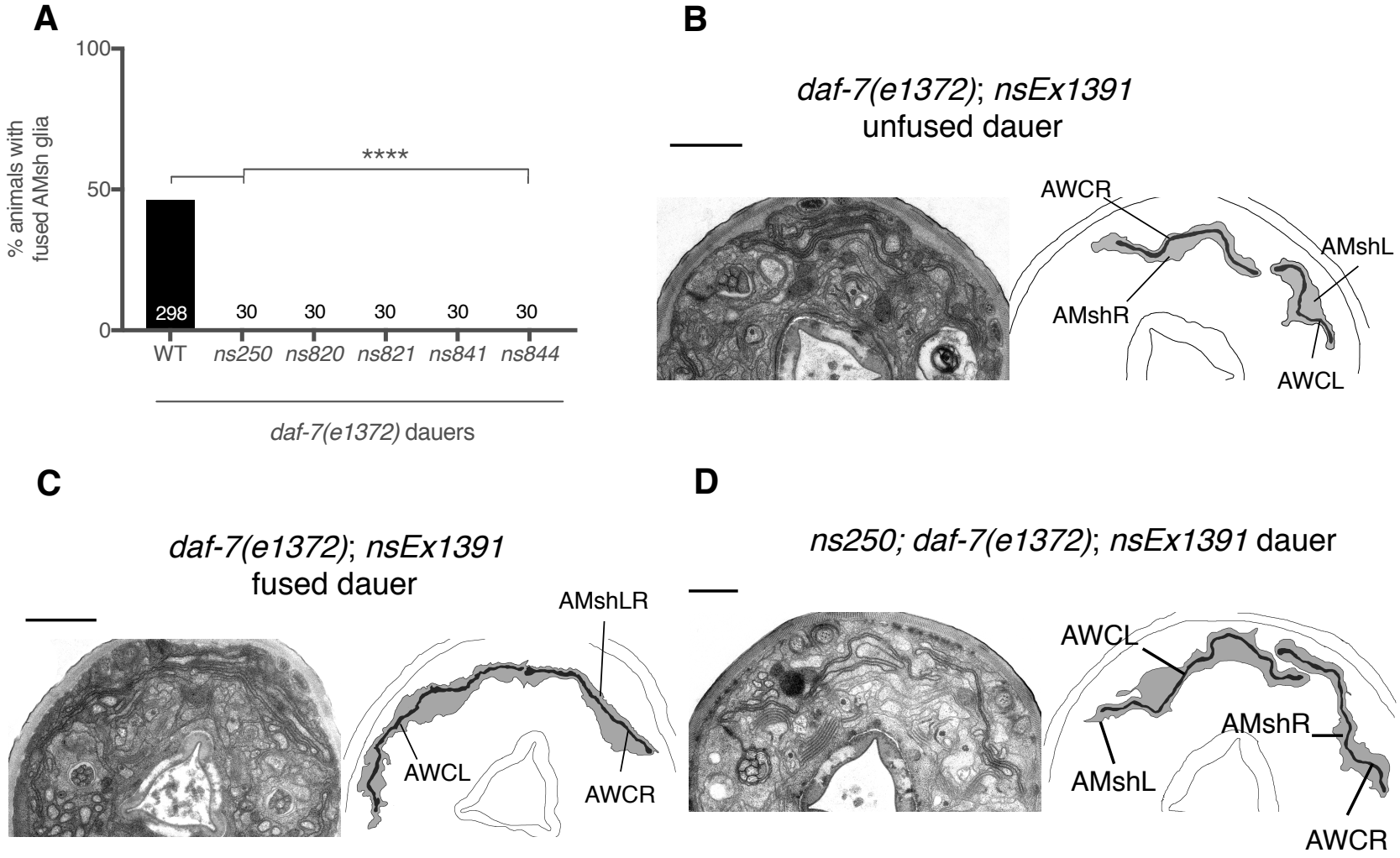
A
100
50
0
% animals with fused AMsh glia
****
298
30
30
30
30
30
WT
ns250
ns820
ns821
ns841
ns844
daf-7(e1372) dauers
B
daf-7(e1372); nsEx1391
unfused dauer
AWCR
AMshL
AMshR
AWCL
C
daf-7(e1372); nsEx1391
fused dauer
AMshLR
AWCL
AWCR
D
ns250; daf-7(e1372); nsEx1391 dauer
AWCL
AMshR
AMshL
AWCR

E

ns820; daf-7(e1372); *nsEx1391* dauer

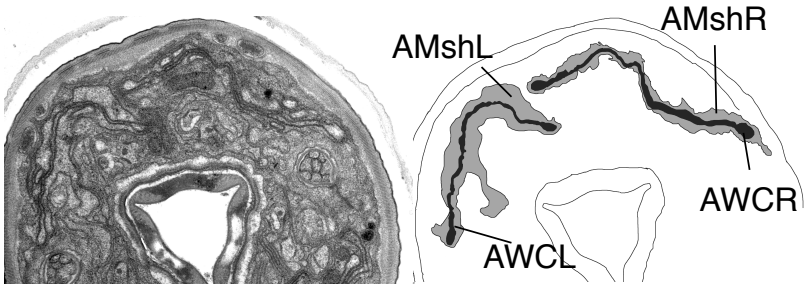

F

ns841; daf-7(e1372); *nsEx1391* dauer

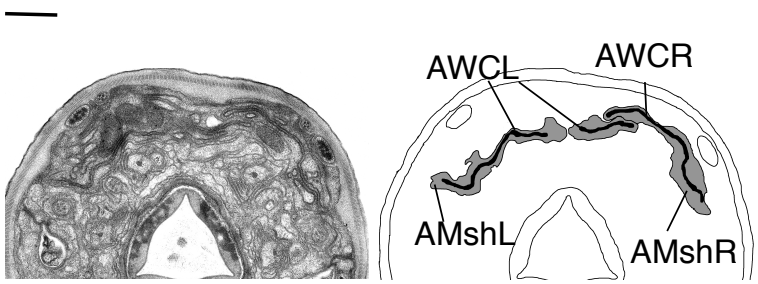

G

ztf-16(ns171); daf-7(e1372) dauer

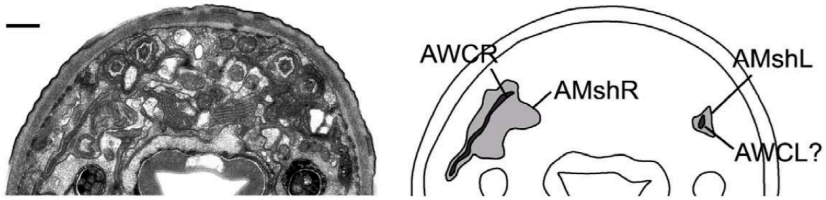

H

ttx-1(p767); daf-7(e1372) dauer

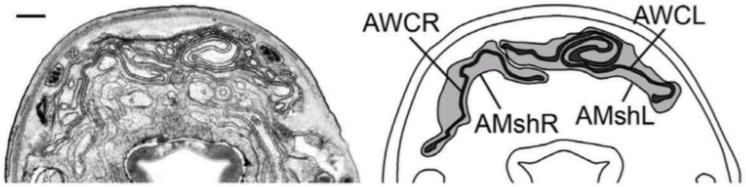

To my surprise, both the premature stop-codon and the 4th TM deletion mutations failed in AMsh glial cell fusion like *ns250* mutants (Fig. 2-8 a, f). These results suggest that *F47D2.11* differentially regulates P*ver-1*::GFP expression and dauer remodeling.

Environmental stress induces both AMsh glial fusion as well as AWC wing expansion. Previous reports have shown that both *ttx-1(p767)* and *ztf-16(ns171)* dauer mutants failed to induce AMsh glial cell fusion [206,207]. However, only *ztf-16(ns171)* mutants showed impaired AWC remodeling (reprinted in Fig. 2-8 g) [207]. In comparison, *ttx-1(p767)* mutants maintained normal AWC wing expansion, forming a distinctive dendritic whorl in the unfused glial cell compartments (reprinted in Fig. 2-8 h) [206]. The mechanism for AWC remodeling is unknown at this time. To test if *F47D2.11* regulates AWC remodeling, I examined *F47D2.11* mutant dauer animals by EM serial reconstructions for AWC dendritic expansion. Using *daf-7(e1372)* temperature-sensitive mutation background, I first induced dauer by cultivating at high temperature. Then, I selected for dauer animals with or without AMsh remodeling, based on the cytoplasmic mixing assay, and looked at the EM serial reconstructions of selected dauer animals. EM image analysis of both *F47D2.11(ns250)* and *F47D2.11(ns841)* dauer mutants in *daf-7(e1372)* background failed to induce AWC dendritic whorl in the unfused AMsh glial cell compartments (Fig. 2-8 d, f). However, the AWC wing does not look as short and constricted as the *ztf-16(ns171)* mutant's unexpanded AWC wings (Fig. 2-8 g).

This suggests *ns250* and *ns841* induce an intermediate AWC expansion defect. Because both cytoplasmic mixing assay and EM analysis are low-throughput and time-consuming, I have only confirmed EM analysis for two *ns250* dauer animals and one *ns841* dauer animal. More EM analysis is needed for further studies. So far, current results suggest *F47D2.11* gene may also function to regulate dauer-induced AWC remodeling.

To aid in faster AWC remodeling analysis, I attempted to use an AWC fluorescent reporter to track the dendritic wing expansion. Based on the EM images of wild type, non-dauer animals, there is a clear separation of space (around 80-120nm) between where the left and the right AWC wing terminals meet. I set out to use AWC reporter (*odr-1* promoter element driving RFP transgene expression) to label the unexpanded AWC wings, hoping that I could clearly see the wing separation. I decided to use the DeltaVision OMX V4/Blaze 3D-SIM super-resolution microscope, which had the highest image resolution of 100nm. Unfortunately, I was unable to differentiate the space between the wings due to resolution limitation.

Environmental stressors initiate other forms of remodeling in the *C. elegans* nervous system (see Chapter 1). To determine whether *F47D2.11* regulates other remodeling events that take place in dauers, I examined IL2 sensory neurons, which exhibit extensive dauer-dependent dendritic arborization [208]. Using an IL2 specific promoter (P*F28A12.3*) driving membrane-targeting myristolated-GFP (myr-GFP) transgene in the *daf-7(e1372)* background with

either wild type or *ns250* point mutation in *F47D2.11* gene, I screened these dauer animals cultivated at high temperature for IL2 remodeling under the compound microscope. In all wild type dauer larvae (P*F28A12.3*::myr-GFP; *daf-7(e1372)*), IL2 neurons arborized their dendrites (Fig. 2-9 a; n=99). Similarly, 98% of *ns250* dauer mutants (P*F28A12.3*::myr-GFP; *daf-7(e1372); F47D2.11(ns250)*) arborized their IL2 dendrites (Fig. 2-9 b; n=95). *ns250* mutants showed no defects in dauer-induced IL2 remodeling, suggesting that *F47D2.11* may function specifically in dauer-induced amphid sensory organ remodeling.

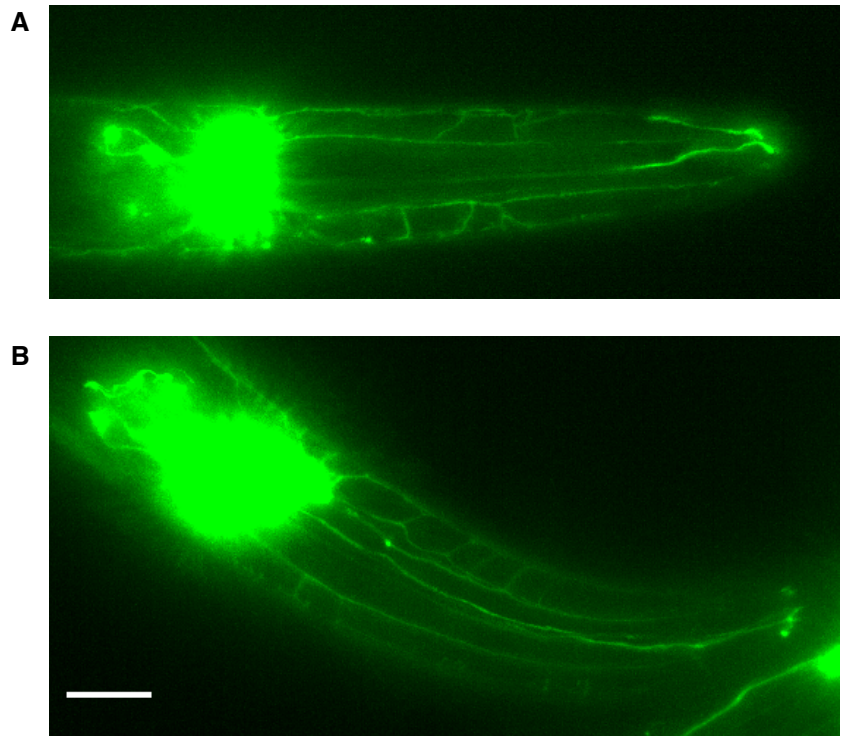

Figure 2-9. *F47D2.11(ns250)* has no effect on IL2 arborization. IL2 dendritic arborization in wild type (A) and *ns250* mutant (B) marked by P*F28A12.3*::myr-GFP in *daf-7(e1372)* background strain. Dauer induced by cultivation at high temperature. Scale bar, 10μm

2.4 Conclusion

In summary, I isolated a novel GPCR gene, *F47D2.11*, that functions in the *ver-1* transcription network and dauer-remodeling pathway. I have characterized *ns250* as the causal mutation which prevents P*ver-1*::GFP expression in the AMsh glia at high temperature and upon dauer entry. It remains unclear how *F47D2.11(ns250)* functions to regulate *ver-1* induction and more study is needed. However, dominance genetic test does suggest *ns250* allele regulate *ver-1* expression in a semi-dominant nature at high temperature. More interestingly, *F47D2.11(ns250)* also fails to induce amphid remodeling in dauer larvae. In the next chapter, I will describe studies aimed at determining in which cell types *F47D2.11* may be expressed and understanding the purpose of stress-induced amphid remodeling using behavioral studies.

3 F47D2.11 GPCR functions in AMsh glia to regulate *ver-1* induction and dauer exit

3.1 P*ver-1*::GFP expression is rescued glia-specifically in *ns250* mutants

F47D2.11 regulates *ver-1* transcription and dauer-remodeling in response to environmental changes. The amphid sensory organ is the primary chemosensory organ in the worm, which forms a glial channel to the external environment that allows some of the amphid sensory dendritic endings to extend and detect changes in the environment (Chapter 1, Fig. 1-1). Given that *F47D2.11* functions in response to environmental stressors to affect amphid glial and neuronal morphology, this suggested that F47D2.11 GPCR might be located at the tip of the amphid sensory organ, near the external opening. However, it is unclear whether *F47D2.11* is expressed in the amphid glial cells or the amphid sensory neurons or both.

To determine in which cell type F47D2.11 GPCR functions, I performed cell-specific rescue experiments aimed at restoring wild type P*ver-1*::GFP expression in *ns250* mutant background by expressing F47D2.11 cDNA in specific subset of cells. I tested for cell-specific rescue using AMsh glia promoter (*F16F9.3)* and amphid sensory neuronal promoter (*dyf-7)* to drive F47D2.11 cDNA. I found that restoring expression of wild type *F47D2.11* in AMsh glia, but not in amphid sensory neurons, could restore P*ver-1*::GFP expression (Fig. 2-5). Three independent lines were observed for each rescue construct. The non-transgenic

siblings for each rescue line served as the controls and all showed no rescue. Therefore, these results suggest *F47D2.11* functions in AMsh glia to regulate P*ver-1*::GFP induction.

3.2 F47D2.11 GPCR may function within AMsh glia to regulate dauer exit

The functional outcome of amphid sensory remodeling in dauers remains unclear. It is possible that the remodeling of AMsh glia and AWC neuron may be a result of radial shrinkage of body circumference, bringing AWC sensory ending pair and two AMsh glia closer together, and serve no physiological purpose [204]. Alternatively, the AMsh glia and AWC neuron of dauer animals may respond differently to their environment, and the remodeling of their morphology may have a functional consequence. For example, these amphid cells may have altered sensitivity to food and other cues that would signal an improvement in their environment and the need to exit dauer to become reproductive adults. Consistent with this hypothesis, the repertoire of odorant receptors expressed in a given sensory neuron is also altered in dauer animals [209]. To date, no AMsh and AWC-mediated behaviors have been described for dauers. It is possible that changes in the amphid sensory structures are required to directly modulate the perception of dauer exit signals. Consistent with this idea, *ttx-1*(*p767*); *daf-7*(*e1372*) mutants have been reported to exit dauer prematurely compared to *daf-7*(*e1372*) single mutants [210]. However, preliminary work suggests that this

effect can be rescued by restoring *ttx-1* function to the AFD thermosensory neurons and not the glia (Carl Procko, unpublished).

To examine if dauer-dependent remodeling serves to facilitate exit from the dauer stage upon favorable environment, I monitored the rate of dauer exit following introduction of food. In dauer state, *C. elegans* stop feeding and the pharyngeal pumping used to rhythmically suck in and trap bacteria is not observed [176,214]. The first visible sign of dauer exit is the recovery of pharyngeal pumping [204]. One way to measure pharyngeal pumping is to screen for pumping movement by eye under a microscope [215]. However, this method is time-consuming and low throughput. Therefore, I developed a new high-throughput assay to monitor dauer recovery, in which dauer animals are exposed to OP50 bacteria expressing GFP. The bacteria serve as both a stimuli to induce dauer exit as well as a marker to measure pumping by observing GFP accumulation in the pharynx. Animals recovered from dauer state can be easily identified by screening for fluorescence in the pharyngeal canal (Fig. 3-1 a). Importantly, the initiation of pharyngeal pumping coincides in time with GFP accumulation in the pharynx. In dauer state, *F47D2.11(ns250)* fail to induce amphid remodeling but are able to enter and exit out of dauer normally. Using both the pumping and OP50-GFP recovery assays, I found that dauer recovery in *ns250* mutants was significantly delayed compared to the recovery in wild type animals. It took 1.4 times longer for both the onset of pharyngeal pumping and GFP accumulation in the pharynx to occur in 50% of *ns250* mutants than in wild

Figure 3-1 OP50-GFP dauer recovery assay. (A) DIC and fluorescence images showing OP50-GFP accumulation in the pharynx in a *daf-7*(*e1372*) animal induced to enter dauer by cultivation at 25°C. Far left image, DIC. The fluorescence images are maximum projections of z-stacks of the entire animal volume. Arrow marks the accumulation of OP50-GFP in the pharynx. Outline of the worm is marked in grey. In all images, above is anterior. Time points in hours are indicated. Each image is of different animals. The animal was anesthetized using 50 mM NaN_3. Scale bar, 10µm. **(B)** The rates of onset of pharyngeal pumping via GFP accumulation in the pharynx at 15°C using OP50-GFP dauer recovery assay were plotted for the indicated genotypes as survival from dauer, and were compared by log-rank test using GraphPad Prism 6. Black dotted line indicates the time-point in which 50% of the given population recovers pumping. Compared to wild-type animals, *ns250* mutants show around 1.4x delay in the onset of pharyngeal pumping recovery in 50% of the animals ($p<0.0001$). This delay is rescued by transgenic expression of F47D2.11 in AMsh glia using F16F9.3 promoter but not with its expression in the amphid sensory neurons, including AWC, using *dyf-7* promoter. Pharynx pumping assay showed similar pattern in WT and *ns250* animals (not shown).

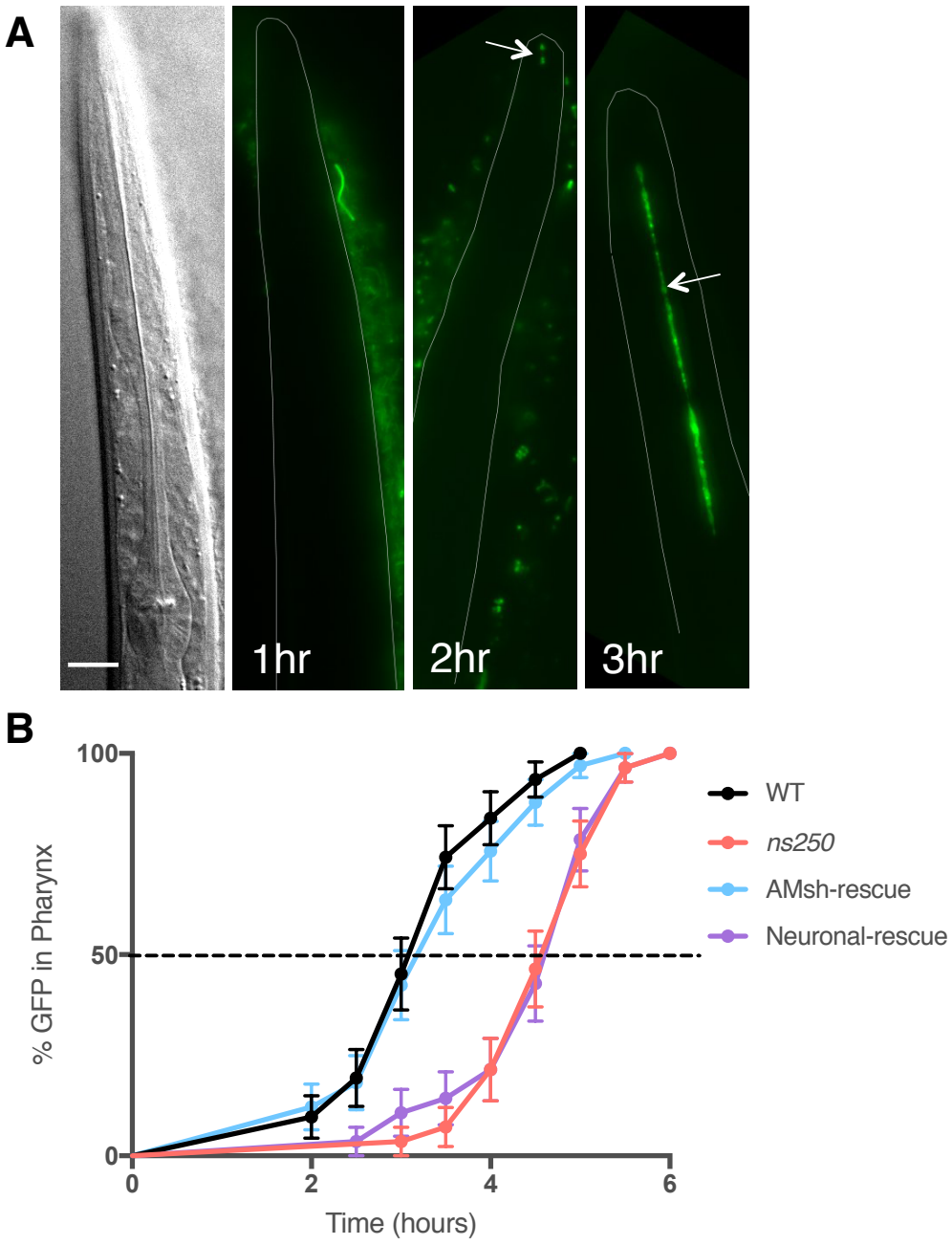
A
1hr
2hr
3hr
B
100
50
0
% GFP in Pharynx
0
2
4
6
Time (hours)
WT
ns250
AMsh-rescue
Neuronal-rescue

type animals following food exposure, suggesting that amphid remodeling facilitate dauer exit.

Next, I performed cell-specific rescue experiments aimed at restoring dauer exit delay in *F47D2.11(ns250)* animals by restoring wild type *F47D2.11* in either AMsh glia using *F16F9.3* promoter or amphid sensory neurons using *dyf-7* promoter to drive F47D2.11 cDNA. Preliminary results show restoring expression of wild type *F47D2.11* in AMsh glia, but not in amphid sensory neurons, was sufficient to rescue dauer exit delay in *ns250* mutant (Fig. 3-1 b), suggesting that *F47D2.11* function in the AMsh glia to regulate dauer exit.

3.3 F47D2.11 GPCR likely to be expressed in the AMsh glia

Next, I set out to identify *F47D2.11* expressing cells using predicted *F47D2.11* promoter regions to make fluorescent transgene reporters. Based on the rescue results above, it is likely that *F47D2.11* is expressed in the AMsh glia. In *C. elegans*, the minimal set of cis-regulatory sequences sufficient to induce proper gene expression is usually found within 2 kb upstream of the translational start codon and restricted to the non-coding, intergenic region [216]. However, the upstream non-coding, intergenic region of *F47D2.11* is only 709bp long, raising concern that important regulatory elements might be missing. Interestingly, *F47D2.11* gene includes a long second intron region (815bp), which seemed likely to contain regulatory elements to drive proper expression of *F47D2.11* gene (Fig. 3-2 a). Therefore, I selected *F47D2.11* promoter region to start from the predicted cis-regulatory motif until the end of the second intron of F47D2.11 gene

(~1.8kb). This predicted 1.8kb promoter region, cloned from the fosmid WRM0612aF01, was used to drive GFP transgene expression using the promoter fusion method to make a transcriptional reporter [217] (see Chapter 6). This transcriptional reporter showed strong expression in the PHsh glia at 25°C in all larval stages (Fig. 3-2b). I also saw very faint expression in the presumed AMsh glia based on cell body morphology and position at 25°C in younger larval stages (image not available due to photo-bleaching) [218]. AMsh and PHsh glia are usually expressed concomitantly by the same promoters. Based on the strong PHsh expression the translational reporter, AMsh glial expression seemed promising.

In case there were other regulatory elements within the *F47D2.11* gene, I also made a translational reporter using predicted 2.5kb promoter region that spans from the start of *F47D2.11* cis-regulatory motif until the end of *F47D2.11* gene to drive GFP transgene expression (Fig. 3-2 a). Predicted 2.5kb promoter region was also cloned from the fosmid WRM0612aF01. This GFP translational reporter also showed similar pattern as the transcriptional reporter above: strong PHsh glia expression and weak AMsh glia expression at high temperature (Fig. 3-2 b). In both reporters, PHsh glia expression gets weaker at 15°C and intermediate expression at 20°C, suggesting *F47D2.11* expression may be temperature-dependent in the PHsh glia (not shown). Between the translational and transcriptional reporter strains, I did not see any noticeable differences in GFP localization within the labeled cells. Occasional AMsh glia expression was

Figure 3-2. AMsh and PHsh glial expression of F47D2.11 GPCR. (A) Schematic of the *F47D2.11* gene and its upstream gene, *ZC132.11*: boxes represent exons. Scale length 100bp. Regions used to create transcriptional (1.8kb) and translational promoter (2.5kb) reporters are depicted in red and green, respectively. **(B)** Fluorescence image of phasmid region of an adult animal carrying a transgene containing the P*F47D2.11* (1.8kb) sequence fused to GFP at 25°C. Fluorescence is seen in the two PHsh glia. Similar expression seen in P*F47D2.11* (2.5kb)::GFP reporter animals at 25°C. Scale bar, 10µm. **(C)** Fluorescence image of the head of an adult animal carrying a transgene containing the P*F47D2.11* (2.5kb) sequence fused to GFP::SL2::NLS::RFP at 25° C. Nuclear RFP fluorescence is seen in the AMsh glia (arrow). Scale bar, 20µm. Dorsal side, top. **(D)** Subcellular localization of F47D2.11 GPCR in AMsh glia. Fluorescence image of an adult animal carrying a transgene containing the *F16F9.3* promoter element to drive the expression of F47D2.11 cDNA fused to mCherry at 25°C. mCherry expression seen in the subcellular vesicles, mostly in the AMsh cell body, excluding the nucleus, and along the anterior processes Scale bar, 20µm. Dorsal side, top. **(E, F)** Fluorescence images of an adult animal (E) or dauer animal (F) carrying CRISPR knock-in Venus transgene following the endogenous *F47D2.11* gene. GFP accumulation at the tip of the amphid region. Animals were cultivated at 25°C and dauer state was induced by starvation. Magnified inset of the Venus accumulation at the tip of the nose. Scale bar, 10µm

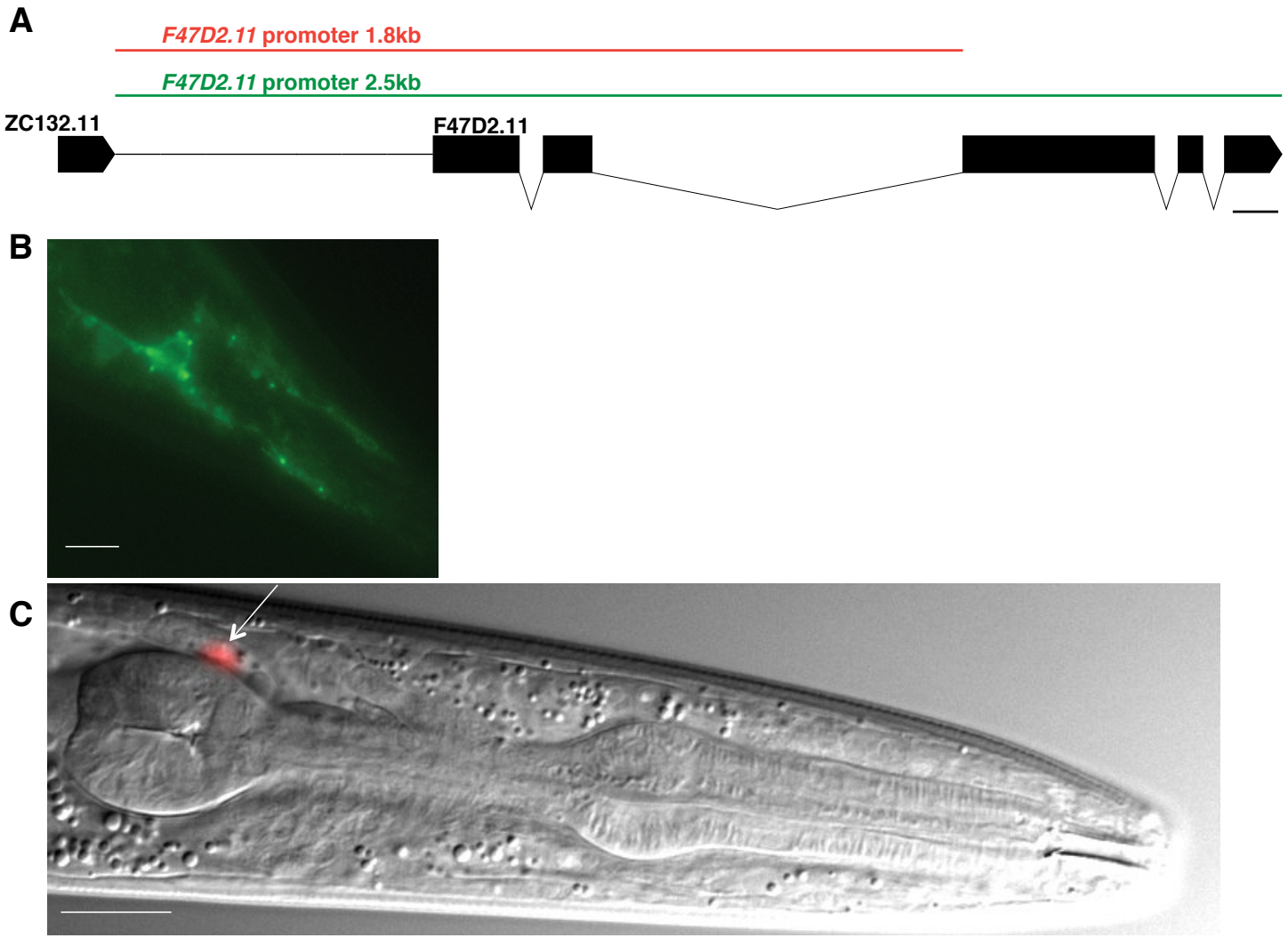
A
F47D2.11 promoter 1.8kb
F47D2.11 promoter 2.5kb
ZC132.11
F47D2.11
B
C

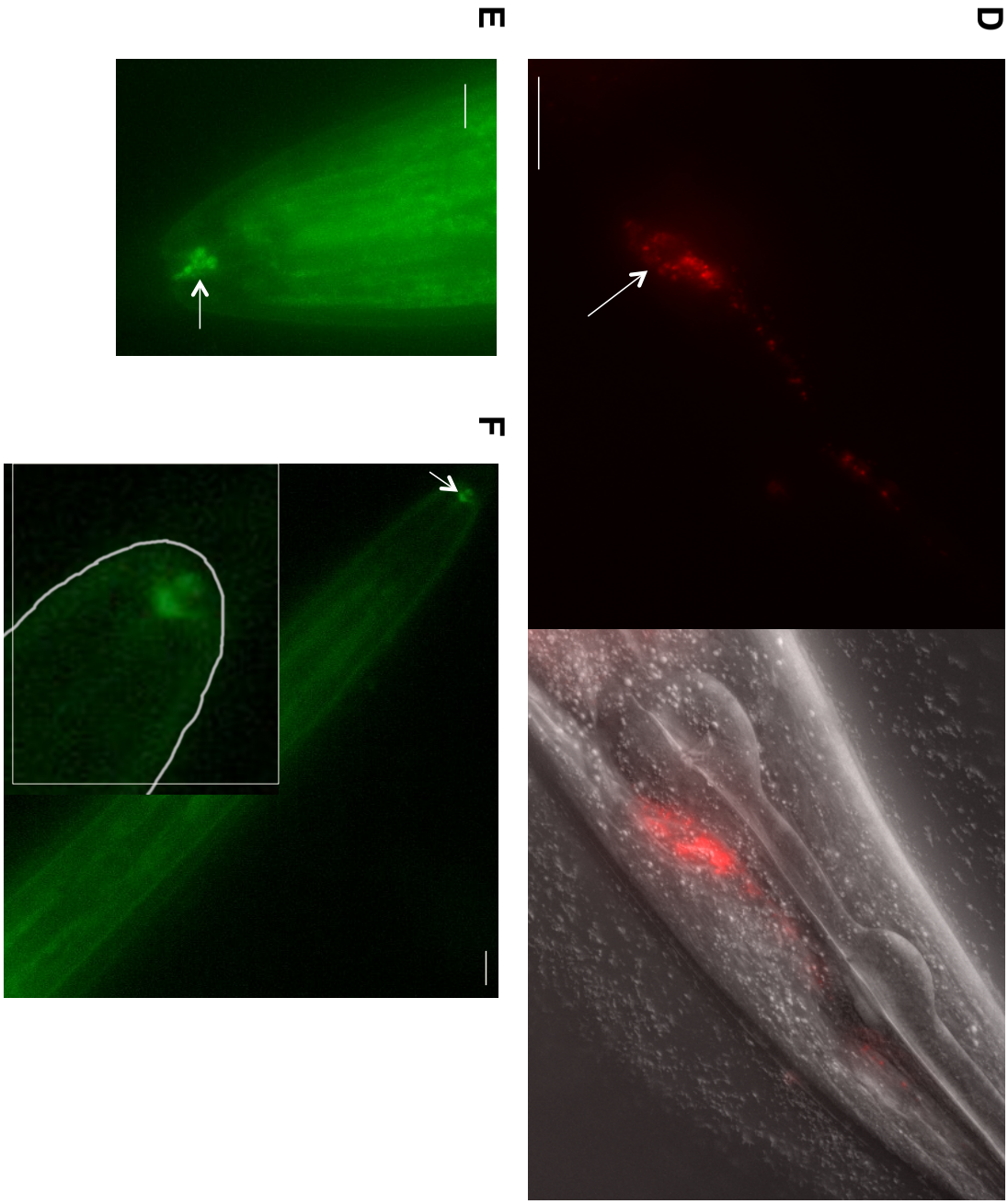
D
E
F

also observed in the translational nuclear reporter based on the positioning of nuclei expression at all larval stages and dauer state (Fig. 3-2 c). For this nuclear reporter, I modified the GFP translational reporter by introducing a trans-splicing sequence followed by a nuclear localization sequence (NLS) and RFP transgene right after the stop codon of GFP transgene (P*F47D2.11*(2.5kb)::GFP::SL2::NLS::RFP).

The faint AMsh glial expression may be explained by the absence of crucial regulatory elements needed for strong expression. Indeed, in *C. elegans*, the promoter regions important for proper glial expression can be far away from the coding region, hence such regions are difficult to predict and identify solely based on the genomic sequence. For example, AMsh expressing promoter region for *ttx-1* gene is 11kb upstream of the gene itself [206]. Instead of searching for the missing regulatory elements blindly, I proceeded to insert a fluorescent transgene reporter in the wild-type genome using CRISPR, thus utilizing the complete endogenous regulatory elements. I inserted the SL2::NLS::RFP transgene after the *F47D2.11* gene using CRISPR knock-in method [219] (Chapter 6). Although PCR analysis confirmed successful insertion, I was not able to detect any fluorescent expression under the compound microscope. The signal may be too weak to be observed due to the low copy number insertion and the overall weak signal emitted by the RFP-tag.

Rescue data and some of these reporters hint that *F47D2.11* is expressed in the AMsh glia. To look at the possible sub-cellular localization of F47D2.11

GPCR, I used the AMsh-specific promoter element (*F16F9.3* promoter) to drive the expression of F47D2.11 cDNA followed by mCherry transgene. I observed GPCR expression in the subcellular vesicles, mostly in the AMsh cell body, excluding the nucleus, and along the anterior processes (Fig. 3-2 d). However, I did not see any expression at the tip of the glia at high temperature or upon dauer entry. This particular AMsh reporter (*F16F9.3* promoter) is known to cause weak defects in the sheath morphology, which may hinder proper expression at the tip of the cell. Another possibility is that *F47D2.11* overexpression may clog up the vesicle trafficking machinery. Lastly, *F47D2.11* may be transiently localized at the tip of the nose, thus capturing it at the right moment might be challenging.

To address some of these technical limitations, I made an endogenous translational reporter using CRISPR. Because CRISPR-inserted SL2::NLS::RFP transgene expression was too weak, I opted to insert Venus transgene after the *F47D2.11* gene instead. In the *F47D2.11*::Venus CRISPR knock-in reporter, I saw a consistent but weak Venus expression in two lateral regions at the tip of the nose in dauer and non-dauer larvae (Fig. 3-2 e, f). These Venus protein accumulations have several lines embedding within the region, which could be the amphid dendritic extensions through the AMsh glia as part of the amphid channel (Fig. 3-2 e, f). As the protein is only localized at the tip of the nose, and not in the cell body, it is difficult to identify the expressing cells with this reporter.

3.4 Conclusion

Altogether, *F47D2.11* regulate P*ver-1*::GFP expression, stress-induced amphid remodeling, and dauer recovery rate. *ns250* mutation affects all three functions and AMsh glial-specific expression of wild type F47D2.11 GPCR rescues both the P*ver-1*::GFP defect and dauer exit delay. Whether glia-specific restoration of wild type *F47D2.11* could rescue the amphid remodeling is to be determined. *F47D2.11* is likely localized at the tip of the glial cells to sense the external environment in order to initiate properly timed dauer exit. My thesis work demonstrates that stress-induced remodeling in the sensory organ has direct functional and behavioral consequences, likely to be important for species propagation.

4 Further studies:

4.1 Characterization of *F47D2.11* expression pattern

Detailed analysis of the complete expression pattern of *F47D2.11* using strains P*F47D2.11*(1.8kb)::GFP transcriptional and P*F47D2.11*(2.5kb)::GFP translational reporters reveals expression in the head muscle, ASI and ASJ and sensory neurons. In addition to strong PHsh glial and weak AMsh glial expression (see Chapter 3), the transcriptional reporter P*F47D2.11*(1.8kb)::GFP show expression in the head muscle as well as ASJ neurons in all larval stages (Fig. 4-1 a) . Similarly, P*F47D2.11*(2.5kb)::GFP translational reporters also showed expression in the head muscle and ASI neuron in all larval stages (Fig. 4-1 b). In these experiments, ASI and ASJ neuronal identities were confirmed using dye-filling assay (see Chapter 6).

To facilitate characterizing *F47D2.11* expression pattern, I made a translational reporter, *F47D2.11*::GFP::SL2::NLS::RFP, to identify both the *F47D2.11*-expressing cells using RFP signal as well as its subcellular localization using GFP signal. In addition to the AMsh glial cell expression (see Chapter 3), this reporter also showed expression in the ASI and ASJ sensory neurons based on cell body expression and DiO co-staining (Fig. 4-1 c). There were GFP accumulations at the tips of both ASI and ASJ neurons (Fig. 4-1 c). However, the morphology of these structures looked different from the protein accumulations I observed using the Venus construct in Chapter 3 (Fig. 3-2 e, f). In the early larval

Figure 4-1. Characterization of *F47D2.11* expression pattern. (A-D) Fluorescence and DIC images of young adult animals (except L2 larva in (D)) carrying different transgene reporters. **(A)** P*F47D2.11* (1.8kb)::GFP transcriptional reporter labels the head muscle (arrow) and ASJ sensory neurons (triangle); confirmed by DiI (not shown) **(B)** P*F47D2.11* (2.5kb)::GFP translational reporter labels the head muscle (arrow) and ASI sensory neurons (triangle); confirmed by DiI (not shown) **(C)** P*F47D2.11* (2.5kb)::GFP::SL2::NLS::RFP reporter labels the nucleus of ASI (right, above arrow) and ASJ sensory neurons (right, lower arrow) in red. GFP shows accumulation of F47D2.11 GPCR mostly at the cell body, excluding the nucleus, along the processes and at the tips. **(D)** Same reporter as (C). L2 larva shows red nuclear labeling in the presumed IL sheath glial cells. Animals cultivated at 25°C. Scale bar, 10µm.

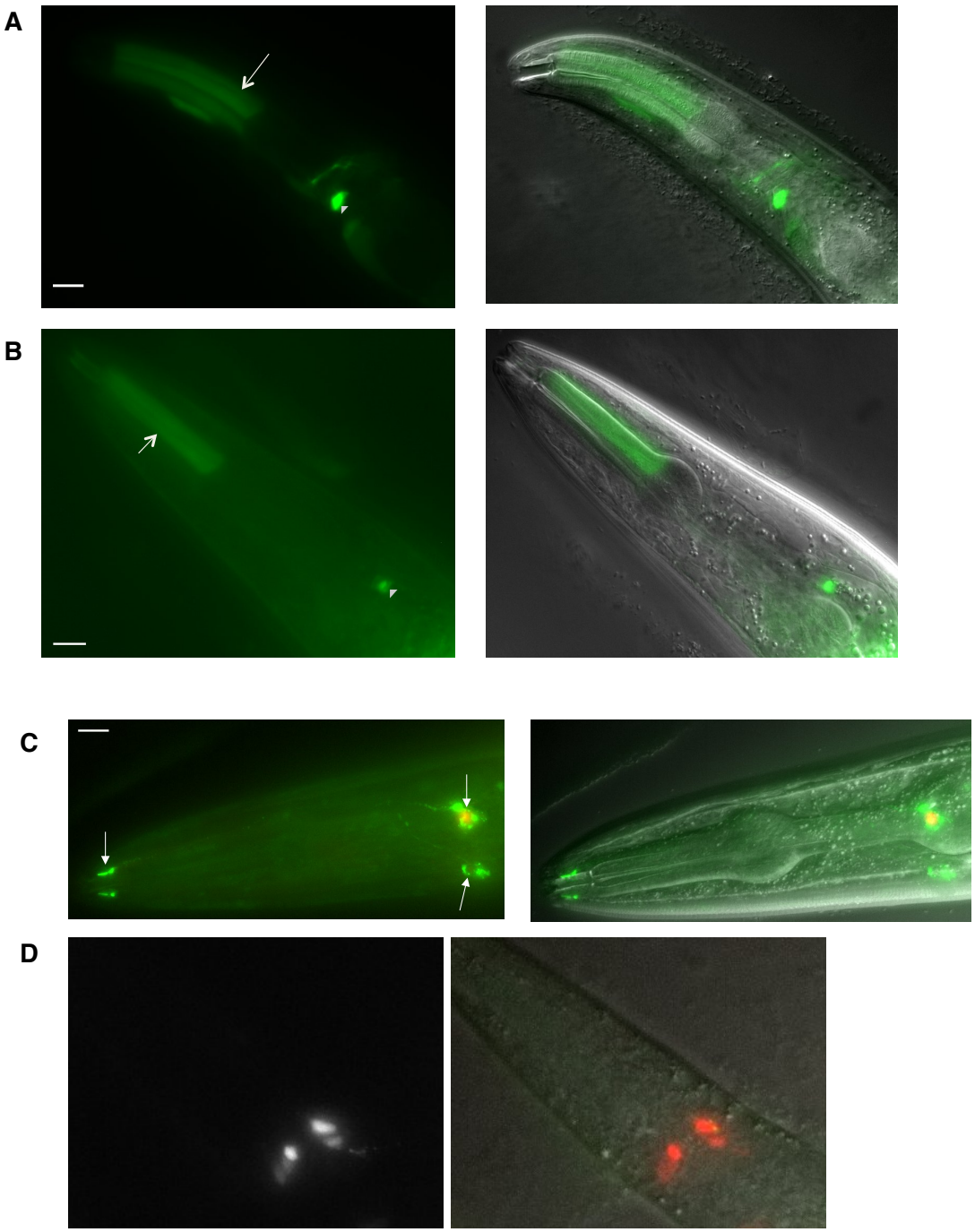
A
B
C
D

states, I see RFP nuclear expression in the IL sheath (ILsh) glia, based on cell body morphology and position (Fig. 4-1 d) [218].

ILsh glia are part of the inner labial sensilla and are thought to guide axons entering the nerve ring neuropil during development [171,172]. Currently, post-embryonic function of ILsh glia is still unknown. There has been no report suggesting correlation between ILsh glia and the dauer state. ILsh glia are associated with IL2 neurons and my studies show IL2 neurons undergo normal dauer-induced remodeling in *ns250* mutant background (Chapter 2). This suggests F47D2.11 GPCR affects remodeling of cilia but not dendrites.

Interestingly, ASI and ASJ are single ciliated amphid sensory neurons and are thought to be important cells for dauer regulation. ASI neurons secrete endocrine signals in response to environmental stressors that induce dauer (see Chapter 1) [165-167]. Upon dauer entry, ASI neurons are shortened and displaced posteriorly in the AMsh glia channel [204]. In addition, ASJ neurons regulate both dauer entry and exit [165-167]. *F47D2.11* expression in ASI and ASJ suggests GPCR may function in these sensory neurons to regulate dauer state. One could imagine ASJ neuron regulating dauer exit by recognizing favorable environmental cues through F47D2.11 GPCR. It's also possible that ASI neuron function through F47D2.11 GPCR to signal its dauer remodeling, increase sensitivity to dauer exit cues in order to signal ASJ for proper dauer exit. However, amphid neuronal rescue using *dyf-7* promoter did not rescue dauer recovery delay. *dyf-7* promoter includes expression in ASI and ASJ neurons,

which suggests the main site of F47D2.11 action is likely in the AMsh glia. An endogenous *F47D2.11* reporter with all of its regulatory elements is needed to confirm all expression.

4.2 *F47D2.11* overexpression may reveal differential control of *ver-1* expression at high temperature and in dauers

I found that ectopic expression of *F47D2.11* (either WT or *ns250* point mutation sequence) in the AMsh glia using the specific promoter from the glial gene *F16F9.3* prevents P*ver-1*::GFP reporter expression in the AMsh glia following cultivation at high temperature in both hermaphrodites and males (Fig. 4-2) but not in dauer state. While the physiological meaning of this effect is not clear, it may suggest that expression of *ver-1* in dauers and in response to high temperature are differentially controlled.

4.3 Exogenous *F47D2.11* expression in all glial cells

Previous reports have demonstrated *ver-1* transcription is upregulated by high temperature [206,207]. Likewise, *F47D2.11(ns250)* prevents *ver-1* induction at high temperature. Since both *F47D2.11* and *ver-1* respond to high temperature, I was curious to see if this GPCR acts as the thermosensor to regulate *ver-1* expression. If *F47D2.11* is a thermosensor, its expression in any given cell would drive *ver-1* expression following high-temperature treatment. To test this idea, I ectopically expressed F47D2.11 GPCR in either all glial cells using pan-glial promoter, *mir-228*, or in a large subset of glial cell using *ptr-10* promoter, at various concentrations (1ng-70ng) in the P*ver-1*::GFP reporter

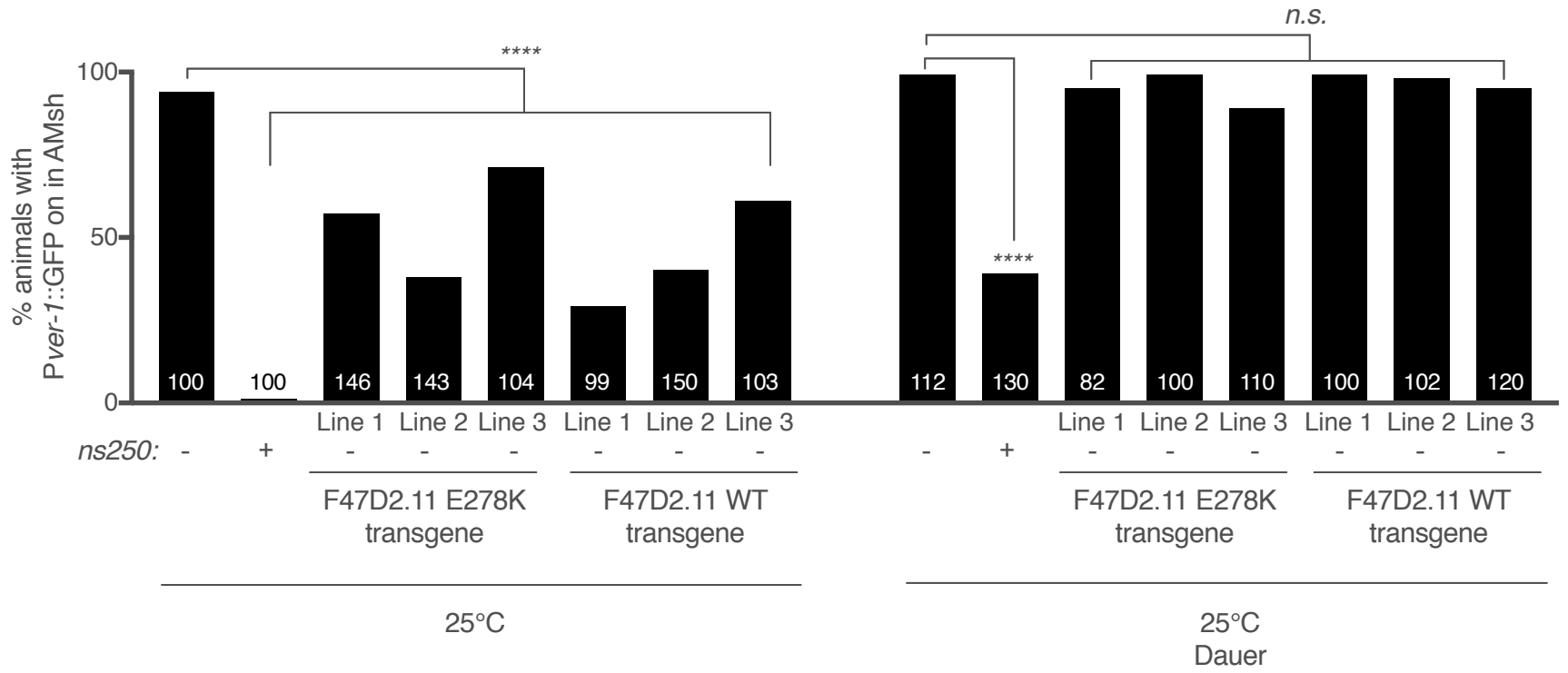

Figure 4-2. Ectopic expression of *F47D2.11* WT or E278K transgene in the AMsh glia. Histogram of P*ver-1*::GFP expression in WT, *ns250* mutant and WT animals with either ectopic overexpression of *ns250* point mutation sequence (E278K) or *F47D2.11* WT sequence in the AMsh glia using *F16F9.3* promoter. Left graph represents hermaphrodites cultivated at 25°C. Similar expression difference is observed in males at 25°C (not shown). Right graph represents dauer animals cultivated at 25°C and dauer-induced by starvation. Animals screened as young adults or dauer larvae. n.s., $p>0.05$, ****, $p<0.0001$, Fisher's exact test. Number of animals scored inside bars.

strain. Upon temperature shift, 15°C to 25°C or vice versa, I did not see ectopic GFP expression in any larval stages indicating that *F47D2.11* expression alone was not sufficient to drive *ver-1* transcription. Thus, *F47D2.11* is likely to not act as a direct thermosensor.

4.4 Redundant GPCR candidates

I've described in Chapter 2 that while *F47D2.11(ns250)* failed to induce *ver-1* expression, *F47D2.11* deletion mutants were able to induce *ver-1* expression normally at 25°C. Given that these deletion mutations are presumed null alleles, this suggested that there might be a compensatory mechanism to induce *ver-1* expression in response to high temperature. To search for the redundant gene that may work in conjunction with *F47D2.11* to regulate P*ver-1*::GFP induction, I looked towards other serpentine receptor class z GPCRs. Previous studies have shown that in *C. elegans*, *srg-36* and *srg-37* serpentine receptor class g GPCRs share 49% conserved regions and act redundantly to detect dauer pheromones [220]. There were two likely candidates: *ZK218.4* and *ZC132.9* GPCR paralogs. *ZK218.4* and *ZC132.9* are part of the serpentine receptor class z GPCR family and share conserved genetic sequences of 35% and 40% respectively with *F47D2.11*. Based on RNAseq studies, *ZK218.4* is enriched in the AMsh glia while *ZC132.9* is enriched in neurons [221-223]. To test for redundancy, I knocked down each of these paralog genes using RNAi in the *F47D2.11* null deletion background and scored for the absence of GFP signal in animals raised at high temperature. While the proper RNAi controls worked (see Chapter 6),

single and double knockdown of the paralog genes did not prevent GFP expression. While these results could be explained by insufficient knockdown of the target genes, it suggested that *ZK218.4* and *ZC132.9* might not work redundantly with *F47D2.11* to regulate *ver-1* expression. It is still possible that a compensatory mechanism exists but requires further analysis.

5 Discussion and future directions

5.1 Discussion:

During my graduate studies, I sought to understand how organisms adapt their fitness in unfavorable conditions in order to survive and maximize reproductive success. To study this, I utilized *C. elegans* because they provide a unique system to study nervous system plasticity in an inducible developmental state of the animal. *C. elegans* evolved an alternative developmental state called dauer, which allows them to persist under high stress conditions. Dauer entry in *C. elegans* is promoted by high population density, low food abundance and high temperature, which initiates a number of morphological changes such as thickening of their cuticles, shrinkage of the body circumference, suppression of movement and alterations in metabolism [176,177,180]. These morphological changes allow increased resistance to environmental challenges [176]. Dauer animals also undergo drastic remodeling in the amphid sensory organ, including the AMsh glia and AWC neurons, but the physiological purpose of this remodeling has been unclear. It is possible that the morphological changes in the amphid sensory organ promote changes in the behavior of the animal. For example, it would be beneficial for dauer animals to perceive their environment in such a way as to effectively locate favorable conditions for exiting dauer and reproduce. Alternatively, the remodeling of glia and AWC neurons may be a result of radial shrinkage of body circumference and serve no physiological purpose [204]. My thesis focused on understanding dauer-induced amphid

remodeling regulation and the functional consequences of this plasticity. Through my work, I found a novel gene, *F47D2.11,* which regulates glial plasticity in dauer animals. *F47D2.11(ns250)* mutation prevents AMsh glial fusion as well as delays dauer recovery. This suggests F47D2.11 GPCR plays an important role in glial plasticity and the change in glial morphology results in behavioral consequences that allows for proper adaptation to the changing environment, revealing a potential new role for glial remodeling.

There still remain open questions in understanding *F47D2.11* and its regulation in dauer remodeling and recovery. Below I will summarize the major questions remaining and outline possibilities and prospects for addressing them.

5.2 Nature of *ns250* mutation

I have described in Chapter 2 that *ns250* has a semi-dominant effect on P*ver-1*::GFP expression. Does *ns250* mutation also regulate glial remodeling semi-dominantly? To test this, I propose using *ns250* heterozygotes mutants in *daf-7(e1372*) background with an unstable extrachromosomal array (*nsEx1391*, AMsh glia::GFP) to perform cytoplasmic mixing assay. L1 animals will be selected for mosaic expression of GFP in only one glial cell and monitored for glial fusion. Each animal will be genotyped at the end of the assay to confirm *ns250* heterozygote mutation. If heterozygote mutants undergo normal glial remodeling, this suggests *ns250* is a recessive mutation. If heterozygote mutants show defect in glial remodeling, this suggests *ns250* is semi-dominant.

If *ns250* has semi-dominant effect on both P*ver-1*::GFP expression and glial remodeling, this suggests *ns250* could be one of four allele types: loss-of-function haploinsufficient, dominant-negative, increased wild type function of the gene or gain of new function. To test if *ns250* is a loss-of-function haploinsufficient allele, I propose to screen for heterozygote *F47D2.11* deletion animals. If they are all completely wild type, then *ns250* cannot be haploinsufficient allele. Next, if overexpression of wild type F47D2.11 GPCR rescues *ns250* mutant defect and the allele is not haploinsufficient, then *ns250* is likely dominant negative allele. In Figure 2-5, I have described that *ns250* defect can be rescued by expression of F47D2.11 transgene and cDNA. If *ns250* is not haploinsufficient, this likely suggests *ns250* is a dominant negative allele. Overexpression of wild type F47D2.11 in *ns250* mutant also tests the last two possibilities. If *ns250* defect is due to increased wild type function of *F47D2.11*, overexpression of wild type F47D2.11 GPCR would make the phenotype worse. If *ns250* is a gain of new function allele, wild type F47D2.11 overexpression should not have any effect. Another way to test if *ns250* allele increases wild type function is to overexpress wild type F47D2.11 protein in a wild type background, which should cause defect. Finally, if overexpression of mutant *ns250* protein in wild type animals results in defects, this suggests *ns250* is either dominant-negative or gain of new function allele.

5.3 Does F47D2.11 GPCR function as a receptor?

My study shows that F47D2.11 GPCR can respond to dauer entry and high temperature, both exogenous stimuli. How does F47D2.11 GPCR perceive environmental stressors to regulate dauer state? One possibility is that F47D2.11 GPCR directly senses the dauer cues from the environment. *F47D2.11* expression in the AMsh glia, ASI and ASJ sensory neurons, and IL sheath glia remains to be determined. Regardless, these four cell types are all exposed to the external environment. As a transmembrane receptor, F47D2.11 GPCR could function in any of these cells to directly sense some environmental stressors that signal dauer state.

Glia-specific rescue data suggest F47D2.11 GPCR likely functions in the AMsh glia. If true, another possibility is that the dauer signals perceived by glia may be secondary signals as a result of dauer entry. These signals could be derived from neuroendocrine pathways that regulate dauer entry. For example, TGF-β/DAF-7 and insulin/DAF-28 signaling from ASI and ASJ neurons may regulate F47D2.11 GPCR to induce dauer remodeling. Alternatively, F47D2.11 GPCR could also respond to dauer-pheromones released by the intestine [224].

Another possibility is that F47D2.11 GPCR functions in the ASJ to detect fatty acids from *E. coli* bacteria to signal dauer exit. I have described in Chapter 1 that dauer recovery is enhanced in the presence of monounsaturated fatty acids (MUFA) and this requires guanylate cyclase *daf-11* [201]. It is possible that

F47D2.11 GPCR could detect the fatty acids in the ASJ sensory neuron to signal downstream DAF-11 via G-protein for dauer recovery.

Interestingly, AMsh glia and ASI neurons undergo dauer-induced remodeling [204]. In addition, IL sheath glia are associated with IL2 neurons which undergo dendritic arborization in dauer state [208]. In my thesis, I have described *F47D2.11(ns250)* mutation interferes with AMsh glia remodeling but has no effect on IL2 neuronal remodeling. I have yet to determine whether *F47D2.11(ns250)* mutation interferes with dauer-induced ASI remodeling. F47D2.11 GPCR expression in AMsh glia, ASI sensory neuron, and IL sheath glia suggests F47D2.11 GPCR could be a generalized receptor for dauer remodeling regulation. It may be that AMsh glia only express F47D2.11 GPCR, whereas ASI and ILsh glia express F47D2.11 GPCR as well as other related redundant GPCRs. This would suggest mutations in *F47D2.11* cause defect in AMsh glia remodeling. However, *F47D2.11* defect may be compensated by other redundant GPCRs in non-AMsh cells. Likely candidates from the serpentine receptor class Z GPCR family are ZK218.4 and ZC132.9, paralogs of F47D2.11 [225]. ZK218.4, ZC132.9, and F47D2.11 all share many conserved amino acid regions including E278, the site of *ns250* mutation. Perhaps ZK218.4 and ZC132.9 are working redundantly with F47D2.11 in both ASI and IL sheath glia to regulate dauer remodeling. I propose to do RNAi knockdowns of these paralogs to see if dauer-induced remodeling in AMsh glia, ASI, and/or IL2 neurons are affected.

5.3.1 If F47D2.11 GPCR is a receptor, what are the downstream regulators?

If F47D2.11 GPCR functions as a receptor in dauer signaling, how does it regulate the changes in morphology? In the canonical model, GPCR signaling is initiated when a ligand-bound receptor activates heterotrimeric G proteins by acting as a GEF for the G protein α subunit (Gα), catalyzing the exchange of guanosine diphosphate (GDP) for guanosine triphosphate (GTP), and causing the release the Gβγ subunits (which form a single unit) (Fig. 5-1). Both GTP-bound Gα and free Gβγ subunits transduce the signal by engaging intracellular effector molecules until the GTP is hydrolyzed and the subunits re-associate [226]. In addition to activating G proteins, GPCRs can also engage β-arrestin that can transmit a signal independently of G proteins [227].

As discussed in Chapter 4, the transcriptional readout of *ver-1* expression (P*ver-1*::GFP) may not be the best proxy to study dauer remodeling. However, this assay is the most convenient and easiest way to screen for mutant alleles at this time. Therefore, to identify the downstream effector of F47D2.11 GPCR, I suggest doing a candidate RNAi screen using P*ver-1*::GFP expression as the readout. I would target individual downstream candidates, such as G proteins and β-arrestins, in *nsIs22* background and look for P*ver-1*::GFP inhibition (see Chapter 6) [213]. I would prioritize the following most likely candidates. First, I would focus on Gα subunits GPA-2 and GPA-3 that are involved redundantly in the dauer decision [185]. Constitutive activation of either protein results in

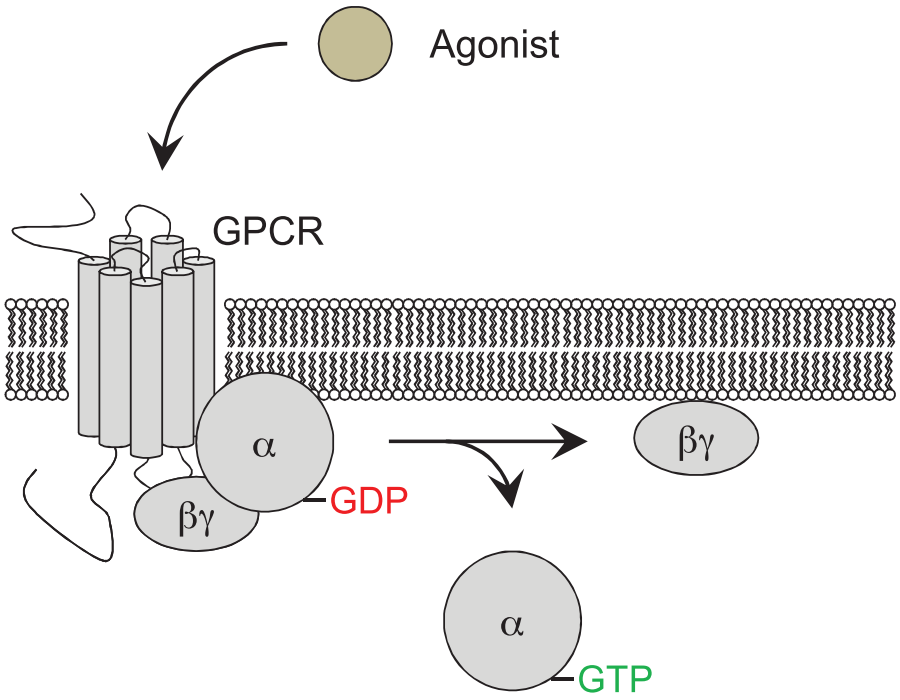

Figure 5-1. Canonical GPCR signaling. Schematic representation of the canonical GPCR signaling. Agonist binds to GPCRs and induces a conformational change that allows the receptor to act as GEF for the Gα subunit, facilitates the exchange of GDP for GTP, triggering release of the complex and dissociation of Gα from Gβγ. Both active, GTP-bound Gα and the released Gβγ dimer stimulate a number of downstream effectors. Figure adapted from Masuho et al., 2015 [230].

constitutive dauer formation [185] while both *gpa-2* and *gpa-3* loss-of-function mutants are partially resistant to dauer entry by pheromone [185,228,229]. I would also prioritize G proteins and β-arrestins that are enriched in the AMsh glia, based on our lab's AMsh glia transcriptome data [221]. Although this gene expression analysis was performed on AMsh glia in the L4/young adult stage, and therefore may not reflect the expression in in dauer larva, enriched transcripts may provide some guidance.

Once a candidate downstream effector protein is identified, I would verify its role in dauer remodeling and recovery by cytoplasmic mixing assays, EM and OP50-GFP recovery assay described in Chapters 2 and 3 using mutant alleles of the candidate protein (see Chapter 6). If mutant alleles are not available, I would generate mutants by inducing mutations in the candidate gene using CRISPR method (see Chapter 6). To determine if the candidate protein functions in AMsh glia to regulate dauer remodeling and exit, I suggest performing cell-specific rescue in AMsh glia and test these strains in the assays (see Chapter 6). Alternatively, if candidate RNAi approach is not fruitful, I propose to do a forward genetic screen using OP50-GFP recovery assay. Cytoplasmic mixing assay and EM analysis are not reasonable methods for screening due to low n and low-throughput nature. Comparatively, OP50-GFP is faster and easier, although still low-throughput compared to P*ver-1*::GFP screen. However, given that OP50-GFP recovery assay would likely reveal other important genes in dauer regulation, this assay may be worth considering.

Previous work in our lab identified *ttx-1* and *ztf-16* transcription factors as well as *aff*-1 fusogen are important regulators of dauer remodeling [206,207]. *ttx-1(p767)* and *ztf-16(ns171)* mutants failed to induce dauer remodeling [206,207] and preliminary data demonstrate dauer recovery delay in *ttx-1(p767)* mutant (not shown). In addition, RNAi knockdowns of *aff-1* show defect in dauer-induced glial remodeling [206]. It is possible that F47D2.11 GPCR regulates *ttx-1*, *ztf-16* and/or *aff-1* transcription in the AMsh glia to induce dauer remodeling. To test this, I propose to create transcriptional reporters of *ttx-1*, *ztf-16,* and *aff-1* using their promoters to drive a GFP transgene and see if *ns250* mutation alters GFP expression. If *F47D2.11* is an upstream regulator of *ttx-1*, *ztf-16,* or *aff-1*, *ns250* mutation would inhibit GFP expression in the AMsh glia. If GFP is not affected, this suggests many possibilities, among which *F47D2.11* could be working in parallel or downstream of these transcriptional factors and fusogen.

Interestingly, AFF-1 is localized at the tip of AMsh glia that undergoes fusion in dauers (Carl Procko, unpublished). To test if F47D2.11 GPCR regulates AFF-1 trafficking to the tip of the glia, I propose to use AFF-1::GFP fusion protein expressed under an AMsh glia promoter and determine if *F47D2.11(ns250)* mutation alters GFP localization at the apical region of AMsh glia. If GFP remains localized at the tip of the glia, this suggests *F47D2.11* does not regulate AFF-1 trafficking and perhaps *F47D2.11* is working in parallel or downstream of *aff-1*. If GFP localization is altered, this suggests many possibilities. It may be that F47D2.11 GPCR signals downstream trafficking machinery to transport AFF-1 to

the tip of the AMsh glia. Another possibility is that F47D2.11(ns250) GPCR inappropriately degrades AFF-1 at the tip of the glia. Further studies may be revealing.

5.4 Does F47D2.11 GPCR function as an adhesion GPCR?

While F47D2.11 GPCR could promote AMsh glia remodeling as a receptor for a diffusible ligand, it could also regulate remodeling as an aGPCR. Many morphological changes occur in dauer animals, including the radial shrinkage of the body circumference. This may physically push the left and right AMsh glia closer in proximity, allowing GPCRs localized at the tip of each cell to interact with one another to signal glial fusion [204]. Several aGPCRs have been shown to undergo similar homophilic trans-trans interactions, and these homophilic associations have been shown to promote aGPCR signaling (see Chapter 1) [145].

To test if F47D2.11 is an aGPCR, I would chimerically restore the expression of *F47D2.11* in one or both AMsh glia and determine the effect on AMsh glial fusion. If hemophilic trans-trans interaction is required to signal amphid glial fusion, I would expect to see fusion rescue only in animals with wild-type GPCR in both AMsh glial cells. This study requires generating animals carrying an unstable extrachromosomal array of the AMsh glia promoter driving expression of both F47D2.11 cDNA and GFP (AMsh glia promoter::GFP::SL2::F47D2.11) in the *F47D2.11(ns841)* early stop mutant with *daf-7(e1372)* temperature-sensitive mutation background to monitor fusion. The

presence of GFP in the glial cells will mark which cells have expression of F47D2.11 wild type protein. First, L1 animals will be selected for GFP expression in one or both glial cells. Then, these animals will be cultivated for more than 48 h at 25°C, which induces dauer entry due to the *daf-7(e1372)* mutation. Similar to the cytoplasmic mixing assay, if L1 animals with mosaic expression in only one of the AMsh glia do not show dauer fusion (as monitored by GFP diffusion), then *F47D2.11* is likely required in both cells. To confirm this, I would select L1 animals with GFP expression in both glial cells, induce dauer by cultivation at 25°C and use EM serial analysis to determine glial fusion (see Chapter 6). If fusion is regulated by aGPCRs through contact-mediated signaling, these animals should exhibit fusion in ~50% of dauer animals.

5.5 Amphid sensory organ remodeling as a model of nervous system plasticity

Although vertebrate glial cells display remarkable morphological plasticity, the relevance of glial plasticity in developmental adaptation remains to be explored. Studying glia in traditional vertebrate models is challenging because these cells are essential for neuronal survival. *C. elegans* possesses glia that resemble vertebrate glia in morphology, function, and molecular characteristics; yet the glia of this animal are not required for neuronal survival [231,232]. Studies in *C. elegans* may prove particularly useful in understanding stress-induced nervous system adaptation. *C. elegans* have a simple and invariant number of neurons and glia, which have stereotyped morphology and connections.

Furthermore, the facile genetics of *C. elegans* facilitates gene discovery, which may prove useful for uncovering the molecular basis of glial actions on facilitating nervous system plasticity and behavioral modification. These observations make *C. elegans* a powerful system in which to understand glial functions in the nervous system and may be able to teach us something about the role of glia in the development and function of the human brain.

6 Materials and Methods

6.1 *C. elegans* strains

C. elegans were cultivated using standard methods [233]. All animals were cultivated at 15°C or 25°C, unless otherwise noted. Bristol N2 strain was used as wild type. Mutants recovered by EMS mutagenesis were outcrossed at least three times before use. Germline transformations were carried out using standard protocols [234]. Co-injection markers used were coelomocyte::GFP, coelomocyte::RFP, or plasmids as otherwise noted. Integrated transgenic strains were generated with UV/trioxalen treatment [235] (Sigma, T6137). Some strains listed below were sourced from the CGC, funded by NIH Office of Research Infrastructure Programs (P40 OD010440).

Alleles and transgenes used or generated in this study:

LGII: *nIs213*[P*egl-6*::GFP; ELK15(*lin-15*(+))]; LGIII: *daf-7(e1372)*; LGIV: *nsIs22*[P*ver-1*::GFP], *dpy-20(e1282);* LGV: *F47D2.11*(*ns250*, *ns820, ns821, ns841, ns842, ns843*, *ns844*, *ns845, ns848, ns852; ns868*, *ttx-1(p767);* LGX: *lin-15(n765), ztf-16(ns171)*; Unmapped: *nsIs855*[P*F28A12.3*::myr-GFP]

Extrachromosomal array used:

nsEx6181/nsEx6182[(fosmid WRM0612aF01); celo::RFP; PBluescript], *nsEx6183*(fosmid WRM0638cF08); celo::RFP; PBluescript], *nsEx6184/nsEx6185*[*F47D2.11* gDNA (fosmid WRM0638cF08); celo::RFP; PBluescript], *nsEx6173*/*nsEx6174*/*nsEx6175*[P*F16F9.3*::F47D2.11 cDNA; celo::GFP; PBluescript], *nsEx6045*/*nsEx6046*/*nsEx6047* [P*dyf-7*::F47D2.11

cDNA; celo::GFP; PBluescript], *nsEx6123*/*nsEx6124*[(P*ptr-10*::F47D2.11 cDNA); celo::RFP; PBluescript], *nsEx6150*[P*F16F9.3*::F47D2.11 cDNA; celo::GFP; PBluescript], *nsEx6125*/ *nsEx6126*/*nsEx6127* [P*F16F9.3*::F47D2.11 cDNA (E278K); celo::GFP; PBluescript], *nsEx6123*[(P*ptr-10*::F47D2.11 cDNA); celo::RFP; PBluescript], *nsEx6124*[(P*mir-228*::F47D2.11 cDNA); celo::RFP; PBluescript], *nsEx6004*[(P*F47D2.11*(2.5kb)::GFP); celo::RFP; PBluescript], *nsEx6005*[(P*F47D2.11*(1.8kb)::GFP); celo::RFP; PBluescript], nsEx6027[celo::RFP; PBluescript], nxEx6187[P*F47D2.11*(2.5kb)::GFP::SL2::NLS::RFP], *nsEx1391*[P*F16F9.3*::GFP; *rol-6(su1006)*], *nsEx5945*[Podr-1::RFP; celo::RFP; PBluescript], *zwEx103*[P*inx-3*::GFP; *lin-15*(+)], *zwEx104*[P*inx-4*::GFP; *lin-15*(+)], *zwEx105*[P*inx-5*::GFP; *lin-15*(+)], *zwEx106*[P*inx-6*::GFP; *lin-15*(+)], *zwEx107*[P*inx-7*::GFP; *lin-15*(+)], *zwEx108*[P*inx-8*::GFP; *lin-15*(+)], *zwEx109*[P*inx-9*::GFP; *lin-15*(+)], *zwEx110*[P*inx-10*::GFP; *lin-15*(+)], *zwEx112*[P*inx-12*::GFP; *lin-15*(+)], *zwEx118*[P*inx-18*::GFP; *lin-15*(+)], *zwEx122*[P*inx-22*::GFP; *lin-15*(+)], *qaEx712* [P*gly-18*::GFP; *dpy-20*(+)]

Table 6-1. *egl-6* promoter bashing plasmids (pSM::GFP vector)

Segment Name	Promoter region
A	Cosmid C46F4: sequence segment 2131-5631
B	Cosmid C46F4: sequence segment 4132-5631
C	Cosmid C46F4: sequence segment 5632-7381
D	Cosmid C46F4: sequence segment 2131-4131

E	Cosmid C46F4: sequence segment 7382-9121
F	Cosmid C46F4: sequence segment 5632-6998
G	Cosmid C46F4: sequence segment 6999-9121
H	Cosmid C46F4: sequence segment 2131-3331
I	Cosmid C46F4: sequence segment 3332-4131
J	Cosmid C46F4: sequence segment 4132-4989
K	Cosmid C46F4: sequence segment 4132-5631
L	Cosmid C46F4: sequence segment 5893-6700
M	Cosmid C46F4: sequence segment 6701-7507
N	Cosmid C46F4: sequence segment 7508-8314
O	Cosmid C46F4: sequence segment 8315-9121
P	Cosmid C46F4: sequence segment 2131-2431
Q	Cosmid C46F4: sequence segment 2432-2731
R	Cosmid C46F4: sequence segment 2732-3031
S	Cosmid C46F4: sequence segment 3032-3331
T	Cosmid C46F4: sequence segment 3332-3631
U	Cosmid C46F4: sequence segment 4990-5390
V	Cosmid C46F4: sequence segment 5391-5790
W	Cosmid C46F4: sequence segment 5791-6190
X	Cosmid C46F4: sequence segment 6721-7201
Y	Cosmid C46F4: sequence segment 7202-7681
Z	Cosmid C46F4: sequence segment 7682-8161

AA	Cosmid C46F4: sequence segment 8162-8641
BB	Cosmid C46F4: sequence segment 8642-9121

6.2 Plasmid construction

Plasmids were constructed using Gibson cloning into the applicable backbone plasmid (Gibson). F47D2.11 cDNA was constructed by cloning each exon sequence from the fosmid WRM0638cF08 and fused using Gibson cloning. For CRISPR-related vectors, plasmids were generated using a site-directed plasmid mutagenesis protocol on pDD162 [236,237].

6.3 Gene identification

A combination of Hawaiian Snip-SNP mapping [212] and whole genome sequencing [238] was used to identify *F47D2.11* using output from galign [239]. *F47D2.11* was confirmed by fosmid rescue, candidate gene analysis, and CRISPR.

6.4 RNAi

Plasmids expressing double-stranded RNA (dsRNA) were obtained from the Ahringer and Vidal libraries [240]. An empty vector was used as the negative control. RNAi was performed by plating L1 *nsIs22* animals onto RNAi bacteria and allowing them to feed at 25°C [241]. ~48 hours later, young adult animals were screened for GFP expression in the AMsh glia.

6.5 Dominance test

Dominance test was performed by crossing hermaphrodite *ns250* mutant to its parental male *nsIs22* strain expressing co-injection marker celo::RFP (and vice versa). F1 cross-progenies with red coelomocytes were selected and screened for GFP expression in the AMsh in both sexes under the dissecting scope.

6.6 Germline transformation and rescue experiments

Plasmid mixes containing the plasmid of interest, co-injection markers, and pBluescript were injected into both gonads of young adult hermaphrodites [234]. Injected animals were singled onto NGM plates and allowed to grow for two generations. Transformed animals based on co-injection markers were picked onto single plates, and screened for stable inheritance of the extrachromosomal array. Only lines from different P_0 injected hermaphrodites were considered independent. For cell-specific rescue experiments, animals expressing co-injection markers were picked as the method above. Lines with stable inheritance of the extrachromosomal array were used to screen for P*ver-1*::GFP restoration.

6.7 Microscopy

P*ver-1*::GFP (*nsIs22*) expression was assayed using a fluorescence dissecting microscope (Leica). Young adult hermaphrodites or dauer animals were scored, excepted as noted. Compound microscope images were taken on an Axioplan II microscope using an AxioCam CCD camera (Zeiss) and analyzed using the Axiovision software (Zeiss). Some images were collected on a DeltaVision Core imaging system (Applied Precision) with a PlanApo 603/1.42 na or UPlanSApo

60x/1.3 oil-immersion objective and a Photometrics CoolSnap HQ camera (Roper Scientific). Images were deconvolved using softWoRx program (GE Healthcare). Some images were collected on a DeltaVision OMX V4/Blaze 3D-SIM super-resolution microscope (GE Healthcare) with a 100x/1.40 UPLSAPO oil objective (Olympus). Structured illumination data sets were reconstructed using softWoRx software (GE Healthcare). Dauer animals for electron microscopy were grown at 25°C and selected for AMsh glial fusion or no fusion based on GFP fluorescence (see cytoplasmic mixing assay for more details). Animals were prepped and sectioned using standard methods [242]. Imaging was performed with an FEI Tecnai G2 Spirit BioTwin transmission electron microscope equipped with a Gatan 4K x 4K digital camera.

6.8 Dauer selection

Animals were starved and dauers selected by treatment with 1% SDS in M9 solution for 15 min. Alternatively, animals carrying the *daf-7*(*e1372*) mutation were induced to form dauers by incubation at 25°C.

6.9 Dye filling assay

DiO (catalog # D-275) or DiI (catalog # D-282) from Molecular Probes stock solution was made at 2 mg/ml in N,N-dimethylformamide. Animals were stained with DiO or DiI (stock solution diluted 1:10,000 in M9 buffer) for 30–60 min, followed by three M9 washes to remove excess dye.

6.10 Cytoplasmic mixing assay to score AMsh glia fusion

Adult animals carrying an *nsEx1391* (AMsh glia::GFP) array were picked to plates seeded with OP50 bacteria, and cultivated at 25°C. From these plates, L1 progeny carrying the *nsEx1391* array in one of the two AMsh glia were picked 24 h later to fresh seeded plates. Mosaic animals were incubated for 48 h at 25°C before scoring GFP presence in either one or both AMsh glia. Animals carrying a *daf-7*(*e1372*) mutation were only scored if they were dauer larvae by morphology at the end of the assay period.

6.11 Dauer recovery assay

6.11.1 Pharyngeal pumping assay

To induce dauer formation, embryos were collected by hypochlorite treatment, washed extensively in water and then approximately 200 embryos were placed onto an NGM plate containing a small lawn of OP50 (~10µL of saturated OP50, 24hr before use). Embryos were allowed to hatch and develop into dauer larva undisturbed at 15°C for at least 120 hours. Failure to include OP50 on the plate resulted in animals that arrested as starved L1 stage larvae. For dauer recovery, dauer animals were individually moved to a plate with a thick lawn of OP50 and incubated at 15°C. Dauers were examined every 30min to 1hour for pharyngeal pumping under the dissecting scope.

6.11.2 OP50-GFP recovery assay

OP50-GFP bacteria (from CGC) were cultivated in LB media. 24 hours before the assay, around 40µL of bacteria were plated evenly on the NGM plates and dried overnight in the dark at 15°C. Dauer animals (see dauer selection) were singled out on the seeded plate and cultivated at 15°C in the dark. Every 30min to 1 hour, dauer animals were screened for GFP accumulation in the pharynx under the dissecting scope.

6.12 Data analysis

Statistical analysis was performed using GraphPad Prism. Statistical parameters including mean ± SEM, and N are reported in the main text, figures, and figure legends. Data is judged to be statistically significant when $p < 0.05$ by Fisher's exact test where appropriate. The rates of onset of OP50-GFP accumulation in the pharynx were plotted as survival from dauer, and were compared by log-rank test using GraphPad Prism 7.

6.13 CRISPR-Cas9 genome editing

Alleles of *F47D2.11* were generated using the co-CRISPR-based genome editing method as previously described [219]. pDD162 was used as a vector backbone, and the following sgRNA sequences were added for each individual CRISPR attempt (E278K and deletion alleles (mix of 2 sgRNAs): 5' ACATGACAACCACTGGAACAAGG 3' and 5' CTTGCTTTTTTTTATTGTTTTGG3'; Venus and SL2::NLS::RFP reporters : 5' ACGGAAATCAAAGCGAACCC 3') to generate *F47D2.11* targeting vectors. A

dpy-10 sgRNA-pDD162-based vector was also generated (5' GCTACCATAGGCACCACGAG 3'). Single-stranded repair oligos were ordered from Sigma (E279K: 5' TTCCTTGTTCCAGTGGTTGTCATGTGGACGaAAATCAAAGCGAACCCGGGTG TTATTCAGA 3'; *dpy-10(cn64):* 5' CACTTGAACTTCAATACGGCAAGATGAGAATGACTGGAAACCGTACCGCATG CGGTGCCTATGGTAGCGGAGCTTCACATGGCTTCAGACCAACAGCCTAT 3'). (Venus and SL2::NLS::RFP transgenes were inserted at the end of *F47D2.11* gene using plasmids: 5' *F47D2.11* homology arm-loxP-reversed *unc-119*(+)-loxP-fluorescent transgene-3' homology arm). For E278K and deletion alleles, N2 animals were injected with the following mix: 50 ng/µl *dpy-10* sgRNA, 50 ng/µl *F47D2.11* targeting vector, 20 ng/µl *dpy-10(cn64)* repair oligo, 20 ng/µl *F47D2.11* repair oligo in 1x injection buffer (20mM potassium phosphate, 3mM potassium citrate, 2% PEG, pH 7.5). F1 animals with Dpy or Rol phenotypes were picked to individual plates, indicating a CRISPR-based editing event had occurred. F1 animals were allowed to lay eggs, and then genotyped for successful co-conversion of the *F47D2.11* locus using PCR and restriction enzyme screening or Cel1 digestion of heteroduplex DNA (Ward 2015). Non-Rol, non-Dpy F2 animals were then singled and homozygosed for the *F47D2.11* mutation or insertion. For Venus and SL2::NLS::RFP transgenes, DP38(*unc-119(ed3)*) animals were injected with the following mix:

10 ng/µl pGH8 (P*rab-8*::mCherry, Addgene #19359), 5 ng/µl pCFJ104 (P*myo-3*::mCherry, Addgene #19328), 2.5 ng/µl pCFJ90 (P*myo-2*::mCherry, Addgene #19327), 50 ng/µl *F47D2.11* targeting vector, 10 ng/µl homologous fluorescent plasmid in 1x injection buffer (20mM potassium phosphate, 3mM potassium citrate, 2% PEG, pH 7.5). Three injected worms per plate were left to starve for 2 weeks at 25°C. Non-red animals were picked individually and allowed to lay eggs, and then genotyped for successful insertion. Removing *unc-119(+)* cassette with Cre recombinase did not change the expression pattern.

7 Appendix 1: Functions of GLR glia in the nervous system of *C. elegans*

7.1 GLR glia of *C. elegans*

My initial thesis proposal aimed to understand the functions of the *C. elegans* GLR glial cells, which are mesodermal glia-like cells. Within the pseudocoelom (body cavity), 3 pairs of GLR cells (dorsal, ventral and lateral) are arranged in a six-fold symmetrical manner around the pharynx, just posterior to the nerve ring (NR), a donut-shaped ring of axons that functions as the brain of the animal [157] (Fig. 7-1). Each GLR cell body projects an anteriorly-directed, sheet-like process that closely apposes the inner face of the NR. These sheet-like processes appear to seal the space between the somatic basement membrane of the muscle and the basement membrane of the pharynx near the anterior end of the NR. Hence, the narrow space between the pharynx and outer tissue anterior to the GLRs is termed accessory pseudocoelom (Z. Altun and D.H. Hall, unpublished). It is not yet clear if there is any material exchange between the accessory and body pseudocoelom. In addition, GLR cells make gap junctions to their target head muscles, as well as to nearby motor neurons that innervate these muscles [157].

Although the morphology and anatomy of GLRs have been characterized, their functions are not well understood. Because of their location, connectivity pattern, and lineage, GLRs seem to share common characteristics with body wall muscle cells. Both GLRs and muscle cells secrete type IV collagen, which is

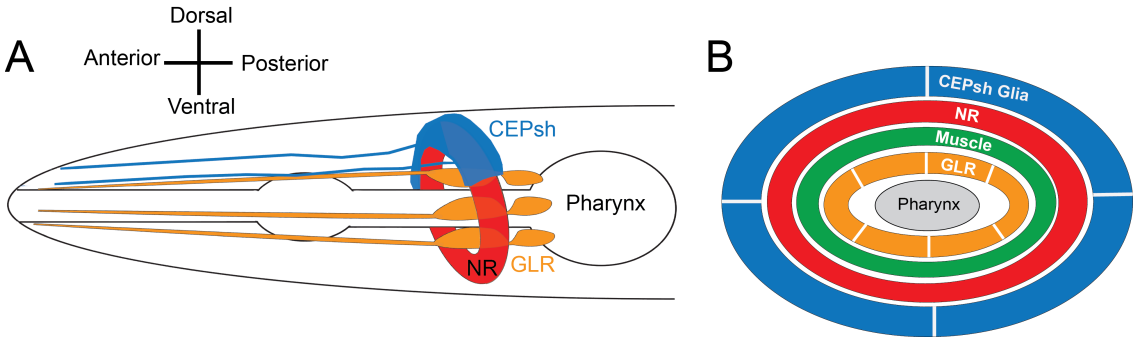

Figure 7-1. Anatomy and positioning of GLR and CEPsh glia respective to the nerve ring (NR). (A) Within the pseudocoelom (body cavity), 3 pairs of GLR cells (dorsal, ventral, and lateral) are arranged in a six-fold symmetrical manner around the pharynx, just posterior to the NR. From each GLR cell body, sheet-like process projects anteriorly to wrap the interior of the muscle-neuron plates of the NR. At the anterior edge of the NR, the processes narrows down to thin rods and terminate at the end of the pharynx. The four CEPsh glia are arranged symmetrically and ensheath the outer face of the NR. **(B)** The schematic of a cross-section through the NR. The four CEPsh glia and six GLR glia are symmetrically oriented without overlapping. The muscle arms insert between the NR and GLR glia.

integrated into the basement membrane of the muscle [243-246]. Furthermore, both cell types express *C. elegans* myoD homolog *hlh-1,* which is required for normal muscle function in late embryogenesis and larval stages [157,247]. *hlh-1* is predicted to drive expression of cell-surface proteins that mediate recognition and contact between GLRs and head muscles [157,247]. Therefore, GLRs are suggested to be mesodermal scaffolding cells that guide muscle arms to

appropriate territories during development [157,231,232]. When any one of the parental cells of the GLRs is killed in the embryo, animals hatch late and arrest at the L1 stage. These animals show an anteriorly-displaced NR and have widespread degeneration and vacuolation in neurons and hypodermis, which may result from disruption of the GLR seal (A. Chisholm, pers. comm.).

What roles might GLR cells have? One exciting possibility is that GLRs modulate coordinated head muscle movement during animal locomotion and foraging. Although glial cells are absent from most neuromuscular junctions in *C. elegans*, GLRs form partnerships with the head muscles and motor neurons that innervate them. These muscles mediate fine motor behaviors that are less stereotypical than the undulations produced by body wall muscles, suggesting a possible need for glial companionship. Such a role would be reminiscent of perisynaptic Schwann cells function in vertebrates [27,243,244,248]. Another appealing possibility is that, together with CEPsh glia, which ensheath the outer portion of the NR [157], GLRs isolate the NR from its surroundings. Thus, GLRs may form a structure resembling the mammalian blood-brain barrier (BBB), which also isolates neurons from their surroundings. However, both functions are, of course, not mutually exclusive.

My studies aim to provide inroads to understanding glial function, and may inform on the roles of glia in coordinating muscle activity as well as in insulating the brain. Determining a potential barrier-like structure around the NR in *C. elegans* would be a novel discovery. This would yield a new model system with

powerful tools of genetic and genomic tools, which, when combined with the complete anatomical reconstruction of the nervous system, will greatly help to understand the development and function of a BBB.

7.2 Determine the existence of a NR barrier in *C. elegans*

To determine whether a barrier shields the NR, I performed a dye penetration assay adapted from dye injection assays in *Drosophila* [249-251]. I collected dyes commonly used in *Drosophila* and zebrafish [249-252] to characterize BBB permeability, including a variety of fluorescent dyes coupled to different sizes of dextran carriers. I performed dye penetration assays by injecting Texas-red (TR) coupled dextran (3, 7, 10kD) and Alexa Fluor (AF)-594 Dextran (10kD) into the pseudocoelomic cavity of *C. elegans* at young adult stage. The NR was visualized using a nematode strain, which carries an integrated GFP transgene (P*nmr-1*::GFP) marking a small number of axons in the NR. If a BBB-like structure exists around the NR, we expect a donut shaped space where the fluorescent dye cannot penetrate. Several injection sites were tested (Fig. 7-2). Potential injection sites included: a) near the isthmus of the pharynx b) near the pharyngeal-intestinal valve c) the space between the distal/proximal gonadal arms (Fig. 7-2). In my hands, the best injection site was between the distal/proximal gonadal arms (Site C Fig. 7-2), which allowed easy access to the pseudocoelomic cavity and showed fast widespread dye dispersal throughout the worm body. Injections at both the

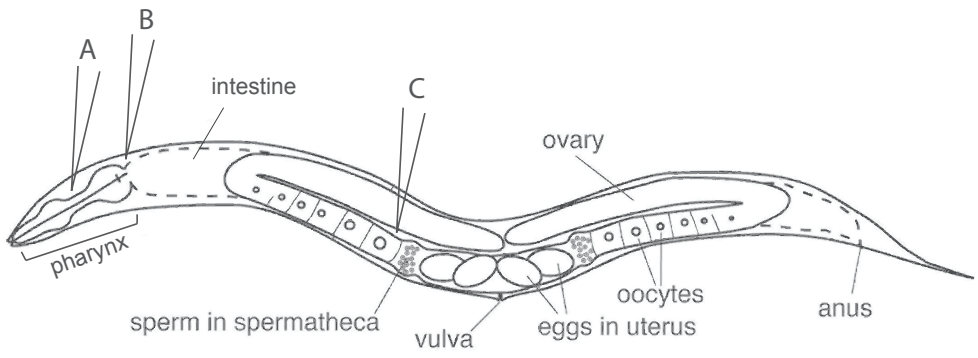

Figure 7-2. Potential injection sites for the dye penetration assay. Dyes were injected into the pseudocoelomic cavity of hermaphrodite *C. elegans* at young adult stage. Potential injection sites include: A) at the isthmus in the pharynx B) near the pharyngeal-intestinal valve C) space between the distal/proximal gonadal arms.

isthmus in the pharynx (Site A Fig. 7-2) and near the pharyngeal-intestinal valve (Site B Fig. 7-2) allowed easy dye dispersal, but I wanted to avoid the chance of damaging the NR area during the procedure.

Next, I tested for the fluorescence persistence of different dyes inside the worm. *C. elegans* possess 3 pairs of coelomocytes in the pseudocoelomic cavity that continuously and nonspecifically endocytose fluid from the pseudocoelom [253]. Initially, I was concerned that the injected dye may be phagocytosed by the coelomocytes before it can reach the NR. Injecting dyes into coelomocyte uptake defective *(Cup)* mutants may allow the dye to accumulate longer in the pseudocoelom. To test, I injected TR-Dextran (3, 7, 10kD) and AF-594 Dextran (10kD) into *cup* mutants and N2 animals. In both strains, all the dyes fluoresced

over 5 hours post-injection. AF-594 Dextran dye fluoresced brighter and more consistently compared to different sized TR-Dextrans. Therefore, I continued the following dye penetration assays using AF-594 Dextran dye.

To visualize the NR, I injected AF-594 Dextran dye into a transgenic strain carrying a P*nmr-1*::GFP reporter that marks few axons around the NR but otherwise is essentially WT. After injection, animals were allowed to recover for 4 hours in the dark. The injected animals were then mounted on 2% agar pads+3mM NaN_3 for paralysis. To generate a transverse view of the worm, injected worms were analyzed using a deconvolution microscope (Deltavision Image Restoration Microscope, Applied Precision/Olympus), available at the Rockefeller BioImaging Facility. Images were analyzed using SoftWoRx software (Applied Precision). Z-stack sections of the worm were reconstructed into 3D images using the Imaris program. Figure 7-3 shows a transverse section through the NR in one of the operated worms. NR is labeled green and the dye is shown in red. AF-594 Dextran dye seems to accumulate in the narrow space between the pharynx and the NR as well as outside of the NR. Preliminary data suggests there exists a donut-shaped barrier around the NR (Fig. 7-3).

7.3 Identification and characterization of GLR markers

GLR-specific reporters were unavailable at the start of this project. Therefore, I set out to identify the regulatory elements that drive gene expression specifically in the six GLRs, which I planned to use to express fluorescent markers in the GLRs. This would allow identification and ablation of GLR cells in

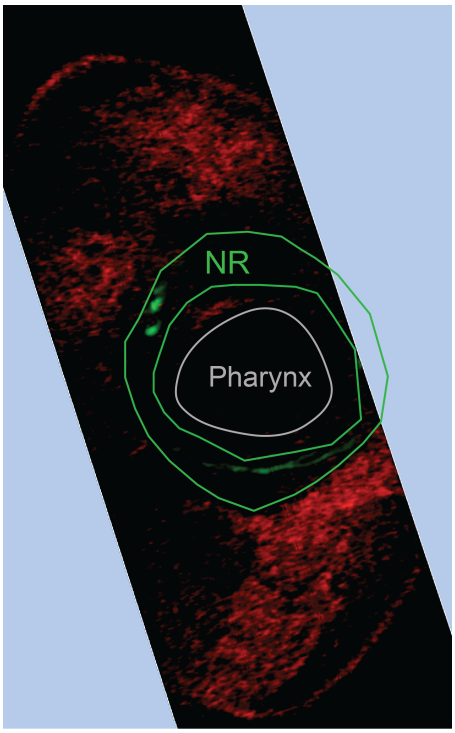

Figure 7-3. Potential barrier around the NR. Transverse section though the NR in young adult hermaphrodites injected with 2.5mM AF-594 Dextran (10kD) dye (red). The NR is shown in green (P*nmr-1*::GFP). The dye accumulates on both sides of the donut-shaped ring, suggesting a potential seal around the NR.

first larval stage animals by laser microsurgery [254,255], or to drive expression of cell-death promoting genes. I identified three classes of reporter genes (*egl-6*, innexins and *gly-18*) driving GFP expression in variable number of GLRs among other cells. I then characterized the expression pattern of these transgenes, which will be described below:

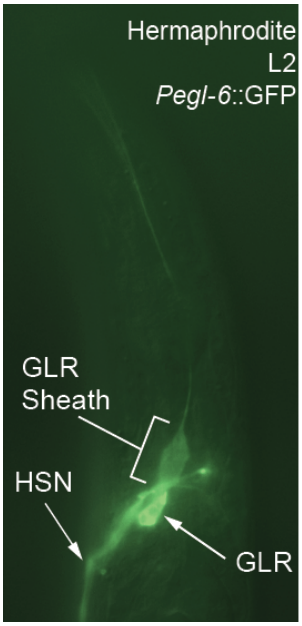

Figure 7-4. Expression pattern of P*egl-6*::GFP reporter transgene.
egl-6 directed expression in L2 hermaphrodite animal shows GFP labeling in GLR and HSN motor neuron.

egl-6 transgene reporter: Worms expressing the transgene P*egl-6*::GFP are labeled primarily in the HSN neurons and GLR cells (two dorsal and two ventral), with weaker expression in DVA tail interneuron and occasional expression in the lateral interneurons SDQL and SDQR. As shown in Figure 7-4, GLR shows a clear cell body with sheet-like process that tapers out anteriorly. P*egl-6*::GFP is brighter in ventral GLRs compared to dorsal GLRs.

Innexins transgene reporters: GLRs express large variety of innexins, including *inx*-3, *inx-4*, *inx-6*, *inx-7*, *inx-8*, *inx-9*, *inx-10*, *inx-12*, *inx-18*, and *inx-22*. All 11 strains showed weak GFP expression in all labeled cells. Five of these strains (*inx-4*, *inx-7*, *inx-8*, *inx-18*, and *inx-22*) express GFP only in the two lateral GLR cells.

gly-18 transgene reporter: The *gly-18* promoter drives GFP expression in all six GLRs at the embryonic stage (Georgia Rapti, pers. comm.). I characterized the expression pattern of these animals in post-embryonic stages. While I can detect the six GLR cell bodies, I am unable to see the sheaths clearly. There are 15 additional cells expressing GFP, most of them in close proximity to the GLRs, making this strain not ideal for laser or genetic ablations.

Promoter bashing

To create a GLR-specific reporter, I conducted promoter bashing on the 7kb *egl-6* locus (bases 2131-9121 in cosmid C46F4). Using molecular cloning techniques, I generated 28 promoter segments as shown in Figure 7-5.

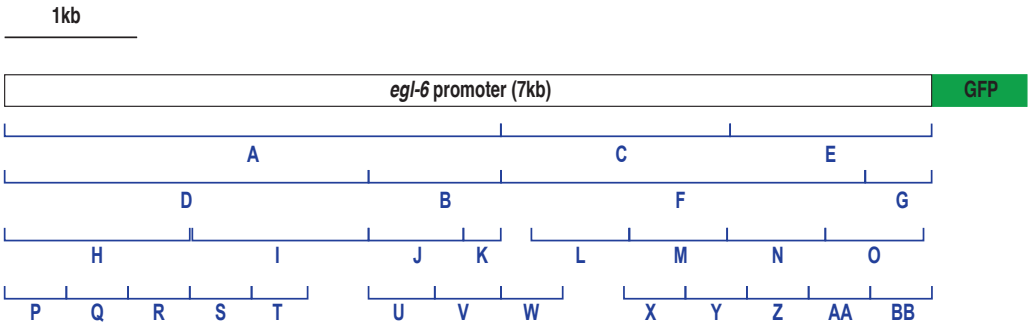

Figure 7-5. Promoter bashing *egl-6* locus (7kb). The original *egl-6* promoter spans 7.0kb across cosmid C46F4. Portions of the original 7kb region were systematically deleted using molecular cloning techniques. Segments A-Z, AA, and BB are regions upstream of *egl-6* gene start site. These promoter segments were cloned into pSM::GFP vector for transformation using N2 animals. Segment regions listed in Chapter 6.

Segments A, B, D, H-K, P-V are regions upstream of *egl-6* gene start site. I cloned these promoter regions into the pSM::GFP vector and injected them individually into N2 animals for transformation (see Chapter 6). I monitored the progeny for GFP expression specifically in GLRs. Unfortunately, none of these regions labeled GLRs specifically. In fact, some segments, like segment H and O, introduced labeling in new cell types. I did not observe any obvious pattern to aid me in selective bashing.

7.4 GLR glia ablation using microbeam laser

I tested GLR laser ablations using transgenic strains described above. I successfully ablated two GLRs in P*egl-6*::GFP worms at L2 larval stage. I found that GLR ablation at L2 stage is easier because the cell bodies are larger and easier to detect. Ablation success was confirmed by the lack of GFP expression and nearby cells looked healthy right after ablation and 48 hours post-ablation. Due to lack of GLR-specific reporter, ablation studies were put on hold.

7.5 Conclusion

GLR glia are poorly characterized cells and only have few speculative reports of their function in the literature. The goal of this project was to identify a novel function of the GLR cells. Although I took the steps discussed in this chapter, I was unable to isolate a GLR-specific reporter, which was a crucial element to continuing this project. Given the inability to progress this project due to the lack of the GLR-specific reporter, I decided to turn my attention to the stress-induced glial remodeling project.

8 Bibliography

[1] McEwen BS, Sapolsky RM. Stress and cognitive function. Current Opinion in Neurobiology 1995;5:205–16.

[2] Nicholson WL, Munakata N, Horneck G, Melosh HJ, Setlow P. Resistance of Bacillus endospores to extreme terrestrial and extraterrestrial environments. Microbiol Mol Biol Rev 2000;64:548–72.

[3] Cano RJ, Borucki MK. Revival and identification of bacterial spores in 25- to 40-million-year-old Dominican amber. Science 1995;268:1060–4.

[4] Schmidt-Nielsen K, Taylor CR, Shkolnik A. Desert snails: problems of heat, water and food. J Exp Biol 1971;55:385–98.

[5] Arad Z, HELLER J. Resistance to desiccation and distribution patterns in the land snail Sphincterochila. Journal of Zoology 2009;218:353–64. doi:10.1111/j.1469-7998.1989.tb02549.x.

[6] Secor SM, Lignot J-H. Morphological plasticity of vertebrate aestivation. Prog Mol Subcell Biol 2010;49:183–208. doi:10.1007/978-3-642-02421-4_9.

[7] Melvin RG, Andrews MT. Torpor induction in mammals: recent discoveries fueling new ideas. Trends Endocrinol Metab 2009;20:490–8. doi:10.1016/j.tem.2009.09.005.

[8] Loomis SH. Diapause and estivation in sponges. Prog Mol Subcell Biol 2010;49:231–43. doi:10.1007/978-3-642-02421-4_11.

[9] Loomis SH, Bettridge A, Branchini BR. The effects of elevated osmotic concentration on control of germination in the gemmules of freshwater sponges Eunapius fragilis and Anheteromeyania ryderi. Physiol Biochem Zool 2009;82:388–95. doi:10.1086/589901.

[10] Wourms JP. Developmental biology of annual fishes. I. Stages in the normal development of Austrofundulus myersi Dahl. J Exp Zool 1972;182:143–67. doi:10.1002/jez.1401820202.

[11] Wourms JP. The developmental biology of annual fishes. 3. Pre-embryonic and embryonic diapause of variable duration in the eggs of annual fishes. J Exp Zool 1972;182:389–414. doi:10.1002/jez.1401820310.

[12] Wourms JP. The developmental biology of annual fishes. II. Naturally occurring dispersion and reaggregation of blastomers during the development of annual fish eggs. J Exp Zool 1972;182:169–200. doi:10.1002/jez.1401820203.

[13] Hrbek T, Larson A. THE EVOLUTION OF DIAPAUSE IN THE KILLIFISH FAMILY RIVULIDAE (ATHERINOMORPHA, CYPRINODONTIFORMES): A MOLECULAR PHYLOGENETIC AND BIOGEOGRAPHIC PERSPECTIVE. Evolution 1999;53:1200–16. doi:10.1111/j.1558-5646.1999.tb04533.x.

[14] Dance A. Live fast, die young. Nature 2016;535:453–5. doi:10.1038/535453a.

[15] Podrabsky JE, Carpenter JF, Hand SC. Survival of water stress in annual fish embryos: dehydration avoidance and egg envelope amyloid fibers. Am J Physiol Regul Integr Comp Physiol 2001;280:R123–31. doi:10.1152/ajpregu.2001.280.1.R123.

[16] Machado BE, Podrabsky JE. Salinity tolerance in diapausing embryos of the annual killifish Austrofundulus limnaeus is supported by exceptionally low water and ion permeability. J Comp Physiol B, Biochem Syst Environ Physiol 2007;177:809–20. doi:10.1007/s00360-007-0177-0.

[17] Podrabsky JE, Somero GN. An inducible 70 kDa-class heat shock protein is constitutively expressed during early development and diapause in the annual killifish Austrofundulus limnaeus. Cell Stress Chaperones 2007;12:199–204.

[18] Romney AL, Podrabsky JE. Transcriptomic analysis of maternally provisioned cues for phenotypic plasticity in the annual killifish, Austrofundulus limnaeus. Evodevo 2017;8:6. doi:10.1186/s13227-017-0069-7.

[19] Podrabsky JE, Garrett IDF, Kohl ZF. Alternative developmental pathways associated with diapause regulated by temperature and maternal influences in embryos of the annual killifish Austrofundulus limnaeus. J Exp Biol 2010;213:3280–8. doi:10.1242/jeb.045906.

[20] Romney ALT, Davis EM, Corona MM, Wagner JT, Podrabsky JE. Temperature-dependent vitamin D signaling regulates developmental trajectory associated with diapause in an annual killifish. Proc Natl

Acad Sci U S A 2018;115:12763–8. doi:10.1073/pnas.1804590115.

[21] Podrabsky JE, Wilson NE. Hypoxia and Anoxia Tolerance in the Annual Killifish Austrofundulus limnaeus. Integr Comp Biol 2016;56:500–9. doi:10.1093/icb/icw092.

[22] Tatar M, Yin C. Slow aging during insect reproductive diapause: why butterflies, grasshoppers and flies are like worms. Exp Gerontol 2001;36:723–38.

[23] Yakubu A-A, Saenz R, Stein J, Jones LE. Monarch butterfly spatially discrete advection model. Math Biosci 2004;190:183–202.

[24] Awasaki T, Lai S-L, Ito K, Lee T. Organization and postembryonic development of glial cells in the adult central brain of Drosophila. J Neurosci 2008;28:13742–53. doi:10.1523/JNEUROSCI.4844-08.2008.

[25] Cajal RS. Histology of the Nervous System. New York: Oxford University Press; 1911.

[26] Doherty J, Logan MA, Tasdemir OE, Freeman MR. Ensheathing glia function as phagocytes in the adult Drosophila brain. J Neurosci 2009;29:4768–81. doi:10.1523/JNEUROSCI.5951-08.2009.

[27] Meyer-Franke A, Kaplan MR, Pfieger FW, Barres BA. Characterization of the signaling interactions that promote the survival and growth of developing retinal ganglion cells in culture. Neuron 1995;15:805–19.

[28] Rakic P. Mode of cell migration to the superficial layers of fetal monkey neocortex. J Comp Neurol 1972;145:61–83. doi:10.1002/cne.901450105.

[29] Rakic P. Neuron-glia relationship during granule cell migration in developing cerebellar cortex. A Golgi and electronmicroscopic study in Macacus Rhesus. J Comp Neurol 1971;141:283–312. doi:10.1002/cne.901410303.

[30] Fishell G, Hatten ME. Astrotactin provides a receptor system for CNS neuronal migration. Development 1991;113:755–65.

[31] Elias LAB, Wang DD, Kriegstein AR. Gap junction adhesion is necessary for radial migration in the neocortex. Nature 2007;448:901–

7. doi:10.1038/nature06063.

[32] Panatier A, Theodosis DT, Mothet J-P, Touquet B, Pollegioni L, Poulain DA, et al. Glia-derived D-serine controls NMDA receptor activity and synaptic memory. Cell 2006;125:775–84. doi:10.1016/j.cell.2006.02.051.

[33] Robitaille R. Modulation of synaptic efficacy and synaptic depression by glial cells at the frog neuromuscular junction. Neuron 1998;21:847–55.

[34] Shimizu H, Watanabe E, Hiyama TY, Nagakura A, Fujikawa A, Okado H, et al. Glial Nax channels control lactate signaling to neurons for brain [Na+] sensing. Neuron 2007;54:59–72. doi:10.1016/j.neuron.2007.03.014.

[35] Porter JT, McCarthy KD. Hippocampal astrocytes in situ respond to glutamate released from synaptic terminals. J Neurosci 1996;16:5073–81.

[36] Wang Y, Apicella AJ, Lee S-K, Ezcurra M, Slone RD, Goldmit M, et al. A glial DEG/ENaC channel functions with neuronal channel DEG-1 to mediate specific sensory functions in C. elegans. Embo J 2008;27:2388–99. doi:10.1038/emboj.2008.161.

[37] Ballanyi K, Panaitescu B, Ruangkittisakul A. Control of breathing by "nerve glue". Sci Signal 2010;3:pe41. doi:10.1126/scisignal.3147pe41.

[38] Gourine AV, Kasymov V, Marina N, Tang F, Figueiredo MF, Lane S, et al. Astrocytes control breathing through pH-dependent release of ATP. Science 2010;329:571–5. doi:10.1126/science.1190721.

[39] Bilbo SD, Block CL, Bolton JL, Hanamsagar R, Tran PK. Beyond infection - Maternal immune activation by environmental factors, microglial development, and relevance for autism spectrum disorders. Experimental Neurology 2018;299:241–51. doi:10.1016/j.expneurol.2017.07.002.

[40] Sofroniew MV. Astrocyte barriers to neurotoxic inflammation. Nat Rev Neurosci 2015;16:249–63. doi:10.1038/nrn3898.

[41] Carter CJ, Blizard RA. Autism genes are selectively targeted by environmental pollutants including pesticides, heavy metals,

bisphenol A, phthalates and many others in food, cosmetics or household products. Neurochem Int 2016. doi:10.1016/j.neuint.2016.10.011.

[42] Zamanian JL, Xu L, Foo LC, Nouri N, Zhou L, Giffard RG, et al. Genomic analysis of reactive astrogliosis. J Neurosci 2012;32:6391–410. doi:10.1523/JNEUROSCI.6221-11.2012.

[43] Anderson MA, Burda JE, Ren Y, Ao Y, O'Shea TM, Kawaguchi R, et al. Astrocyte scar formation aids central nervous system axon regeneration. Nature 2016;532:195–200. doi:10.1038/nature17623.

[44] Crotti A, Ransohoff RM. Microglial Physiology and Pathophysiology: Insights from Genome-wide Transcriptional Profiling. Immunity 2016;44:505–15. doi:10.1016/j.immuni.2016.02.013.

[45] Liddelow SA, Guttenplan KA, Clarke LE, Bennett FC, Bohlen CJ, Schirmer L, et al. Neurotoxic reactive astrocytes are induced by activated microglia. Nature 2017;541:481–7. doi:10.3758/BF03193146.

[46] Herz J, Filiano AJ, Smith A, Yogev N, Kipnis J. Myeloid Cells in the Central Nervous System. Immunity 2017;46:943–56. doi:10.1016/j.immuni.2017.06.007.

[47] Klein RS, Hunter CA. Protective and Pathological Immunity during Central Nervous System Infections. Immunity 2017;46:891–909. doi:10.1016/j.immuni.2017.06.012.

[48] Kim SU, de Vellis J. Microglia in health and disease. J Neurosci Res 2005;81:302–13. doi:10.1002/jnr.20562.

[49] Rivest S. Regulation of innate immune responses in the brain. Nat Rev Immunol 2009;9:429–39. doi:10.1038/nri2565.

[50] Rio-Hortega PD, Penfield W. Cytology & [and] cellular pathology of the nervous system. New York: Hoeber; 1932.

[51] Ginhoux F, Greter M, Leboeuf M, Nandi S, See P, Gokhan S, et al. Fate mapping analysis reveals that adult microglia derive from primitive macrophages. Science 2010;330:841–5. doi:10.1126/science.1194637.

[52] Deverman BE, Patterson PH. Cytokines and CNS development.

Neuron 2009;64:61–78. doi:10.1016/j.neuron.2009.09.002.

[53] McHugh D, Hu SSJ, Rimmerman N, Juknat A, Vogel Z, Walker JM, et al. N-arachidonoyl glycine, an abundant endogenous lipid, potently drives directed cellular migration through GPR18, the putative abnormal cannabidiol receptor. BMC Neurosci 2010;11:44. doi:10.1186/1471-2202-11-44.

[54] Salter MW, Beggs S. Sublime microglia: expanding roles for the guardians of the CNS. Cell 2014;158:15–24. doi:10.1016/j.cell.2014.06.008.

[55] Nimmerjahn A, Kirchhoff F, Helmchen F. Resting microglial cells are highly dynamic surveillants of brain parenchyma in vivo. Science 2005;308:1314–8. doi:10.1126/science.1110647.

[56] Frost JL, Schafer DP. Microglia: Architects of the Developing Nervous System. Trends Cell Biol 2016;26:587–97. doi:10.1016/j.tcb.2016.02.006.

[57] Mosser C-A, Baptista S, Arnoux I, Audinat E. Microglia in CNS development: Shaping the brain for the future. Prog Neurobiol 2017;149-150:1–20. doi:10.1016/j.pneurobio.2017.01.002.

[58] Gemma C, Bachstetter AD. The role of microglia in adult hippocampal neurogenesis. Front Cell Neurosci 2013;7:229. doi:10.3389/fncel.2013.00229.

[59] Nistico R, Salter E, Nicolas C, Feligioni M, Mango D, Bortolotto ZA, et al. Synaptoimmunology - roles in health and disease. Mol Brain 2017;10:26. doi:10.1186/s13041-017-0308-9.

[60] Schafer DP, Stevens B. Synapse elimination during development and disease: immune molecules take centre stage. Biochem Soc Trans 2010;38:476–81. doi:10.1042/BST0380476.

[61] Schafer DP, Lehrman EK, Stevens B. The “quad-partite” synapse: microglia-synapse interactions in the developing and mature CNS. Glia 2013;61:24–36. doi:10.1002/glia.22389.

[62] Tremblay M-E, Lowery RL, Majewska AK. Microglial interactions with synapses are modulated by visual experience. PLoS Biol 2010;8:e1000527. doi:10.1371/journal.pbio.1000527.

[63] Chen Z, Trapp BD. Microglia and neuroprotection. J Neurochem 2016;136 Suppl 1:10–7. doi:10.1111/jnc.13062.

[64] Vinet J, Weering HRJV, Heinrich A, Kalin RE, Wegner A, Brouwer N, et al. Neuroprotective function for ramified microglia in hippocampal excitotoxicity. J Neuroinflammation 2012;9:27. doi:10.1186/1742-2094-9-27.

[65] Lyman M, Lloyd DG, Ji X, Vizcaychipi MP, Ma D. Neuroinflammation: the role and consequences. Neurosci Res 2014;79:1–12. doi:10.1016/j.neures.2013.10.004.

[66] Ransohoff RM, Schafer D, Vincent A, Blachere NE, Bar-Or A. Neuroinflammation: Ways in Which the Immune System Affects the Brain. Neurotherapeutics 2015;12:896–909. doi:10.1007/s13311-015-0385-3.

[67] Liu Z, Fan Y, Won SJ, Neumann M, Hu D, Zhou L, et al. Chronic treatment with minocycline preserves adult new neurons and reduces functional impairment after focal cerebral ischemia. Stroke 2007;38:146–52. doi:10.1161/01.STR.0000251791.64910.cd.

[68] Kettenmann H, Hanisch U-K, Noda M, Verkhratsky A. Physiology of microglia. Physiol Rev 2011;91:461–553. doi:10.1152/physrev.00011.2010.

[69] Cherry JD, Olschowka JA, O'Banion MK. Neuroinflammation and M2 microglia: the good, the bad, and the inflamed. J Neuroinflammation 2014;11:98. doi:10.1186/1742-2094-11-98.

[70] Loane DJ, Kumar A. Microglia in the TBI brain: The good, the bad, and the dysregulated. Experimental Neurology 2016;275 Pt 3:316–27. doi:10.1016/j.expneurol.2015.08.018.

[71] Nakagawa Y, Chiba K. Diversity and plasticity of microglial cells in psychiatric and neurological disorders. Pharmacol Ther 2015;154:21–35. doi:10.1016/j.pharmthera.2015.06.010.

[72] Orihuela R, McPherson CA, Harry GJ. Microglial M1/M2 polarization and metabolic states. British Journal of Pharmacology 2016;173:649–65. doi:10.1111/bph.13139.

[73] Ransohoff RM. A polarizing question: do M1 and M2 microglia exist? Nat Neurosci 2016;19:987–91. doi:10.1038/nn.4338.

[74] Xu H, Wang Z, Li J, Wu H, Peng Y, Fan L, et al. The Polarization States of Microglia in TBI: A New Paradigm for Pharmacological Intervention. Neural Plast 2017;2017:5405104. doi:10.1155/2017/5405104.

[75] Mahad DJ, Ransohoff RM. The role of MCP-1 (CCL2) and CCR2 in multiple sclerosis and experimental autoimmune encephalomyelitis (EAE). Semin Immunol 2003;15:23–32.

[76] Kawanokuchi J, Mizuno T, Takeuchi H, Kato H, Wang J, Mitsuma N, et al. Production of interferon-gamma by microglia. Mult Scler 2006;12:558–64. doi:10.1177/1352458506070763.

[77] Mosser DM, Edwards JP. Exploring the full spectrum of macrophage activation. Nat Rev Immunol 2008;8:958–69. doi:10.1038/nri2448.

[78] Chhor V, Le Charpentier T, Lebon S, Ore M-V, Celador IL, Josserand J, et al. Characterization of phenotype markers and neuronotoxic potential of polarised primary microglia in vitro. Brain Behav Immun 2013;32:70–85. doi:10.1016/j.bbi.2013.02.005.

[79] Davis MJ, Tsang TM, Qiu Y, Dayrit JK, Freij JB, Huffnagle GB, et al. Macrophage M1/M2 polarization dynamically adapts to changes in cytokine microenvironments in Cryptococcus neoformans infection. MBio 2013;4:e00264–13. doi:10.1128/mBio.00264-13.

[80] Franco R, Fernandez-Suarez D. Alternatively activated microglia and macrophages in the central nervous system. Prog Neurobiol 2015;131:65–86. doi:10.1016/j.pneurobio.2015.05.003.

[81] Subramanian A, Siefert M, Banerjee S, Vishal K, Bergmann KA, Curts CCM, et al. Remodeling of peripheral nerve ensheathment during the larval-to-adult transition in Drosophila. Dev Neurobiol 2017;77:1144–60. doi:10.1002/dneu.22502.

[82] Che Y, Hou L, Sun F, Zhang C, Liu X, Piao F, et al. Taurine protects dopaminergic neurons in a mouse Parkinson's disease model through inhibition of microglial M1 polarization. Cell Death Dis 2018;9:435. doi:10.1038/s41419-018-0468-2.

[83] Ponomarev ED, Maresz K, Tan Y, Dittel BN. CNS-derived interleukin-4 is essential for the regulation of autoimmune inflammation and induces a state of alternative activation in microglial cells. J Neurosci

2007;27:10714–21. doi:10.1523/JNEUROSCI.1922-07.2007.

[84] Colton CA. Heterogeneity of microglial activation in the innate immune response in the brain. J Neuroimmune Pharmacol 2009;4:399–418. doi:10.1007/s11481-009-9164-4.

[85] Zhou X, Spittau B, Krieglstein K. TGFbeta signalling plays an important role in IL4-induced alternative activation of microglia. J Neuroinflammation 2012;9:210. doi:10.1186/1742-2094-9-210.

[86] Holcomb IN, Kabakoff RC, Chan B, Baker TW, Gurney A, Henzel W, et al. FIZZ1, a novel cysteine-rich secreted protein associated with pulmonary inflammation, defines a new gene family. Embo J 2000;19:4046–55. doi:10.1093/emboj/19.15.4046.

[87] Willment JA, Lin H-H, Reid DM, Taylor PR, Williams DL, Wong SYC, et al. Dectin-1 expression and function are enhanced on alternatively activated and GM-CSF-treated macrophages and are negatively regulated by IL-10, dexamethasone, and lipopolysaccharide. J Immunol 2003;171:4569–73.

[88] Raes G, Van den Bergh R, De Baetselier P, Ghassabeh GH, Scotton C, Locati M, et al. Arginase-1 and Ym1 are markers for murine, but not human, alternatively activated myeloid cells. J Immunol 2005;174:6561–authorreply6561–2.

[89] Morris SMJ. Arginine metabolism: boundaries of our knowledge. J Nutr 2007;137:1602S–1609S. doi:10.1093/jn/137.6.1602S.

[90] Neumann H, Takahashi K. Essential role of the microglial triggering receptor expressed on myeloid cells-2 (TREM2) for central nervous tissue immune homeostasis. J Neuroimmunol 2007;184:92–9. doi:10.1016/j.jneuroim.2006.11.032.

[91] Saba K, Denda-Nagai K, Irimura T. A C-type lectin MGL1/CD301a plays an anti-inflammatory role in murine experimental colitis. Am J Pathol 2009;174:144–52. doi:10.2353/ajpath.2009.080235.

[92] Shechter R, London A, Varol C, Raposo C, Cusimano M, Yovel G, et al. Infiltrating blood-derived macrophages are vital cells playing an anti-inflammatory role in recovery from spinal cord injury in mice. PLoS Med 2009;6:e1000113. doi:10.1371/journal.pmed.1000113.

[93] Lisi L, Ciotti GMP, Braun D, Kalinin S, Curro D, Russo Dello C, et al.

Expression of iNOS, CD163 and ARG-1 taken as M1 and M2 markers of microglial polarization in human glioblastoma and the surrounding normal parenchyma. Neurosci Lett 2017;645:106–12. doi:10.1016/j.neulet.2017.02.076.

[94] Subramaniam SR, Federoff HJ. Targeting Microglial Activation States as a Therapeutic Avenue in Parkinson's Disease. Front Aging Neurosci 2017;9:176. doi:10.3389/fnagi.2017.00176.

[95] Gao Z, Zhu Q, Zhang Y, Zhao Y, Cai L, Shields CB, et al. Reciprocal modulation between microglia and astrocyte in reactive gliosis following the CNS injury. Mol Neurobiol 2013;48:690–701. doi:10.1007/s12035-013-8460-4.

[96] da Fonseca ACC, Matias D, Garcia C, Amaral R, Geraldo LH, Freitas C, et al. The impact of microglial activation on blood-brain barrier in brain diseases. Front Cell Neurosci 2014;8:362. doi:10.3389/fncel.2014.00362.

[97] Dudvarski Stankovic N, Teodorczyk M, Ploen R, Zipp F, Schmidt MHH. Microglia-blood vessel interactions: a double-edged sword in brain pathologies. Acta Neuropathol 2016;131:347–63. doi:10.1007/s00401-015-1524-y.

[98] Sofroniew MV, Vinters HV. Astrocytes: biology and pathology. Acta Neuropathol 2010;119:7–35. doi:10.1007/s00401-009-0619-8.

[99] Clarke LE, Barres BA. Emerging roles of astrocytes in neural circuit development. Nat Rev Neurosci 2013;14:311–21. doi:10.1038/nrn3484.

[100] Chung W-S, Clarke LE, Wang GX, Stafford BK, Sher A, Chakraborty C, et al. Astrocytes mediate synapse elimination through MEGF10 and MERTK pathways. Nature 2013;504:394–400. doi:10.1038/nature12776.

[101] Liddelow S, Barres B. SnapShot: Astrocytes in Health and Disease. Cell 2015;162:1170–1. doi:10.1016/j.cell.2015.08.029.

[102] Hawkins B, Davis T. The Blood-Brain Barrier/Neurovascular Unit in Health and Disease. Pharmacol Rev 2005;57:173–85. doi:10.1124/pr.57.2.4.

[103] Shi L, Adams M, Long A, Carter C, Bennett C, Sonntag W, et al.

Spatial Learning and Memory Deficits after Whole-Brain Irradiation are Associated with Changes in NMDA Receptor Subunits in the Hippocampus. Radiation Research 2007;166:892–9. doi:10.1667/RR0588.1.

[104] Tariot PN, Farlow MR, Grossberg GT, Graham SM, McDonald S, Gergel I. Memantine treatment in patients with moderate to severe Alzheimer disease already receiving donepezil: a randomized controlled trial. Jama 2004;291:317–24.

[105] Chamoun R, Suki D, Gopinath SP, Goodman JC, Robertson C. Role of extracellular glutamate measured by cerebral microdialysis in severe traumatic brain injury. J Neurosurg 2010;113:564–70. doi:10.3171/2009.12.JNS09689.

[106] Sanchez MC, Benitez A, Ortloff L, Green LM. Alterations in glutamate uptake in NT2-derived neurons and astrocytes after exposure to gamma radiation. Radiation Research 2009;171:41–52. doi:10.1667/RR1361.1.

[107] Pandya JD, Pauly JR, Nukala VN, Sebastian AH, Day KM, Korde AS, et al. Post-Injury Administration of Mitochondrial Uncouplers Increases Tissue Sparing and Improves Behavioral Outcome following Traumatic Brain Injury in Rodents. J Neurotrauma 2007;24:798–811. doi:10.1089/neu.2006.3673.

[108] Radak D, Katsiki N, Resanovic I, Jovanovic A, Sudar-Milovanovic E, Zafirovic S, et al. Apoptosis and Acute Brain Ischemia in Ischemic Stroke. Curr Vasc Pharmacol 2017;15:115–22.

[109] Vijayan M, Reddy PH. Stroke, Vascular Dementia, and Alzheimer's Disease: Molecular Links. J Alzheimers Dis 2016;54:427–43. doi:10.3233/JAD-160527.

[110] Rosenberg PA, Aizenman E. Hundred-fold increase in neuronal vulnerability to glutamate toxicity in astrocyte-poor cultures of rat cerebral cortex. Neurosci Lett 1989;103:162–8.

[111] Lepore AC, O'Donnell J, Kim AS, Yang EJ, Tuteja A, Haidet-Phillips A, et al. Reduction in expression of the astrocyte glutamate transporter, GLT1, worsens functional and histological outcomes following traumatic spinal cord injury. Glia 2011;59:1996–2005. doi:10.1002/glia.21241.

[112] Tanaka K, Watase K, Manabe T, Yamada K, Watanabe M, Takahashi K, et al. Epilepsy and exacerbation of brain injury in mice lacking the glutamate transporter GLT-1. Science 1997;276:1699–702.

[113] Hayakawa K, Esposito E, Wang X, Terasaki Y, Liu Y, Xing C, et al. Transfer of mitochondria from astrocytes to neurons after stroke. Nature 2016;535:551–5. doi:10.1038/nature18928.

[114] Iwata-Ichikawa E, Kondo Y, Miyazaki I, Asanuma M, Ogawa N. Glial Cells Protect Neurons Against Oxidative Stress via Transcriptional Up-Regulation of the Glutathione Synthesis. J Neurochem 1999;72:2334–44. doi:10.1046/j.1471-4159.1999.0722334.x.

[115] Eftekharpour E, Holmgren A, Juurlink BH. Thioredoxin reductase and glutathione synthesis is upregulated by t-butylhydroquinone in cortical astrocytes but not in cortical neurons. Glia 2000;31:241–8. doi:10.1002/1098-1136(200009)31:3<241::AID-GLIA50>3.0.CO;2-9.

[116] Messing A, Brenner M. GFAP: functional implications gleaned from studies of genetically engineered mice. Glia 2003;43:87–90. doi:10.1002/glia.10219.

[117] Sofroniew MV. Astrogliosis. Cold Spring Harb Perspect Biol 2014;7:a020420. doi:10.1101/cshperspect.a020420.

[118] Martinez FO, Gordon S. The M1 and M2 paradigm of macrophage activation: time for reassessment. F1000Prime Rep 2014;6:13.

[119] Heppner FL, Ransohoff RM, Becher B. Immune attack: the role of inflammation in Alzheimer disease. Nat Rev Neurosci 2015;16:358–72. doi:10.1038/nrn3880.

[120] Fung S, Cherry AE, Xu C, Stella N. Alkylindole-sensitive receptors modulate microglial cell migration and proliferation. Glia 2015;63:1797–808. doi:10.1002/glia.22845.

[121] Bradley SJ, Challiss RAJ. G protein-coupled receptor signalling in astrocytes in health and disease: a focus on metabotropic glutamate receptors. Biochem Pharmacol 2012;84:249–59. doi:10.1016/j.bcp.2012.04.009.

[122] Dixon RA, Kobilka BK, Strader DJ, Benovic JL, Dohlman HG, Frielle T, et al. Cloning of the gene and cDNA for mammalian beta-

adrenergic receptor and homology with rhodopsin. Nature 1986;321:75–9. doi:10.1038/321075a0.

[123] Gloriam DE, Fredriksson R, Schioth HB. The G protein-coupled receptor subset of the rat genome. BMC Genomics 2007;8:338. doi:10.1186/1471-2164-8-338.

[124] Ghanemi A. Targeting G protein coupled receptor-related pathways as emerging molecular therapies. Saudi Pharm J 2015;23:115–29.

[125] Rosenbaum DM, Rasmussen SGF, Kobilka BK. The structure and function of G-protein-coupled receptors. Nature 2009;459:356–63. doi:10.1038/nature08144.

[126] Katritch V, Cherezov V, Stevens RC. Structure-function of the G protein-coupled receptor superfamily. Annu Rev Pharmacol Toxicol 2013;53:531–56. doi:10.1146/annurev-pharmtox-032112-135923.

[127] Venkatakrishnan AJ, Deupi X, Lebon G, Tate CG, Schertler GF, Babu MM. Molecular signatures of G-protein-coupled receptors. Nature 2013;494:185–94. doi:10.1038/nature11896.

[128] Hurowitz EH, Melnyk JM, Chen YJ, Kouros-Mehr H, Simon MI, Shizuya H. Genomic characterization of the human heterotrimeric G protein alpha, beta, and gamma subunit genes. DNA Res 2000;7:111–20.

[129] Oldham WM, Hamm HE. Heterotrimeric G protein activation by G-protein-coupled receptors. Nat Rev Mol Cell Biol 2008;9:60–71. doi:10.1038/nrm2299.

[130] Dorsam RT, Gutkind JS. G-protein-coupled receptors and cancer. Nat Rev Cancer 2007;7:79–94. doi:10.1038/nrc2069.

[131] Lagerstrom MC, Schioth HB. Structural diversity of G protein-coupled receptors and significance for drug discovery. Nat Rev Drug Discov 2008;7:339–57. doi:10.1038/nrd2518.

[132] Kolakowski LFJ. GCRDb: a G-protein-coupled receptor database. Receptors Channels 1994;2:1–7.

[133] Collingridge GL, Isaac JTR, Wang YT. Receptor trafficking and synaptic plasticity. Nat Rev Neurosci 2004;5:952–62. doi:10.1038/nrn1556.

[134] Hnasko TS, Edwards RH. Neurotransmitter corelease: mechanism and physiological role. Annu Rev Physiol 2012;74:225–43. doi:10.1146/annurev-physiol-020911-153315.

[135] Fredriksson R, Lagerstrom MC, Lundin L-G, Schioth HB. The G-protein-coupled receptors in the human genome form five main families. Phylogenetic analysis, paralogon groups, and fingerprints. Mol Pharmacol 2003;63:1256–72.

[136] Dijksterhuis JP, Petersen J, Schulte G. WNT/Frizzled signalling: receptor-ligand selectivity with focus on FZD-G protein signalling and its physiological relevance: IUPHAR Review 3. British Journal of Pharmacology 2014;171:1195–209. doi:10.1111/bph.12364.

[137] Jukkola PI, Rogers JT, Kaspar BK, Weeber EJ, Nishijima I. Secretin deficiency causes impairment in survival of neural progenitor cells in mice. Hum Mol Genet 2011;20:1000–7. doi:10.1093/hmg/ddq545.

[138] Hamann J, Aust G, Arac D, Engel FB, Formstone C, Fredriksson R, et al. International Union of Basic and Clinical Pharmacology. XCIV. Adhesion G protein-coupled receptors. Pharmacol Rev 2015;67:338–67. doi:10.1124/pr.114.009647.

[139] Langenhan T, Piao X, Monk KR. Adhesion G protein-coupled receptors in nervous system development and disease. Nature Publishing Group 2016;17:550–61. doi:10.1038/nrn.2016.86.

[140] Krasnoperov VG, Bittner MA, Beavis R, Kuang Y, Salnikow KV, Chepurny OG, et al. alpha-Latrotoxin stimulates exocytosis by the interaction with a neuronal G-protein-coupled receptor. Neuron 1997;18:925–37.

[141] Arac D, Boucard A, F Bolliger M, Nguyen J, Michael Soltis S, C Südhof T, et al. A novel evolutionarily conserved domain of cell-adhesion GPCR mediates autoproteolysis. Embo J 2012;31:1364–78. doi:10.1038/emboj.2012.26.

[142] Lin H-H, Chang G-W, Davies JQ, Stacey M, Harris J, Gordon S. Autocatalytic cleavage of the EMR2 receptor occurs at a conserved G protein-coupled receptor proteolytic site motif. J Biol Chem 2004;279:31823–32.

[143] Paavola KJ, Stephenson JR, Ritter SL, Alter SP, Hall RA. The N terminus of the adhesion G protein-coupled receptor GPR56 controls

receptor signaling activity. J Biol Chem 2011;286:28914–21. doi:10.1074/jbc.M111.247973.

[144] Chen P-L, Clandinin TR. The cadherin Flamingo mediates level-dependent interactions that guide photoreceptor target choice in Drosophila. Neuron 2008;58:26–33. doi:10.1016/j.neuron.2008.01.007.

[145] Paavola KJ, Hall RA. Adhesion G protein-coupled receptors: signaling, pharmacology, and mechanisms of activation. Mol Pharmacol 2012;82:777–83. doi:10.1124/mol.112.080309.

[146] Kuhnert F, Mancuso MR, Shamloo A, Wang H-T, Choksi V, Florek M, et al. Essential regulation of CNS angiogenesis by the orphan G protein-coupled receptor GPR124. Science 2010;330:985–9. doi:10.1126/science.1196554.

[147] Anderson KD, Pan L, Yang X-M, Hughes VC, Walls JR, Dominguez MG, et al. Angiogenic sprouting into neural tissue requires Gpr124, an orphan G protein-coupled receptor. Proc Natl Acad Sci U S A 2011;108:2807–12. doi:10.1073/pnas.1019761108.

[148] Cullen M, Elzarrad MK, Seaman S, Zudaire E, Stevens J, Yang MY, et al. GPR124, an orphan G protein-coupled receptor, is required for CNS-specific vascularization and establishment of the blood-brain barrier. Proc Natl Acad Sci U S A 2011;108:5759–64. doi:10.1073/pnas.1017192108.

[149] Hernández-Vásquez MN, Adame-García SR, Hamoud N, Chidiac R, Reyes-Cruz G, Gratton JP, et al. Cell adhesion controlled by adhesion G protein-coupled receptor GPR124/ADGRA2 is mediated by a protein complex comprising intersectins and Elmo-Dock. J Biol Chem 2017;292:12178–91. doi:10.1074/jbc.M117.780304.

[150] Mellor H. The role of formins in filopodia formation. Biochim Biophys Acta 2010;1803:191–200. doi:10.1016/j.bbamcr.2008.12.018.

[151] Rio C, Dikkes P, Liberman MC, Corfas G. Glial fibrillary acidic protein expression and promoter activity in the inner ear of developing and adult mice. J Comp Neurol 2002;442:156–62. doi:10.1002/cne.10085.

[152] Flock A, Flock B, Fridberger A, Scarfone E, Ulfendahl M. Supporting cells contribute to control of hearing sensitivity. J Neurosci 1999;19:4498–507.

[153] Bernardos RL, Barthel LK, Meyers JR, Raymond PA. Late-stage neuronal progenitors in the retina are radial Muller glia that function as retinal stem cells. J Neurosci 2007;27:7028–40. doi:10.1523/JNEUROSCI.1624-07.2007.

[154] Fischer AJ, Reh TA. Muller glia are a potential source of neural regeneration in the postnatal chicken retina. Nat Neurosci 2001;4:247–52.

[155] Kevany BM, Palczewski K. Phagocytosis of retinal rod and cone photoreceptors. Physiology (Bethesda) 2010;25:8–15. doi:10.1152/physiol.00038.2009.

[156] Ward S, Thomson N, White JG, Brenner S. Electron microscopical reconstruction of the anterior sensory anatomy of the nematode Caenorhabditis elegans. J Comp Neurol 1975;160:313–37. doi:10.1002/cne.901600305.

[157] White JG, Southgate E, THOMSON JN, Brenner S. The Structure of the Nervous-System of the Nematode Caenorhabditis-Elegans. Philos Trans R Soc Lond B Biol Sci 1986;314:1–340.

[158] Shaham S. Glia-neuron interactions in the nervous system of Caenorhabditis elegans. Current Opinion in Neurobiology 2006;16:522–8. doi:10.1016/j.conb.2006.08.001.

[159] Perkins LA, Hedgecock EM, Thomson JN, Culotti JG. Mutant sensory cilia in the nematode Caenorhabditis elegans. Dev Biol 1986;117:456–87. doi:10.1016/0012-1606(86)90314-3.

[160] Shaham S. Chemosensory organs as models of neuronal synapses. Nature Publishing Group 2010;11:212–7. doi:10.1038/nrn2740.

[161] Bargmann CI, Hartwieg E, Horvitz HR. Odorant-selective genes and neurons mediate olfaction in C. elegans. Cell 1993;74:515–27.

[162] Bargmann CI, Horvitz HR. Chemosensory neurons with overlapping functions direct chemotaxis to multiple chemicals in C. elegans. Neuron 1991;7:729–42.

[163] Mori I, Ohshima Y. Neural regulation of thermotaxis in Caenorhabditis elegans. Nature 1995;376:344–8. doi:10.1038/376344a0.

[164] Kaplan JM, Horvitz HR. A dual mechanosensory and chemosensory neuron in Caenorhabditis elegans. Proc Natl Acad Sci U S A 1993;90:2227–31.

[165] Bargmann CI, Horvitz HR. Control of larval development by chemosensory neurons in Caenorhabditis elegans. Science 1991;251:1243–6.

[166] Kim K, Sato K, Shibuya M, Zeiger DM, Butcher RA, Ragains JR, et al. Two chemoreceptors mediate developmental effects of dauer pheromone in C. elegans. Science 2009;326:994–8. doi:10.1126/science.1176331.

[167] Schackwitz WS, Inoue T, Thomas JH. Chemosensory neurons function in parallel to mediate a pheromone response in C. elegans. Neuron 1996;17:719–28.

[168] Chalasani SH, Chronis N, Tsunozaki M, Gray JM, Ramot D, Goodman MB, et al. Dissecting a circuit for olfactory behaviour in Caenorhabditis elegans. Nature 2007;450:63–70. doi:10.1038/nature06292.

[169] Biron D, Wasserman S, Thomas JH, Samuel ADT, Sengupta P. An olfactory neuron responds stochastically to temperature and modulates Caenorhabditis elegans thermotactic behavior. Proc Natl Acad Sci U S A 2008;105:11002–7. doi:10.1073/pnas.0805004105.

[170] Kuhara A, Okumura M, Kimata T, Tanizawa Y, Takano R, Kimura KD, et al. Temperature sensing by an olfactory neuron in a circuit controlling behavior of C. elegans. Science 2008;320:803–7. doi:10.1126/science.1148922.

[171] Wadsworth WG, Bhatt H, HEDGECOCK EM. Neuroglia and pioneer neurons express UNC-6 to provide global and local netrin cues for guiding migrations in C. elegans. Neuron 1996;16:35–46.

[172] Antebi A, Norris CR, Hedgecock EM, Garriga G. Cell and Growth Cone Migrations 1997.

[173] Hart AC, Sims S, Kaplan JM. Synaptic code for sensory modalities revealed by C. elegans GLR-1 glutamate receptor. Nature 1995;378:82–5. doi:10.1038/378082a0.

[174] Driscoll M, Kaplan J. Mechanotransduction 1997.

[175] Hilliard MA, Bargmann CI, Bazzicalupo P. C. elegans responds to chemical repellents by integrating sensory inputs from the head and the tail. Curr Biol 2002;12:730–4.

[176] Cassada RC, Russell RL. The dauerlarva, a post-embryonic developmental variant of the nematode Caenorhabditis elegans. Dev Biol 1975;46:326–42.

[177] Holt SJ, Riddle DL. SAGE surveys C. elegans carbohydrate metabolism: evidence for an anaerobic shift in the long-lived dauer larva. Mech Ageing Dev 2003;124:779–800.

[178] Gems D, Sutton AJ, Sundermeyer ML, Albert PS, King KV, Edgley ML, et al. Two pleiotropic classes of daf-2 mutation affect larval arrest, adult behavior, reproduction and longevity in Caenorhabditis elegans. Genetics 1998;150:129–55.

[179] Lee H, Choi M-K, Lee D, Kim H-S, Hwang H, Kim H, et al. Nictation, a dispersal behavior of the nematode Caenorhabditis elegans, is regulated by IL2 neurons. Nat Neurosci 2011;15:107–12. doi:10.1038/nn.2975.

[180] Golden JW, Riddle DL. The Caenorhabditis elegans dauer larva: developmental effects of pheromone, food, and temperature. Dev Biol 1984;102:368–78.

[181] Golden JW, Riddle DL. A pheromone-induced developmental switch in Caenorhabditis elegans: Temperature-sensitive mutants reveal a wild-type temperature-dependent process. Proc Natl Acad Sci U S A 1984;81:819–23.

[182] Golden JW, Riddle DL. A pheromone influences larval development in the nematode Caenorhabditis elegans. Science 1982;218:578–80.

[183] Li W, Kennedy SG, Ruvkun G. daf-28 encodes a C. elegans insulin superfamily member that is regulated by environmental cues and acts in the DAF-2 signaling pathway. Genes Dev 2003;17:844–58.

[184] Roayaie K, Crump JG, Sagasti A, Bargmann CI. The G alpha protein ODR-3 mediates olfactory and nociceptive function and controls cilium morphogenesis in C. elegans olfactory neurons. Neuron 1998;20:55–67.

[185] Zwaal RR, Mendel JE, Sternberg PW, Plasterk RH. Two neuronal G proteins are involved in chemosensation of the Caenorhabditis elegans Dauer-inducing pheromone. Genetics 1997;145:715–27.

[186] Kimura KD, Tissenbaum HA, Liu Y, Ruvkun G. daf-2, an insulin receptor-like gene that regulates longevity and diapause in Caenorhabditis elegans. Science 1997;277:942–6.

[187] Ren P, Lim CS, Johnsen R, Albert PS, Pilgrim D, Riddle DL. Control of C. elegans larval development by neuronal expression of a TGF-beta homolog. Science 1996;274:1389–91.

[188] Estevez M, Attisano L, Wrana JL, Albert PS, Massague J, Riddle DL. The daf-4 gene encodes a bone morphogenetic protein receptor controlling C. elegans dauer larva development. Nature 1993;365:644–9. doi:10.1038/365644a0.

[189] Georgi LL, Albert PS, Riddle DL. daf-1, a C. elegans gene controlling dauer larva development, encodes a novel receptor protein kinase. Cell 1990;61:635–45.

[190] Ogg S, Paradis S, Gottlieb S, Patterson GI, Lee L, Tissenbaum HA, et al. The Fork head transcription factor DAF-16 transduces insulin-like metabolic and longevity signals in C. elegans. Nature 1997;389:994–9. doi:10.1038/40194.

[191] Lin K, Dorman JB, Rodan A, Kenyon C. daf-16: An HNF-3/forkhead family member that can function to double the life-span of Caenorhabditis elegans. Science 1997;278:1319–22.

[192] Antebi A, Yeh WH, Tait D, HEDGECOCK EM, Riddle DL. daf-12 encodes a nuclear receptor that regulates the dauer diapause and developmental age in C. elegans. Genes Dev 2000;14:1512–27.

[193] Larsen PL, Albert PS, Riddle DL. Genes that regulate both development and longevity in Caenorhabditis elegans. Genetics 1995;139:1567–83.

[194] Riddle DL, Swanson MM, Albert PS. Interacting genes in nematode dauer larva formation. Nature 1981;290:668–71.

[195] Motola DL, Cummins CL, Rottiers V, Sharma KK, Li T, Li Y, et al. Identification of ligands for DAF-12 that govern dauer formation and reproduction in C. elegans. Cell 2006;124:1209–23.

doi:10.1016/j.cell.2006.01.037.

[196] Fielenbach N, Antebi A. C. elegans dauer formation and the molecular basis of plasticity. Genes Dev 2008;22:2149–65. doi:10.1101/gad.1701508.

[197] Golden JW, Riddle DL. ACaenorhabditis elegans dauer-inducing pheromone and an antagonistic component of the food supply. J Chem Ecol 1984;10:1265–80. doi:10.1007/BF00988553.

[198] Grogan DW, Cronan JEJ. Cyclopropane ring formation in membrane lipids of bacteria. Microbiol Mol Biol Rev 1997;61:429–41.

[199] Brooks KK, Liang B, Watts JL. The influence of bacterial diet on fat storage in C. elegans. PLoS ONE 2009;4:e7545. doi:10.1371/journal.pone.0007545.

[200] Baba T, Ara T, Hasegawa M, Takai Y, Okumura Y, Baba M, et al. Construction of Escherichia coli K-12 in-frame, single-gene knockout mutants: the Keio collection. Mol Syst Biol 2006;2:2006.0008. doi:10.1038/msb4100050.

[201] Kaul TK, Reis Rodrigues P, Ogungbe IV, Kapahi P, Gill MS. Bacterial fatty acids enhance recovery from the dauer larva in Caenorhabditis elegans. PLoS ONE 2014;9:e86979. doi:10.1371/journal.pone.0086979.

[202] Murakami M, Koga M, Ohshima Y. DAF-7/TGF-beta expression required for the normal larval development in C. elegans is controlled by a presumed guanylyl cyclase DAF-11. Mech Dev 2001;109:27–35.

[203] Bargmann C. Chemosensation in C. elegans. WormBook 2006. doi:10.1895/wormbook.1.123.1.

[204] Albert PS, Riddle DL. Developmental alterations in sensory neuroanatomy of the Caenorhabditis elegans dauer larva. J Comp Neurol 1983;219:461–81. doi:10.1002/cne.902190407.

[205] Ward DM, Ferris MJ, Nold SC, Bateson MM. A natural view of microbial biodiversity within hot spring cyanobacterial mat communities. Microbiol Mol Biol Rev 1998;62:1353–70.

[206] Procko C, Lu Y, Shaham S. Glia delimit shape changes of sensory neuron receptive endings in C. elegans. Development

2011;138:1371–81. doi:10.1242/dev.058305.

[207] Procko C, Lu Y, Shaham S. Sensory organ remodeling in Caenorhabditis elegans requires the zinc-finger protein ZTF-16. Genetics 2012;190:1405–15. doi:10.1534/genetics.111.137786.

[208] Schroeder NE, Androwski RJ, Rashid A, Lee H, Lee J, Barr MM. Dauer-specific dendrite arborization in C. elegans is regulated by KPC-1/Furin. Curr Biol 2013;23:1527–35. doi:10.1016/j.cub.2013.06.058.

[209] Peckol EL, Troemel ER, Bargmann CI. Sensory experience and sensory activity regulate chemosensory receptor gene expression in Caenorhabditis elegans. Proc Natl Acad Sci U S A 2001;98:11032–8.

[210] Satterlee JS, Sasakura H, Kuhara A, Berkeley M, Mori I, Sengupta P. Specification of thermosensory neuron fate in C. elegans requires ttx-1, a homolog of otd/Otx. Neuron 2001;31:943–56.

[211] Hall SE, Beverly M, Russ C, Nusbaum C, Sengupta P. A cellular memory of developmental history generates phenotypic diversity in C. elegans. Curr Biol 2010;20:149–55. doi:10.1016/j.cub.2009.11.035.

[212] Wicks SR, Yeh RT, Gish WR, Waterston RH, Plasterk RH. Rapid gene mapping in Caenorhabditis elegans using a high density polymorphism map. Nat Genet 2001;28:160–4.

[213] Fraser AG, Kamath RS, Zipperlen P, Martinez-Campos M, Sohrmann M, Ahringer J. Functional genomic analysis of C. elegans chromosome I by systematic RNA interference. Nature 2000;408:325–30. doi:10.1038/35042517.

[214] Chow DK, Glenn CF, Johnston JL, Goldberg IG, Wolkow CA. Sarcopenia in the Caenorhabditis elegans pharynx correlates with muscle contraction rate over lifespan. Exp Gerontol 2006;41:252–60. doi:10.1016/j.exger.2005.12.004.

[215] Chou HT, Vazquez RG, Wang K, Campbell R, Milledge GZ, Walthall WW, et al. HES-Mediated Repression of Pten in Caenorhabditis elegans. G3 2015;5:2619–28. doi:10.1534/g3.115.019463.

[216] Reinke V, Krause M, Okkema P. Transcriptional regulation of gene expression in *C. elegans*. WormBook; 2013.

[217] Hobert O. PCR fusion-based approach to create reporter gene constructs for expression analysis in transgenic C. elegans. Biotechniques 2002;32:728–30.

[218] Sulston JE, Horvitz HR. Post-embryonic cell lineages of the nematode, Caenorhabditis elegans. Dev Biol 1977;56:110–56. doi:10.1016/0012-1606(77)90158-0.

[219] Arribere JA, Bell RT, Fu BXH, Artiles KL, Hartman PS, Fire AZ. Efficient marker-free recovery of custom genetic modifications with CRISPR/Cas9 in Caenorhabditis elegans. Genetics 2014;198:837–46. doi:10.1534/genetics.114.169730.

[220] McGrath PT, Xu Y, Ailion M, Garrison JL, Butcher RA, Bargmann CI. Parallel evolution of domesticated Caenorhabditis species targets pheromone receptor genes. Nature 2011;477:321–5. doi:10.1038/nature10378.

[221] Wallace SW, Singhvi A, Liang Y, Lu Y, Shaham S. PROS-1/Prospero Is a Major Regulator of the Glia- Specific Secretome Controlling Sensory-Neuron Shape and Function in C. elegans. Cell Rep 2016;15:550–62. doi:10.1016/j.celrep.2016.03.051.

[222] Watson JD, Wang S, Stetina Von SE, Spencer WC, Levy S, Dexheimer PJ, et al. Complementary RNA amplification methods enhance microarray identification of transcripts expressed in the C. elegans nervous system. BMC Genomics 2008;9:84. doi:10.1186/1471-2164-9-84.

[223] Stetina Von SE, Watson JD, Fox RM, Olszewski KL, Spencer WC, Roy PJ, et al. Cell-specific microarray profiling experiments reveal a comprehensive picture of gene expression in the C. elegans nervous system. Genome Biol 2007;8:R135. doi:10.1186/gb-2007-8-7-r135.

[224] Butcher RA, Ragains JR, Li W, Ruvkun G, Clardy J, Mak HY. Biosynthesis of the Caenorhabditis elegans dauer pheromone. Proc Natl Acad Sci U S A 2009;106:1875–9. doi:10.1073/pnas.0810338106.

[225] Thomas JH, Kelley JL, Robertson HM, Ly K, Swanson WJ. Adaptive evolution in the SRZ chemoreceptor families of Caenorhabditis elegans and Caenorhabditis briggsae. Proc Natl Acad Sci U S A 2005;102:4476–81. doi:10.1073/pnas.0406469102.

[226] Neer EJ. Heterotrimeric G proteins: organizers of transmembrane signals. Cell 1995;80:249–57.

[227] Shukla AK, Xiao K, Lefkowitz RJ. Emerging paradigms of beta-arrestin-dependent seven transmembrane receptor signaling. Trends Biochem Sci 2011;36:457–69. doi:10.1016/j.tibs.2011.06.003.

[228] Jansen G, Thijssen KL, Werner P, van der Horst M, Hazendonk E, Plasterk RH. The complete family of genes encoding G proteins of Caenorhabditis elegans. Nat Genet 1999;21:414–9. doi:10.1038/7753.

[229] Hilliard MA, Bergamasco C, Arbucci S, Plasterk RHA, Bazzicalupo P. Worms taste bitter: ASH neurons, QUI-1, GPA-3 and ODR-3 mediate quinine avoidance in Caenorhabditis elegans. Embo J 2004;23:1101–11.

[230] Masuho I, Ostrovskaya O, Kramer GM, Jones CD, Xie K, Martemyanov KA. Distinct profiles of functional discrimination among G proteins determine the actions of G protein-coupled receptors. Sci Signal 2015;8. doi:10.1126/scisignal.aab4068.

[231] Bacaj T, Tevlin M, Lu Y, Shaham S. Glia are essential for sensory organ function in C. elegans. Science 2008;322:744–7. doi:10.1126/science.1163074.

[232] Yoshimura S, Murray JI, Lu Y, Waterston RH, Shaham S. mls-2 and vab-3 Control glia development, hlh-17/Olig expression and glia-dependent neurite extension in C. elegans. Development 2008;135:2263–75. doi:10.1242/dev.019547.

[233] Brenner S. The genetics of Caenorhabditis elegans. Genetics 1974;77:71–94.

[234] Mello C, FIRE A. DNA transformation. Methods Cell Biol 1995;48:451–82.

[235] Mello CC, Kramer JM, Stinchcomb D, Ambros V. Efficient gene transfer in C.elegans: extrachromosomal maintenance and integration of transforming sequences. Embo J 1991;10:3959–70.

[236] Liu H, Naismith JH. An efficient one-step site-directed deletion, insertion, single and multiple-site plasmid mutagenesis protocol. BMC Biotechnol 2008;8:91. doi:10.1186/1472-6750-8-91.

[237] Dickinson DJ, Ward JD, Reiner DJ, Goldstein B. Engineering the Caenorhabditis elegans genome using Cas9-triggered homologous recombination. Nat Methods 2013;10:1028–34. doi:10.1038/nmeth.2641.

[238] Zuryn S, Le Gras S, Jamet K, Jarriault S. A strategy for direct mapping and identification of mutations by whole-genome sequencing. Genetics 2010;186:427–30. doi:10.1534/genetics.110.119230.

[239] Shaham S. galign: a tool for rapid genome polymorphism discovery. PLoS ONE 2009;4:e7188. doi:10.1371/journal.pone.0007188.

[240] Kamath RS, Fraser AG, Dong Y, Poulin G, Durbin R, Gotta M, et al. Systematic functional analysis of the Caenorhabditis elegans genome using RNAi. Nature 2003;421:231–7.

[241] Timmons L, FIRE A. Specific interference by ingested dsRNA. Nature 1998;395:854. doi:10.1038/27579.

[242] Lundquist EA, Reddien PW, Hartwieg E, Horvitz HR, Bargmann CI. Three C. elegans Rac proteins and several alternative Rac regulators control axon guidance, cell migration and apoptotic cell phagocytosis. Development 2001;128:4475–88.

[243] Feng Z, Ko C-P. Neuronal glia interactions at the vertebrate neuromuscular junction. Curr Opin Pharmacol 2007;7:316–24. doi:10.1016/j.coph.2006.12.003.

[244] Rousse I, St-Amour A, Darabid H, Robitaille R. Synapse-glia interactions are governed by synaptic and intrinsic glial properties. Neuroscience 2010;167:621–32. doi:10.1016/j.neuroscience.2010.02.036.

[245] Graham PL, Johnson JJ, Wang S, Sibley MH, Gupta MC, Kramer JM. Type IV collagen is detectable in most, but not all, basement membranes of Caenorhabditis elegans and assembles on tissues that do not express it. J Cell Biol 1997;137:1171–83. doi:10.2307/1618070.

[246] Norman KR, Moerman DG. The let-268 Locus of Caenorhabditis elegans Encodes a Procollagen Lysyl Hydroxylase That Is Essential for Type IV Collagen Secretion. Dev Biol 2000;227:690–705.

doi:10.1006/dbio.2000.9897.

[247] KRAUSE M, Harrison SW, XU SQ, Chen L, FIRE A. Elements regulating cell- and stage-specific expression of the C. elegans MyoD family homolog hlh-1. Dev Biol 1994;166:133–48. doi:10.1006/dbio.1994.1302.

[248] Chen S, Rio C, Ji R-R, Dikkes P, Coggeshall RE, Woolf CJ, et al. Disruption of ErbB receptor signaling in adult non-myelinating Schwann cells causes progressive sensory loss. Nat Neurosci 2003;6:1186–93. doi:10.1038/nn1139.

[249] Schwabe T, Bainton RJ, Fetter RD, Heberlein U, Gaul U. GPCR Signaling Is Required for Blood-Brain Barrier Formation in Drosophila. Cell 2005;123:133–44. doi:10.1016/j.cell.2005.08.037.

[250] Stork T, Engelen D, Krudewig A, Silies M, Bainton RJ, Klämbt C. Organization and function of the blood-brain barrier in Drosophila. J Neurosci 2008;28:587–97. doi:10.1523/JNEUROSCI.4367-07.2008.

[251] Hoxha V, Lama C, Chang PL, Saurabh S, Patel N, Olate N, et al. Sex-specific signaling in the blood-brain barrier is required for male courtship in Drosophila. PLoS Genet 2013;9:e1003217. doi:10.1371/journal.pgen.1003217.

[252] Watanabe K, Nishimura Y, Nomoto T, Umemoto N, Zhang Z, Zhang B, et al. In vivo assessment of the permeability of the blood-brain barrier and blood-retinal barrier to fluorescent indoline derivatives in zebrafish. BMC Neurosci 2012;13:101. doi:10.1186/1471-2202-13-101.

[253] Fares H, Greenwald I. Genetic analysis of endocytosis in Caenorhabditis elegans: coelomocyte uptake defective mutants. Genetics 2001;159:133–45.

[254] Bargmann CIC, Avery LL. Laser killing of cells in Caenorhabditis elegans. Methods Cell Biol 1995;48:225–50.

[255] Fang-Yen C, Gabel CV, Samuel ADT, Bargmann CI, Avery L. Laser microsurgery in Caenorhabditis elegans. Methods Cell Biol 2012;107:177–206. doi:10.1016/B978-0-12-394620-1.00006-0.